DLR-IB-FA-BS-2019-59

Analytical and Numerical
Investigation of Multi-fastener
Joints in Composite Structures

Masterarbeit

Luca Massera und Josef Koord

Deutsches Zentrum
DLR für Luft- und Raumfahrt

Institut für Faserverbundleichtbau und Adaptronik

DLR-IB-FA-BS-2019-59

Analytical and Numerical Investigation of Multi-fastener Joints in Composite Structures

Zugänglichkeit:

Stufe 2 DLR intern zugänglich

Braunschweig, *März, 2019*

Abteilungsleiter:

Prof. Dr.-Ing. Christian Hühne

Der Bericht umfasst: 167 Seiten

Autoren:

Luca Massera

Betreuer:

Josef Koord

Deutsches Zentrum
DLR   für Luft- und Raumfahrt

ANALYTICAL AND NUMERICAL INVESTIGATION OF MULTI-FASTENER JOINTS IN COMPOSITE STRUCTURES

DEUTSCHES ZENTRUM FÜR LUFT- UND RAUMFAHRT

ÉCOLE POLYTECHNIQUE FÉDÉRALE DE LAUSANNE

Luca Massera

Supervisors:

Prof. William Curtin

Josef Koord

March 2019

Ma più sovente mi tormenta il dubbio
che questo confine non esista

—————————

BUZZATI, I sette messaggeri

Abstract

In this study, the reaction forces arising in multi-fastener joints subject to different forms of in-plane loading are investigated. Different approaches are considered with the goal of designing a tool capable of predicting fastener loads in the context of early preliminary joint design. A review of the relevant literature on the topic is provided. The analytical models retained from the literature, as well as models modified or proposed as part of the study, are presented and discussed. The models accounting for the deformation of both the connected members and of the fasteners are based on a one-dimensional discretization of the joint through linear springs. The stiffness of the fasteners is calculated with empirically based methods. The applicability of the analytical models to joint design is assessed both in terms of accuracy and conservatism. The limits of validity of the assumptions underlying the analytical models are evaluated through comparison with detailed numerical models. Through 3D Finite Element analysis with linear material deformation, the parts composing the joint and their interactions are modelled. Joint design guidelines stemming from the findings of the numerical and analytical investigations are suggested.

Table of content

List of Figures

List of Tables

List of Symbols

A	Area [mm^2]
cl	Bolt-hole distance [μm]
D	Diameter [mm]
E	Modulus of elasticity [GPa]
F	Force reaction [N]
f	Load fraction [-]
G	Shear modulus [GPa]
I	Section modulus [mm^3]
K	Stiffness [Nm^{-1}]
$\underline{\underline{K}}$	Stiffness matrix [Nm^{-1}]
$\underline{L}$	Loading vector [N]
$l_{\mathbf{end}}$	Last bolt edge distance [mm]
M	Moment [Nm]
N	Number of fasteners [-]
P	Applied load [N]
p	Bolt spacing [mm]
R$_{\mathbf{N}}$	Bolt shear capacity [N]
r	Radius of rotation [mm]
T	Temperature [K]
t	Thickness [mm]
u	Displacement [mm]
w	Width [mm]
$\underline{x}$	Nodal displacement vector [mm]
α	CTE of plate A [K^{-1}]
β	CTE of plate B [K^{-1}]
γ	Shear strain [-]

$\boldsymbol{\Delta}$	Bolt deformation [mm] or [in]
$\boldsymbol{\delta}$	Member deformation [mm]
$\boldsymbol{\varepsilon}$	Normal strain [-]
$\boldsymbol{\theta}$	Angle [°]
$\boldsymbol{\lambda}$	Bolt-hole clearance [μm]
$\boldsymbol{\mu}$	Static friction coefficient [-]
$\boldsymbol{\nu}$	Poisson ratio [-]
$\boldsymbol{\sigma}$	Stress [MPa]

List of Abbreviations

BC	Boundary Conditions
CFRP	Carbon Fiber Reinforced Polymer
CG	Fastener group centroid
CLT	Classical Lamination Theory
CTE	Coefficient of Thermal Expansion
DLR	German Aerospace Center
FE	Finite Element
FEM	Finite Element Method
HSB	Handbuch Struktur Berechnung
IC	Instantaneous Center
ICoR	Instantaneous Center of Rotation
LC	Load Case
SF	Scaling Factor
SLSQP	Sequential Least SQuares Programming

1 Introduction

1.1 Context and objective

Composite materials have found extensive application in aviation and space technology in recent decades, with a potential for lightweight design of both primary and secondary structures. The vastness of composite applications is reflected in the variety of technological challenges designers are faced with.

Bolted joints are commonly employed for the assembly of different members in composite or hybrid structures. Joint analysis can be crucial when evaluating a structure's safety from failure, which may need to be ensured for very different loading conditions.

A tool for preliminary joint design is currently under development at the German Aerospace Center (DLR). Considering an as wide as possible array of loading conditions, the tool will determine at first the reaction forces at each fastener. These predicted loads will then be used as input to determine the 2D stress distribution around the bolt holes. Finally, failure of the joint will be evaluated through the application of failure criteria to the obtained stress distribution.

This thesis study focused exclusively on the prediction of the reaction loads, the first of the tool's modules. The key goal was to identify, evaluate and, when possible, modify existing models for predicting reaction loads in composite bolted joints.

The tool is intended to be used at an early design stage and specifically in early preliminary design, providing indications regarding the influence on joint failure of parameters such as member thickness or bolt spacing. The intended use makes it necessary for the tool to require little time for setup and computation, as well as little input from the user. Complex analysis practices, such as 3D Finite Element (FE) modelling, could provide precise information regarding joint failure but would not be suitable for joint optimization because of their high computational requirements.

Nonetheless, numerical approaches were considered in this thesis study for evaluation of the results obtained with the preliminary design tool. The goal of such a comparison was to evaluate under what conditions a simpler model, incapable of reproducing the level of detail of a 3D FE model, could provide reasonably accurate load predictions. The level of accuracy and conservatism of the predictions was assessed as part of the present study.

1.2 Bolted joints under in-plane loading: an early discussion

Let us consider a bolted connection in which two plates are clamped together by a single bolt. The nut has been torqued sufficiently so that a non-negligible preload is

present in the bolt. The bolt has an a shank diameter smaller than the hole diameter in the plates, so that a certain clearance is present between bolt and hole.

Such an assembly is held fixed at one end of the top plate, while a horizontal load is applied to the opposite end of the bottom plate, as shown in Fig.1. The behavior of the joint can be described through a load-deflection curve. Four distinct regions can be observed in the curve of Fig.1, where the red lines indicate possible linear approximations of quasi-linear phenomena.
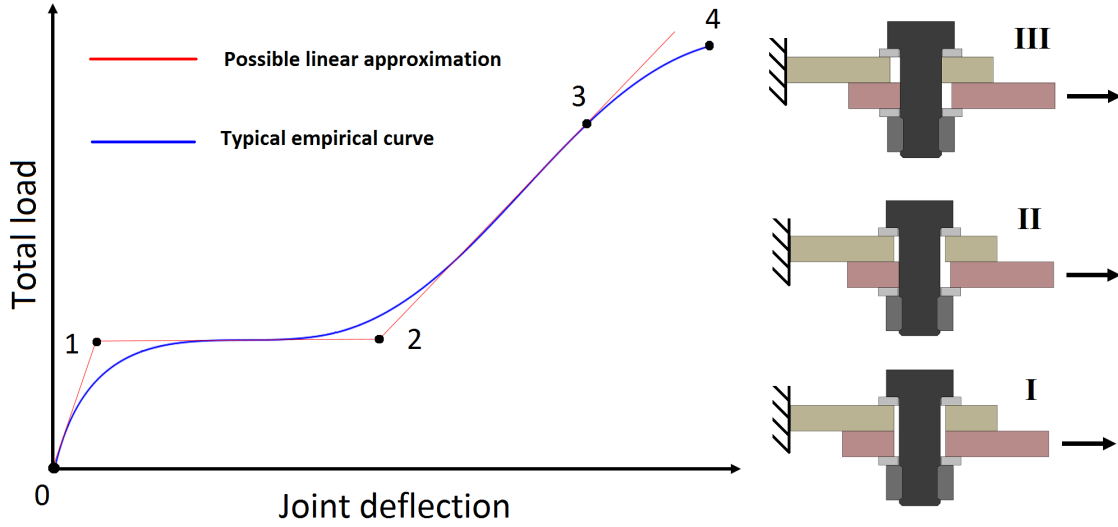
Figure 1: Typical load-deflection curve for a single-bolt joint (Adapted from [1])

Small applied loads correspond to the initial quasi-linear region I (0-1), in which the external load is reacted by the static friction forces between the parts in contact. The bolt-torque is sufficient to ensure that no slipping of the plates is possible. The shear deformation of the plates dominates the overall joint deformation. As a consequence, the slope of the quasi-linear curve in this region depends strongly on the elastic properties of the plates for such a shear loading.

When the applied load is large enough for the static friction effects to be overcome, a displacement of the bottom plate with respect to the top plate is initiated. After initiation, the slipping of the transition region II (1-2) takes place with little resistance, which results in a significantly flatter load-deflection curve compared to the previous region.

The transition region ends when contact is established between bolt shank and plates. In the early bolt load transmittal region III (2-3), the contact area is small but rapidly increasing with an increase in applied load. The curve becomes nearly linear when a substantial bolt shank-plates contact is reached. In this phase, the elastic properties of the plates, as well as of the bolt, dominate the load transfer.

For cases in which bearing failure is critical, as considered in Fig.1, the non-linear region after point 3 is the final stage before failure of the joint. Non-linear deformation of the plates has the potential to modify load distribution in the bolts since, at different bolts, the plates will reach this stage at different moments, depending on the distribution in region III.

For metal joints where significant bearing deformation takes place, the load distribution among fasteners can become almost even thanks to the effects of non-linear member deformation. Since composite laminates often show less significant non-linear deformation compared to metals, it is sometimes possible to assume that the load-distribution in a composite joint at failure does not change after the bolt-transmittal region [4]. However, when non-linear effects are believed to play an important role in joint failure, they need to be accounted for in the modelling approach.

While the presented discussion showed a joint subject to tensile loading, a similar behavior in load transfer would be observable with other forms of in-plane loading in presence of bolt-hole clearance and preload.

2 Joint description and properties

2.1 Geometry definitions

Bolted joints transferring loads from one member to another were investigated in this study. As presented in more detail in Section 3.1, the focus of the study was on in-plane loading of joints. In the case of shear joints, external in-plane loads are reacted, at least partially, by the fasteners through shear forces. Lap joints belong to the family of shear joints and can be divided in single-lap and double-lap joints depending on the number of connected plates.
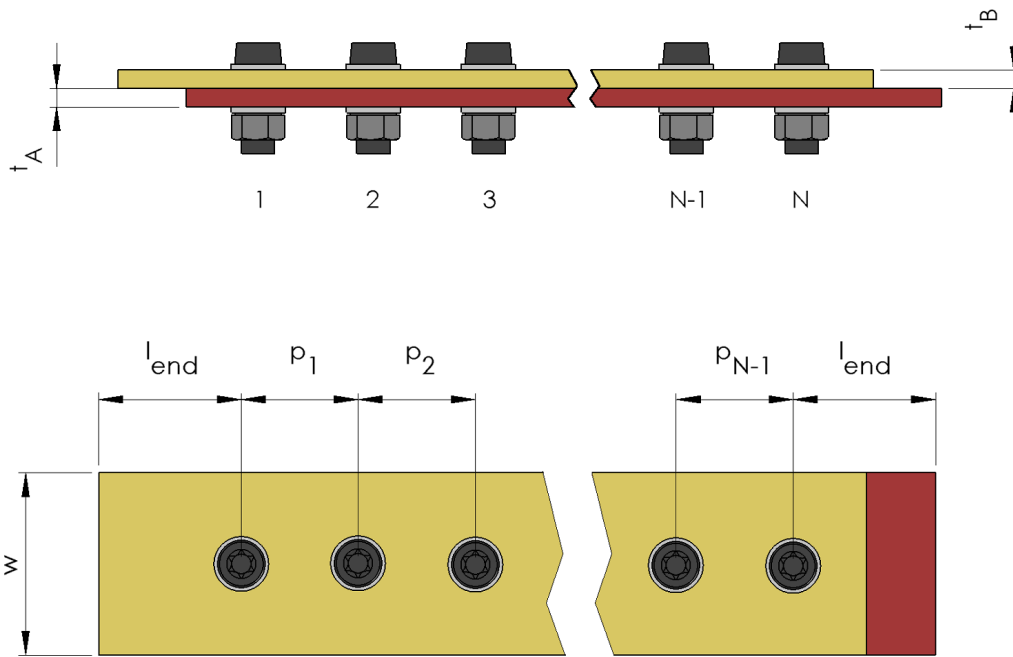
Figure 2: Dimensions and numbering for a generic single-lap joint

Fig.2 shows a generic single-lap joint. Two plates A and B of uniform thickness t_A and t_B are connected with N fasteners. Both plates have a constant width w. The fasteners are separated by a distance p, with p_1 indicating the spacing between fasteners number 1 and 2. l_{end} refers to the distance of bolt 1 to the edge of plate B and of bolt N to the edge of plate A. In later sections, the subscript j is used to indicate a generic fastener, such that $1 \leq j \leq N$, and when referring to the value of parameters at that fastener location, for example for a bolt diameter D_j. Similarly, the subscript i is used to indicate a generic location in between fasteners, with $1 \leq i \leq N - 1$. It can be used to indicate a spacing p_i or quantities related to this distance, such as the local A plate stiffness K_{A_i}. It should be noted that a

value $i = 1$ corresponds to the position between fasteners 1 and 2, while the position $i = N - 1$ is located between fasteners N-1 and N.

A double-lap joint is shown in Fig.3. The top and bottom plates are both referred to as A plates, while the central plate is called B. In this thesis study, it is always considered that both the A plates have equal thickness at the same fastener. Bolt and spacing numbering follow the same pattern previously introduced for single-lap joints.
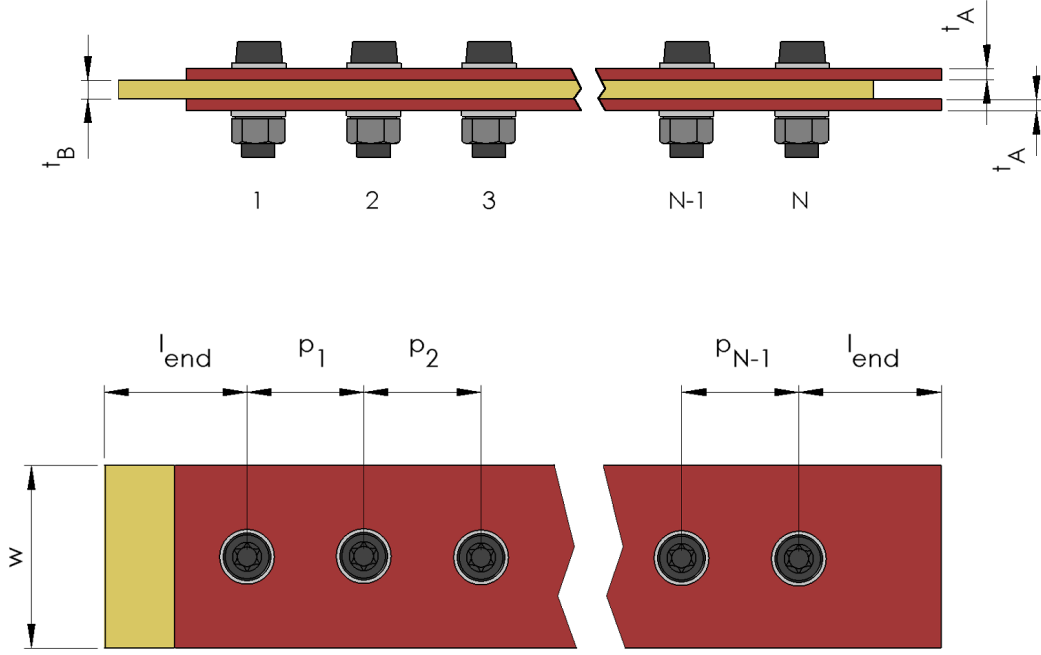
Figure 3: Dimensions and numbering for a generic double-lap joint

While the two previously presented joints have uniform plate thickness, lap-joints can also have different plate thickness at different fasteners. Fig.4 shows a schematic representation of a stepped-double-lap joint.
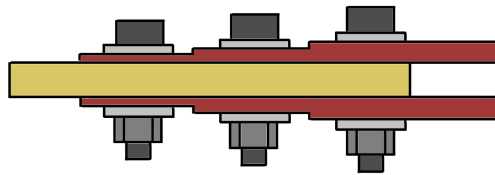
Figure 4: Example of stepped-double-lap joint with three fasteners

When discussing shear joints, the total joint is sometimes divided in smaller portions of fasteners in a line. These portions are defined as "strips". Fig.5 shows an example

of a strip composing a double-lap joint, schematically represented. The terms "row" and "column" are also sometimes employed. While, as "strip", both refer to the joint geometry, the direction of the load applied to the structure is implicitly considered. If the plates that compose the joint were divided in strips, columns would be the strips parallel to the applied load and the rows would be the strips perpendicular to it. Considering the joints of Figures 2 and 3, if a load were applied along a line passing through all the fasteners, then these joints would have N rows and 1 column. The term "strip" is therefore broader than "row" and "column" and simply refers to the joint geometry.
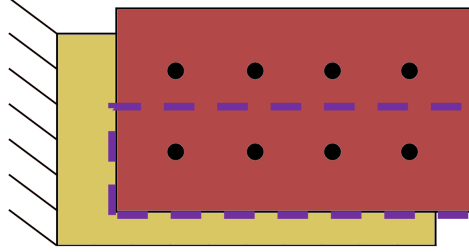
Figure 5: Example of a strip, indicated in purple

The numbering and definitions provided in this section are sufficient to fully define the majority of joint geometries considered in the study and to understand the tool formulation presented in Chapter 4. Additional information is provided whenever necessary to avoid ambiguity in the joint geometry definition.

2.2   Clearance and tolerance effects

The effects on load distribution of bolt-hole clearance were taken into consideration in the thesis study. Table 1 presents the possible clearance values λ with the f7/H10 fitting for bolts of nominal diameter 8 mm, as used in this study, see ISO 286 [5]. Such fitting was indicated as typical for the aerospace industry and considered in several studies, among which [2]. Clearance is calculated as the difference between hole and bolt diameters.

Table 1: Tolerance values with an f7/H10 fitting for M8 bolts

Bolt tol$_{max}$ [μm]	Bolt tol$_{min}$ [μm]	Hole tol$_{max}$ [μm]	Hole tol$_{min}$ [μm]	λ_{min} [μm]	λ_{max} [μm]
-28	-13	0	+58	13	86

The table shows that no clearance smaller than 13 μm or larger than 86 μm is possible with the f7/H10 fitting. The knowledge of the bolt-hole clearance in a joint

is of primary importance since it introduces the possibility of bolts not being in contact with the hole surface, with the effects that were presented in Section 1.2.

Having introduced the bolt-hole clearance values, a clarification regarding joint displacement needs to be made. Considering a generic bolt j subject to uniaxial loading as presented in Section 1.2, no load is transferred through the bolt until contact with the hole surface is established. The displacement of the joint induced by the applied load before bolt-hole contact is established does not correspond to λ_j. The actual joint displacement, defined as cl_j, cannot be exactly known and depends on how the bolt holes are aligned. It could vary from $cl_j = 0$ to $cl_j = 2\lambda_j$. Fig.6 shows two scenarios for which λ_j is the same but cl_j is different because of the different hole alignment. In Fig.6(a), after a very small joint displacement cl_j, contact is established on both sides of the bolt, which starts transferring a load in shear. In Fig.6(b), however, a much larger cl_j displacement is necessary to be completed before the bolt can enter the bolt load transmittal region, despite the clearance λ_j being the same. Fig.61 in the Appendix shows in detail the evolution of the case of Fig.6(b) before load transfer through the bolt in shear can take place.

<center>(a)   (b)</center>
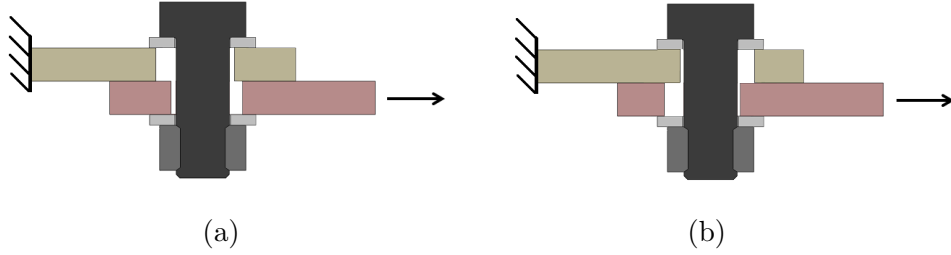
Figure 6: Examples of different cl_j due to different hole alignment

In this thesis study, cl_j was considered equal to the clearance expressed at the diameter: $cl_j = \lambda_j$. This represents an average case and is equivalent to consider the bolt exactly at the center of the hole.

A clearance of 20 μm was considered as a small clearance, while 100 μm corresponds to the largest possible clearance with the f7/H10 fitting. This choice was made for simplicity, and without loss of conservatism, based on the values presented in Table 1. An ideal case of 0 μm and an intermediate value 40 μm were also considered in the study. To facilitate the description of the clearance conditions in a joint, the clearance values are indicated in later sections through the $\boldsymbol{\lambda}$ vector:

$$\boldsymbol{\lambda} = \{\lambda_1, \lambda_2 \cdots \cdot \lambda_N\} \tag{1}$$

Defined here for a generic joint with N fasteners. Bolt numbering definition is provided whenever necessary.

Finally, it should be noted that position tolerance, unlike the clearance fit considered above, cannot increase the actual distance between bolt and hole surfaces. A clarification is provided through Fig.7.

(a)   (b)
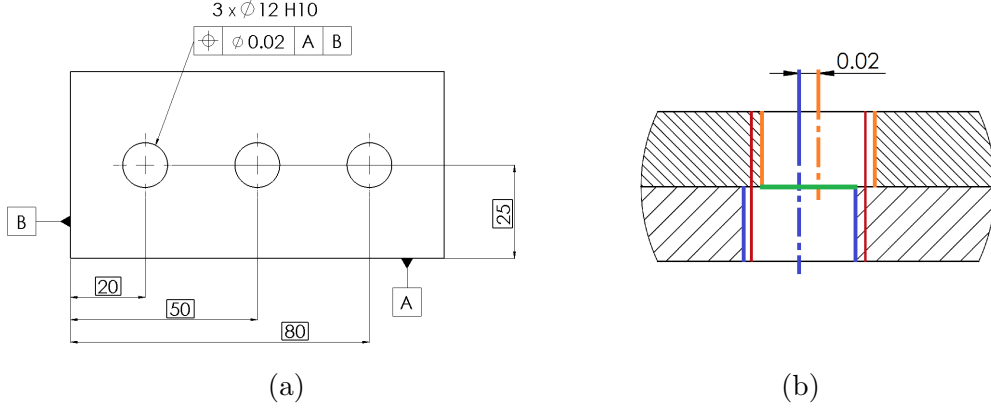
Figure 7: Effects of position tolerance on bolt-hole distance

Let us consider two identical plates to be joined with three bolts. Fig.7(a) shows the locations of the holes. While the location where the holes on the top and bottom plates are drilled is theoretically the same, the uncertainty due to the manufacturing process has to be taken into account. Considering a commonly employed tolerance grade IT6 as per ISO 286, position tolerance values of 13 μm, 16 μm and 19 μm could be ensured in the part manufacturing for the specified bolt distances. For simplicity, a 20 μm tolerance is considered and indicated in Fig.7. With such a position tolerance, the drilling locations are confined within a circle of diameter 20 μm centered at the theoretical drilling location. Therefore, a hole misalignment of at most 20 μm, shown in Fig.7(b), can be generated with drilling. The red lines indicate where the hole surface would be for an ideal case of zero position tolerance, while the orange and blue lines refer to the case of worst misalignment possible. It is evident from the picture how any misalignment due to manufacturing would reduce the surface through which the bolt has to pass during assembly, indicated in green in the picture. The largest possible distance between bolt and hole surfaces corresponds to the ideal case of zero position tolerance, since the misalignment it introduces can only reduce bolt-hole clearance.

2.3   Bolt preload

Three levels of bolt preload were considered in the thesis study. The corresponding values of axial force F_N for M8 bolts are presented in Table 2.

Table 2: Considered bolt preload values and corresponding axial force for M8 bolts

Denomination	Bolt Torque [Nm]	F_N [kN]
Finger-tight	0.5	0.362
Intermediate	8	5
Torque-tight	16	11.4

Finger-tight and torque-tight conditions were already considered in [3]. The same study provided measurements of the axial force F_N for those torque conditions obtained with instrumented fasteners. Intermediate torque was also considered, being recommended for assembly by the standard ASTM D5961 [6]. The corresponding F_N value was obtained as in [7].

2.4 Material data and material properties calculation

When discussing material properties, the 123 right-handed coordinate system is used. The 1 direction corresponds to the fiber orientation, while 2 lies in the plane of the fibers and is perpendicular to 1. The 3 axis is directed perpendicularly to the plane of the fibers. Following this convention, θ is used to indicate the angle of a ply with respect to the 1 direction, 90° being aligned with 2. The right-handed XYZ coordinate system is instead used throughout the report to indicate the orientation of structures.

The material orientations were defined with respect to a coordinate system oriented as in Fig.8 for all the single-column cases. The 0° angle corresponds to the direction indicated by the X axis, while the Z axis indicates the stacking direction.
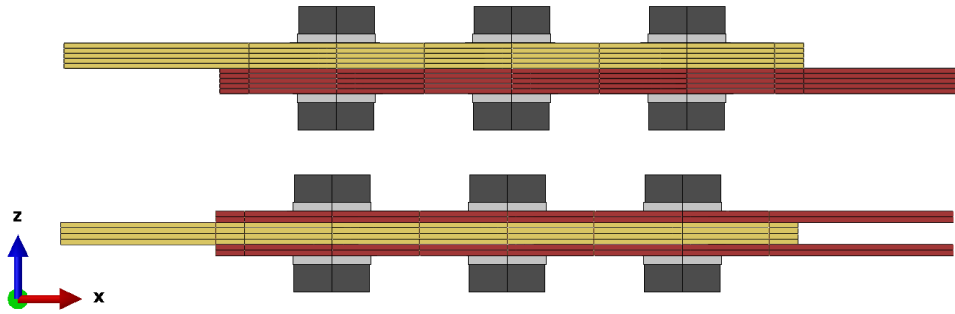
Figure 8: Coordinate system definition for material orientation

Whenever necessary, additional information about material orientation is indicated throughout the report.

2.4.1 Stiffness properties

HTA/6376, a carbon fiber–epoxy material currently used for primary structures in the aerospace industry, was considered in this study. The prepreg has a nominal ply thickness of 0.13 mm and its unidirectional stiffness properties are summarized in Table 3. The material properties were obtained from [8].

Table 3: Stiffness properties of a unidirectional layer of HTA/6376

E_{11} [GPa]	E_{22} [GPa]	E_{33} [GPa]	G_{12} [GPa]	G_{13} [GPa]	G_{23} [GPa]	ν_{12} [-]	ν_{13} [-]	ν_{23} [-]
140	10	10	5.2	5.2	3.9	0.3	0.3	0.5

The second carbon-epoxy material modelled in the study is M21/T700GC. The unidirectional stiffness properties for this prepreg, which also has a nominal ply thickness of 0.13 mm, were implemented as shown in Table 4. These properties were obtained from the DLR material library. A distinction is made between ply properties in tensile and compressive loading.

Table 4: Stiffness properties of a unidirectional layer of M21/T700GC

	E_{11} [GPa]	E_{22} [GPa]	E_{33} [GPa]	G_{12} [GPa]	G_{13} [GPa]	G_{23} [GPa]	ν_{12} [-]	ν_{13} [-]	ν_{23} [-]
Tens.	125.5	8.33	8.33	4.135	3.5	3	0.3	0.3	0.4
Comp.	102.8	8.26	8.26						

The composite layups modelled with the described prepreg materials are presented in Section 2.5.

Steel plates were modelled with isotropic elastic properties. These properties, indicated as "Generic steel", were also used to model washers and were reported in [8]. The same properties were employed for the steel sheets in hybrid laminates. Laminate hybridization is further discussed in section 2.5. An isotropic material behavior was also considered in the studies with ASTM A36 steel plates, with properties obtained from the database of AZoMaterials[i]. Material properties for steel are presented in Table 5.

---

[i] azom.com

Table 5: Material properties for generic steel (left) and ASTM A36 plates (right)

E [GPa]	ν [-]
210	0.3

E [GPa]	ν [-]
200	0.26

Fasteners and plates were modelled in some cases with isotropic titanium alloy properties with a purely elastic behavior. The properties, obtained from [8], are shown in Table 6.

Table 6: Material properties for titanium

E [GPa]	G [GPa]	ν [-]
110	36	0.29

In Section 7.1, fasteners were modelled in a Finite Element model as ASTM A325 bolts in order to allow comparison of numerical results with an empirically based model developed for such fasteners. The equivalence of this standard of fasteners to the metric grade 8.8 is established in [9]. The material properties of these fasteners were taken as equivalent to the metric standard of grade 8.8 and obtained from ISO 898-1 [10]. The implemented values are shown in Table 7.

Table 7: Material properties for ASTM A325 / Grade 8.8 metric bolts

E [GPa]	σ_{Y} [MPa]	σ_{uts} [MPa]	Elongation [-]	ν [-]
210	640	830	0.12	0.3

The material deformation for these bolts was modelled as piece-wise linear. The plastic strain at ultimate elongation was implemented in Abaqus FEA following the official documentation.[ii] The bolt shear capacity calculation is presented in the Appendix (Section 11.5).

2.4.2 Thermal expansion properties

When investigating the loads generated by thermal loading, thermal expansion of the materials was modelled. The material properties for the considered models are summarized in Table 8.

[ii]dsk.ippt.pan.pl/docs/abaqus/v6.13/books/gsk/default.htm

Table 8: Coefficients of Thermal Expansion (CTE) of the considered materials

	CTE$\cdot 10^6$[K^{-1}]	
	1 Direction	2 Direction
M21/T700GC	0.21	29.8
Steel	17.3	17.3
Titanium	8.6	8.6

The effective properties of an M21/T700GC cured ply were reported in [11], while the thermal properties for steel were taken from the material database of ASM Aerospace Specification Metals, Inc.[iii] The properties corresponding to ASTM Grade 7 titanium and AISI Type 304 stainless steel were selected from the database. These material properties refer to a temperature of 20° C.

2.4.3 Laminate properties calculation in the tool

Global stiffness properties for the laminate are necessary as input for the tool. These are derived through Classical Lamination Theory (CLT). The values of E_{11}, E_{22}, G_{12} and ν_{12} for a single ply are needed as input for the calculation, together with the fractions of 0°,±45° and 90° plies or metal sheets. Tensile or compressive stiffness properties are used as input depending on the considered joint loading. The outputs of the theory, programmed in a Python script, are the global laminate stiffness properties E_x, E_y, G_{xy} and ν_{xy}.
Similarly, the tool calculates the global CTE of a laminate from the single ply properties. A description of the model for CTE calculation, also based on CLT, is presented in the Appendix (Section 11.4).

2.5 Composite Layups

Several laminate layups were considered in this thesis study. This was due to both a need to reproduce results from the literature for comparison and to investigate relevant aspects of load distribution under different conditions. The layups differed on the basis of four parameters. A four-entry code of the type X-X-X-X was defined to avoid confusion when referring to the layups. The X letters are replaced by letters that specify the four parameters for a certain layup:

- **Material**
  The letter for the material is the first to be indicated in the layup code. Two prepreg materials were presented in Section 2.4. They both have a nominal ply thickness of 0.13 mm. Since tensile loading was mostly considered in this thesis study, when no particular mention is made, tensile properties of the

---

[iii]aerospacemetals.com

materials are used in the definition of the layup. HTA/6376 is identified by "H", while M21/T700GC by "M" for layups to be used with tensile loading. Only in Section 6.2.3 compression loading is considered and the material in the layup code is indicated with "M*"

- **Joint configuration**
  This parameter is expressed in second position in the code. It can either be expressed by "SL" for single-lap joints or "DL" for double-lap joints.

- **Layup orientation**
  The third letter in the code takes either the value "Q" for a (25-50-25)% quasi-isotropic layup or "D" for a (62.5-25-12.5)% layup with higher stiffness in the X direction.

- **Metal hybridization**
  The last entry in the code indicates if a laminate is entirely made of a carbon-epoxy material or if it is partially hybridized with steel sheets. Hybridized laminates, "H", differ from those entirely made from CFRP, "C", only by the fact that the fraction of 90° plies, indicated by the third code entry is replaced by steel sheets. The letter "m" is used to indicate a metal sheet in a hybrid laminate.

Keeping in mind the defined layup identification code, the following layups were considered in this thesis study:

- **H-SL-Q-C**
  - A plate: $[45/0/\text{-}45/90]_{5s}$, 5.2 mm total thickness
  - B plate: $[45/0/\text{-}45/90]_{5s}$, 5.2 mm total thickness

- **H-DL-Q-C**
  - A plates: $[45/0/\text{-}45/90]_{2s}$, 2.08 mm total thickness
  - B plate: $[45/0/\text{-}45/90]_{4s}$, 4.16 mm total thickness

- **M-SL-D-C**
  - A plate: $[0/45/0/\text{-}45/0/0/90/0/0/45/0/\text{-}45/0/0/90/0]_s$, 4.16 mm total thickness
  - B plate: $[0/45/0/\text{-}45/0/0/90/0/0/45/0/\text{-}45/0/0/90/0]_s$, 4.16 mm total thickness

- **M-DL-D-C**
  - A plates: $[0/45/0/\text{-}45/0/0/90/0]_s$, 2.08 mm total thickness
  - B plate: $[0/45/0/\text{-}45/0/0/90/0/0/45/0/\text{-}45/0/0/90/0]_s$, 4.16 mm total thickness

– **M*-DL-D-C**
This layup was considered in a study of compression loading. It is almost identical to M-DL-D-C, with the exception that compression and not tensile ply stiffness properties are used as input for the calculation of the global properties.
  – A plates: $[0/45/0/\text{-}45/0/0/90/0]_s$, 2.08 mm total thickness
  – B plate: $[0/45/0/\text{-}45/0/0/90/0/0/45/0/\text{-}45/0/0/90/0]_s$, 4.16 mm total thickness

– **M-DL-Q-C**
  – A plates: $[45/90/\text{-}45/0]_{2s}$, 2.08 mm total thickness
  – B plate: $[45/90/\text{-}45/0]_{4s}$, 4.16 mm total thickness

– **M-DL-D-H**
  – A plates: $[0/45/0/\text{-}45/0/0/m/0]_s$, 2.08 mm total thickness
  – B plate: $[0/45/0/\text{-}45/0/0/m/0/0/45/0/\text{-}45/0/0/m/0]_s$, 4.16 mm total thickness

– **M-DL-Q-H**
  – A plates: $[45/m/\text{-}45/0]_{2s}$, 2.08 mm total thickness
  – B plate: $[45/m/\text{-}45/0]_{4s}$, 4.16 mm total thickness

The difference between the $[45/0/\text{-}45/90]$ and $[45/90/\text{-}45/0]$ quasi-isotropic layups was modelled to allow metal hybridization of the latter laminates. Hybridization requires no two adjacent metal sheets to be present in the stacking sequence. As a consequence, the corresponding composite layup cannot have two adjacent 90° plies which would be replaced by metal sheets.

3 Load cases and literature review

3.1 Load cases

Having introduced the joint geometries considered in the thesis study, the Load Cases (LC) of interest are presented and numbered in this section.

The tool was designed to account for different forms of in-plane loading, while out-of-plane loads are of no interest for the intended tool application. As a consequence, for all cases, the fasteners can only be purely loaded in shear by the external load and no tensile reactions take place, with the exception of minor secondary effects due to loading eccentricity in single-lap joints.

The first considered load case is uniaxial loading. Keeping in mind the previous geometry definitions, a load is applied to an edge of the A plates of a double-lap joint, while the central plate B is held fixed at the opposite edge. The applied load is thus transferred to the central plate. A schematic representation is provided in Fig.9, where the black dots indicate the fasteners. The fastener pattern is arbitrary here. Also, while double-lap joints are shown here from the top view, the discussion of this section equally applies to single-lap joints. A distinction is made between Fig.9(a) and Fig.9(b), where the former represents uniaxial tension (LC1) and the latter uniaxial compression (LC2). Both forms of loading were investigated in this study.

(a)   (b)
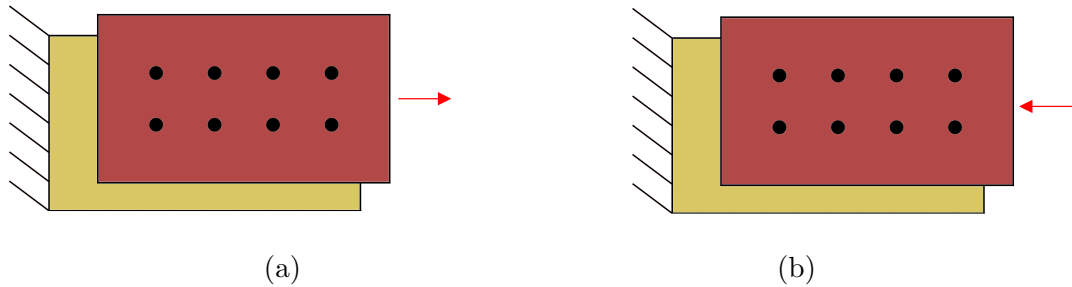
Figure 9: Uniaxial loading of a joint: tension (a) and compression (b)

With the uniaxial loading previously mentioned, the external load is applied along a line passing through the fastener group center. In the case of shear loading (LC3), shown in Fig.10, an eccentric load, i.e. not applied along a line passing through the center of the fastener group, is considered. A rigorous definition of group center and eccentricity is provided in Section 4.1.5, here it is sufficient to mention that the fastener reactions depend on the load application point as well as its direction. It should be noted that, when discussing this load case, "shear" refers to the loading itself and should not be confused with the fastener shear reactions. As already

mentioned, any form of in-plane loading, and not just the shear loading of Fig.10, can generate shear reactions in the fasteners.
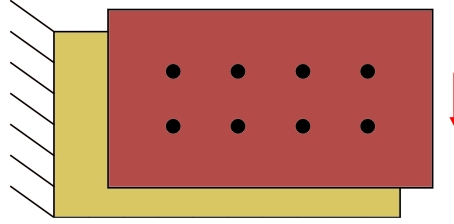
Figure 10: Shear loading of a joint

Another considered load case is biaxial loading. In this case, non-eccentric loads are applied to the A plates of the joint, while the central plate B is held fixed on two edges against displacement in any direction. A schematic representation of this load case is shown in Fig.11 with tensile loads applied in both directions. Three more forms of biaxial loading would also be possible, with compression in both directions or tension in one direction and compression in the other. The four cases of biaxial loading are all of interest and are grouped within LC4.
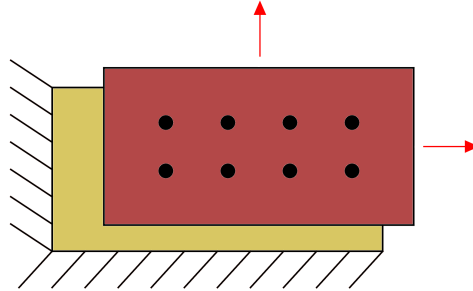
Figure 11: Biaxial loading of a joint

Lastly, thermal loading was also considered in this study. This load case (LC5) refers to the loads that can arise in some joints subject to a temperature difference between assembly and operational conditions. To discuss these thermal loads, let us consider a single-lap joint. For plate A, α is the global CTE along a certain direction, while β is the global CTE for plate B along the same direction. If the properties of the plates were different in terms of global CTE, the plates would expand differently in presence of a temperature difference between assembly and operational conditions. This could result in the appearance of shear loads at the fasteners due to the different displacement of the bolt at the top and bottom plates. Equivalent reasoning can be applied to explain the appearance of such thermal forces for a double-lap joint.

3.2   Literature review

Several practices are currently employed in the design of bolted connections. They can be grouped in three families: analytical approaches, experimental testing and FE modelling. While the last two can provide important insights by capturing fundamental effects as those generated by bolt-hole clearance and friction, they are often impractical for optimization, being expensive and time consuming.

While lacking accuracy under certain circumstances, analytical models are rapid and cost-effective. Regarding uniaxial loading, the earliest analytical study in the literature is by Tate and Rosenfeld [12], in which a linear spring model for the analysis of double-lap joints with isotropic materials was presented. The model was later modified to account for anisotropic materials by Nelson [13]. This kind of linear models has been extensively used both in academia and in industry. In these methods, the fastener load distribution is calculated by considering that both the fastener and the joint members deform when subject to a load. Many following studies [14][15] are based on the model by Tate and Rosenfeld but they all suggest different ways to account for the fastener stiffness. M.A. McCarthy [2] introduced a modification to the spring model that could take into account the presence of bolt-hole clearance. This model was further developed by C.T. McCarthy [3] to also consider the effects of bolt torque and friction between the laminates. All the aforementioned models assume material linearity and cannot take into account non-linear bearing deformation.

Other kinds of analytical models for uniaxial loading include boundary element formulations [16] and boundary collocation methods [17][18], which however gave rise to very limited following literature. This thesis study focused on spring-based approaches.

No model specifically dealing with in-plane shear loading of composite joints was identified in the literature. Models for conventional metal structures were therefore investigated. Two different methods of analysis are presented in the AISC Manual of Steel Construction [19]: the elastic method and the instantaneous center of rotation method. The former is based on a well-known work by Reilly [20] and assumes that a fastener group subject to an eccentric load rotates around the group centroid with the connected plates being infinitely rigid. The latter, originally formulated by Crawford and Kulak [21], considers that the eccentric load generates both a rotation around the group centroid and a translation of the fastener group. The model relies on an empirical relation to account for bolt deformation. Both models were retained and investigated.

While a few semi-analytical models [22] based on stress superposition exist to calculate load distribution, biaxial loading was found to be mostly investigated in the literature with empirical and numerical approaches. The study by Kapidžić [23] was retained as a reference for numerical modelling of joints subject to biaxial loading.

The Handbuch Struktur Berechnung (HSB) [24] and Esp [4] propose a modification to the classical spring-based model for uniaxial loading [12] to predict load distribution in case of thermal loading as described in Section 3.1. The model was retained and investigated as part of the thesis study. The investigation on single-bolt joint by Santiuste [25] was retained for the numerical modelling of composite joints under thermal loading.

In addition to the already mentioned works by Kapidžić and Santiuste, other relevant studies regarding the 3D FE modelling of bolted joints were also considered, being comparison of the analytical tool with numerical models part of the thesis study. The majority of the considered numerical investigations followed the meshing approach of Ireman [26]. Ireman himself based part of the modelling approach on earlier numerical studies on bolt-hole contact by Chen [27][28]. The meshing strategy by Ireman was retained and partially reproduced. The numerical and experimental results from [3] were retained for comparison of the numerical results under axial loading. In addition to these studies, Egan [29] provides a valuable description of the best practices for FE modelling and experimental testing of composite bolted joints as of 2018.

While the previously introduced analysis practices are the most commonly employed, it is worth mentioning here another category of analysis. In the 1970s and 1980s, efforts were made by the American aerospace and defense industry, funded by the United States Air Force, to develop analytical or semi-analytical techniques to allow the analysis of mechanically fastened composite structures. Under the Composite Joint Analysis Program, these methods resulted in the formulation of several computer codes. Snyder [30] presented the features of each code and tested their capabilities. Three codes can be used in the analysis of multiple bolted joints: JOINT [31], A4EJ [32] and SAMCJ [33][34]. The earliest of the three, JOINT, was developed by the Douglas Aircraft Company. Its reliance on empirical test data was found to severely limit its application. A few years later, A4EJ was also developed by the Douglas Aircraft Company as a tool capable of analyzing multi-row joints accounting for the non-linear behavior of the fasteners, as well as of the adherends. The code is based on continuum mechanics techniques. SAMCJ is a test data-independent code developed by the Northrop Corporation. The code has a finite element based formulation. The three codes can model both single-lap and double-lap joints subject to uniaxial tension, compression or in-plane loading, as well as thermal loading. It should be noted that both [4] and [30] suggest employing A4EJ for advanced and non-linear multi-fastener analyses. Despite these codes being now in the public domain [35], difficulties of availability make it impossible to directly use them for comparison. The results obtained with some of these codes have however been reported and were considered for comparison of later studies, as in Poon and Xiong [36].

4 Joint modelling in the tool

4.1 Retained models

Some of the models from the literature could be directly implemented in the tool to evaluate load distribution with one or more of the considered load cases. These models are presented in this section. Further discussion and analysis on these models is presented in Chapter 6.

The models that were modified in this study before being implemented in the tool are described in Section 4.2. Alongside these models, proposed approaches to extend the application of the retained models are presented. The thermal loading model is presented in Section 4.1.3 and not there since its formulation, but not the modelling approach, was modified. Similarly, the uniaxial loading model for single-column joints of Section 4.1.2 is presented among the retained methods since it was generalized for any number of bolts, and not just three, but its modelling approach remained the same. Also the results from the modified models were analyzed and a discussion is presented in Chapter 7.

4.1.1 A note on spring model formulations

All the spring-based methods considered in the thesis study are based on the same joint discretization, shown in Fig.12 for a single-lap-two-bolt joint and presented in more detail in Section 4.1.2. However, these methods can be divided in two groups depending on the problem formulation: those expressed in terms of member flexibility and those formulated through direct stiffness.
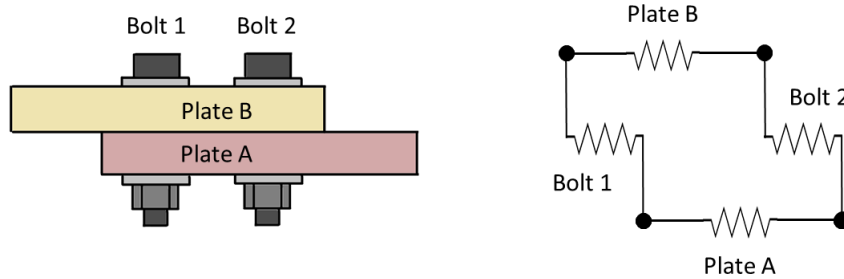
Figure 12: Example of single-lap joint discretization

In the case of the former group, the problem is expressed through a series of displacement compatibility equations. As shown by the red arrows in Fig.13(a), it is possible to express an equation for each pair of adjacent fasteners in terms of member deflection δ and flexibility C. A matrix problem can therefore be assembled under the form:

$$\underline{\underline{C}} \cdot \underline{R} = \underline{P} \qquad (2)$$

Where, for a joint composed of N fasteners, $\underline{\underline{C}}$ is an N×N compliance matrix, while $\underline{R}$ and $\underline{P}$ are the fasteners' reactions vector and loading vector respectively.

Alternatively, the problem can be expressed by solving equilibrium equations at each node, thus obtaining the nodal displacements $\underline{x}$. The matrix problem corresponding to the discretization of Fig.13(b) is expressed in the form:

$$\underline{\underline{K}} \cdot \underline{x} = \underline{L} \qquad (3)$$

Where $\underline{\underline{K}}$ is the stiffness matrix of the problem and $\underline{L}$ the loading vector. Unlike the flexibility matrix $\underline{\underline{C}}$, the size of the stiffness matrix $\underline{\underline{K}}$ is n×n, where n=2N+1. The fastener reaction can be retrieved as the product of its stiffness and the difference in displacement between the corresponding top and bottom node. It should be noted that the loading vector here is expressed differently than $\underline{P}$.
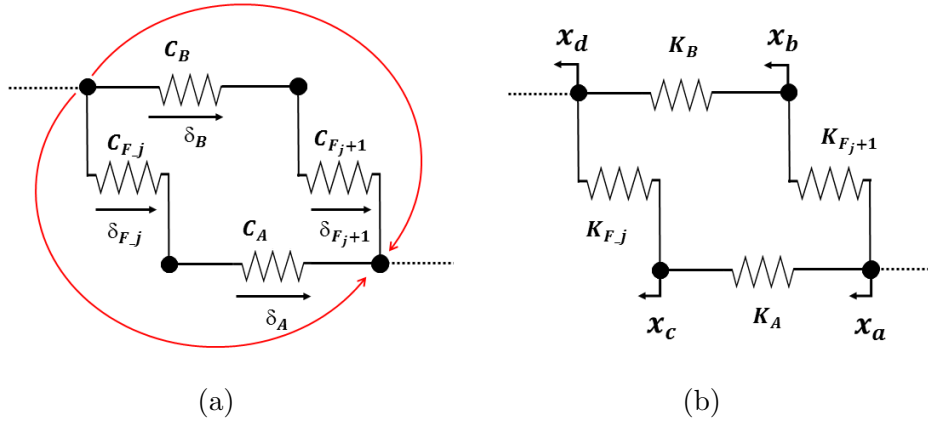
Figure 13: Flexibility formulation (a) and direct stiffness formulation (b)

To maintain coherence throughout the discussion, all the models in this thesis study were expressed in terms of direct member stiffness. Being the modelling approach equivalent, the two formulations yield identical results, with purely formal differences.

4.1.2 Uniaxial loading model for single-column joints

The model from M.A. McCarthy [2] was retained from the literature and generalized. This model allows to calculate the load distribution in a single-column joint where a non-zero bolt-hole clearance can be specified. It is both applicable to single-lap and

double-lap configurations, for tension (LC1) loading as well as compression loading (LC2). While the formulation proposed by the authors only considers a 3-row joint, the model was generalized for this thesis work to consider any number of fastener rows. It should be noted that the model is an extension of what was introduced by Tate and Rosenfeld [12], in which no bolt-hole clearance was considered. None of these studies takes into account the effects of bolt preload and friction. They can therefore be employed for predicting load distribution in finger-tight joint.

Fig.14 shows the discretization of a single-lap joint's bottom and top plates, A and B respectively, fastened by N bolts. A horizontal load P is applied to one end of plate B while the opposite end of plate A is held fixed. The joint was discretized by introducing two nodes at every fastener location, one node for each plate. An additional node is placed at the free end of plate B where the load P is applied.

The stiffness $K_{\mathrm{B\_i}}$ indicates the stiffness of plate B at a generic spacing i. The same applies to $K_{\mathrm{A\_i}}$ for plate A. The stiffness $K_{\mathrm{F\_j}}$ refers to the stiffness of a generic fastener j in case of a difference in the displacement of the corresponding top and bottom nodes.

It is considered that only a purely horizontal node displacement is possible, with the positive direction indicated in Fig.14 by the coordinate systems x_1 to x_{2N+1}. It follows that all the stiffnesses are defined considering such a horizontal displacement.
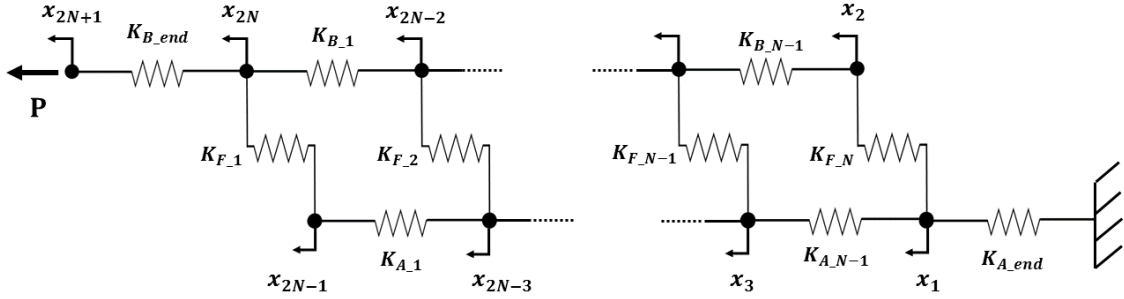
Figure 14: Definition of the quantities for the uniaxial loading model of single-lap-single-column joints

The springs are used to model either the stiffness of a portion of a plate or of a fastener in shear. The plate stiffness between adjacent fasteners at a location i is defined as:

$$K_{\mathrm{A\_i}} = \frac{E_{x_A} t_{A\_i} w}{p_i} \qquad \text{and} \qquad K_{\mathrm{B\_i}} = \frac{E_{x_B} t_{B\_i} w}{p_i} \quad , \quad 1 \le i \le N \qquad (4)$$

With t_{A_i} and t_{B_i} being the effective thickness of the plates over the fastener separation p_i and plate width w. These quantities were introduced in Figures 2 and 3. The

thickness of a plate is calculated as the average thickness between the two adjacent fasteners, as suggested in HSB 21031-01 [24]. The plates' longitudinal direction is aligned with the axis of loading of the joint, so that the relevant moduli of elasticity are E_{x_A} and E_{x_B}. Several models to account for fastener stiffness K_{F_i} exist and they are discussed in Section 4.1.4. Lastly, K_{A_end} and K_{B_end} are calculated with the corresponding distance $l_{\_end}$.

The stiffness values are therefore all known and they are used to express the forces acting on each node as a function of the nodal displacement. It is then possible to calculate the force balance at every node. Fig.15 shows free body diagrams of a generic node $k+1$, belonging to the top plate B, and the neighbouring node k, located on the bottom plate A.
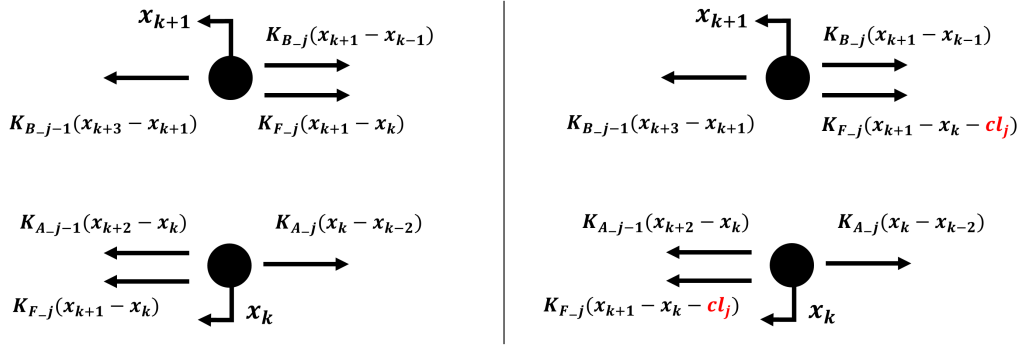
Figure 15: Force balance with classical model (left) and clearance model (right)

On the left-hand side of Fig.15, the nodal force balance with a classical spring-based model, such as considered by Tate and Rosenfeld [12], is shown. The balance modification proposed by M.A. McCarthy in [2] to account for bolt-hole clearance is shown on the right-hand side. The balance is expressed for a generic fastener j. Based on the geometrical definitions of Section 2.1, the plate stiffness on the right of the node can be expressed with the subscript j, while the stiffness on the left with $j-1$. The difference between the two methods lies in the fact that a delay in load take-up is introduced for a fastener with non-zero clearance, so that the reaction force is given by:

$$
F_j = \begin{cases} 0 & \text{for} & 0 \leq x_{k+1} - x_k \leq cl_j \\ K_{F\_j}(x_{k+1} - x_k - cl_j) & \text{for} & x_{k+1} - x_k > cl_j \end{cases} \tag{5}
$$

With the delay term cl_j as defined in Section 2.2. Since only a displacement in the X direction is possible in the model, F_j is purely directed along X. For loadings such that a fastener reaction can have more than one component, a distinction is made between the reaction along X and Y, defined as F_{X_j} and F_{Y_j} respectively.

Considering the free body diagrams for the clearance model, the following equilibrium equations can be written:

$$-K_{\text{B-j}} \cdot x_{k-1} - K_{\text{F-j}} \cdot x_k + (K_{\text{B-j}} + K_{\text{B-j-1}} + K_{\text{F-j}})x_{k+1} - K_{\text{B-j-1}} \cdot x_{k+3} = K_{\text{F-j}} \cdot cl_j \quad (6)$$

$$-K_{\text{A-j}} \cdot x_{k-2} - (K_{\text{A-j-1}} + K_{\text{A-j}} + K_{\text{F-j}})x_k - K_{\text{F-j}} \cdot x_{k+1} - K_{\text{A-j-1}} \cdot x_{k+2} = K_{\text{F-j}} \cdot cl_j \quad (7)$$

Such equations can be written for all nodes, with the nodal displacements as unknowns. Care needs to be taken when considering the equilibrium at nodes 2, 2N-1 and 2N+1, being the forces acting on the nodes slightly different with respect to the other locations.

To simplify the discussion, a stiffness matrix and load vectors corresponding to an N=3 joint are presented below. However, their generalized forms were derived and can be found in the appendix. The system of equations can be written in matrix form as $\underline{\underline{K}} \cdot \underline{x} = \underline{L}$, with the loading vector $\underline{L}$ composed by the terms of the equilibrium equations independent from $\underline{x}$:

$$\underline{\underline{K}} = \begin{bmatrix} K_{\text{A-end}} + K_{\text{A-2}} + K_{\text{F-3}} & -K_{\text{F-3}} & -K_{\text{A-2}} \\ -K_{\text{F-3}} & K_{\text{F-3}} + K_{\text{B-2}} & 0 \\ -K_{\text{A-2}} & 0 & K_{\text{A-2}} + K_{\text{A-1}} + K_{\text{F-2}} \\ 0 & -K_{\text{B-2}} & -K_{\text{F-2}} \\ 0 & 0 & -K_{\text{A-1}} \\ 0 & 0 & 0 \\ 0 & 0 & 0 \end{bmatrix}$$

$$\begin{bmatrix} 0 & 0 & 0 & 0 \\ -K_{\text{A-2}} & 0 & 0 & 0 \\ -K_{\text{F-2}} & -K_{\text{A-1}} & 0 & 0 \\ K_{\text{B-2}} + K_{\text{B-1}} + K_{\text{F-2}} & 0 & -K_{\text{B-1}} & 0 \\ 0 & K_{\text{A-1}} + K_{\text{F-1}} & -K_{\text{F-1}} & 0 \\ K_{\text{B-1}} & -K_{\text{F-1}} & K_{\text{B-1}} + K_{\text{B-end}} + K_{\text{F-1}} & -K_{\text{B-end}} \\ 0 & 0 & -K_{\text{B-end}} & K_{\text{B-end}} \end{bmatrix}$$

$$\underline{L} = \begin{bmatrix} -K_{\text{F-3}} \cdot cl_3 \\ K_{\text{F-3}} \cdot cl_3 \\ -K_{\text{F-2}} \cdot cl_2 \\ K_{\text{F-2}} \cdot cl_2 \\ -K_{\text{F-1}} \cdot cl_1 \\ K_{\text{F-1}} \cdot cl_1 \\ P \end{bmatrix} \qquad \underline{x} = \begin{bmatrix} x_1 \\ x_2 \\ x_3 \\ x_4 \\ x_5 \\ x_6 \\ x_7 \end{bmatrix}$$

The above system of equations can be solved to obtain the nodal displacements. The fastener reactions are then derived from Eq.5. It is to be noted that the problem is non-linear because of bolt-hole clearance, which introduces zones where no reactions are generated in the fasteners. When solving for a certain load value P, the applied load is incrementally stepped up from zero.

As stated above, the model is equally applicable to single-lap and double-lap joints. The former case was shown in the above discussion for simplification. The model can be easily modified to account for double-lap joints by considering a factor 2 when calculating the stiffness of plate A:

$$ K_{\text{A\_i}} = \frac{2E_{x_A} t_{A\_i} w}{p_i} \quad , \quad 1 \leq i \leq N \tag{8} $$

The same factor is to be considered when calculating $K_{\text{A\_end}}$. This approach is justified under the assumption that the thickness of the top and bottom A plates is equal.

Finally, the overall joint displacement was defined as the sum of the individual displacements of all the bolts composing the joint. The bolt displacement is equal to the difference in displacement between the top and bottom nodes, as already introduced in Eq.5 where the displacement is compared to the bolt clearance. The overall joint displacement can be used when showing in a graph the evolution of the bolt reactions for different applied loads.

4.1.3   Thermal loading model for single-strip joints

As presented in Section 3.1, modelling thermal loads generated by a temperature gradient ΔT in a joint with different expansion properties was considered as part of this study (LC5). An analytical model to calculate these thermal loads was presented in HSB 21031-01 [24] and by Esp [4] for a single-strip joint. However, these models are expressed in terms of member flexibility and not direct stiffness, see Section 4.1.1. No model formulation in terms of direct member stiffness was identified in the literature. Having the model for uniaxial loading been formulated in terms of stiffness, the thermal loading model was re-formulated as part of this study to maintain consistency and to facilitate a combination of the two models if desired.

The thermal loading model re-formulation was derived for a three-bolt-single-lap joint, shown in Fig.16, and then generalized to any number of fasteners.
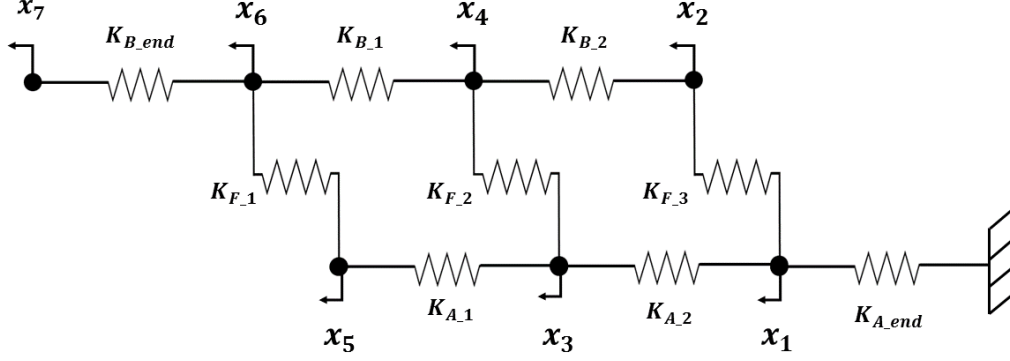
Figure 16: Definition of quantities for thermal loading model of single-strip joints

As a first step, equations representing the displacement of the first and last node due to thermal expansion are written as:

$$x_1 = \alpha \cdot l_{end} \cdot \Delta T \tag{9}$$

$$x_7 = x_6 + \beta \cdot l_{end} \cdot \Delta T \tag{10}$$

Where α and β are the global CTE values in the X direction for plate A and B respectively. It should be noted that the expansion properties of composite materials can be significantly different in different directions, see Table 8. The computation of the global properties for a laminate is described in the Appendix (Section 11.4). The letters α and β were used rather than $\mathrm{CTE_{X\_A}}$ and $\mathrm{CTE_{X\_B}}$ to simplify the notation.

A condition is also imposed on the reactions of the fasteners. Because of the internal nature of thermal forces, the sum of the bolt reactions is set equal to zero:

$$F_1 + F_2 + F_3 = 0 \tag{11}$$

In addition to Equations 9 to 11, four more equations representing nodal force balances complete the linear system of 7 equations to determine 7 unknown nodal displacements. This system can be expressed in terms of the stiffness matrix of the structure $\underline{\underline{K}}$ and of a thermal loading vector $\underline{L}_{ther}$. Because of the lengthy algebraic manipulation required to express the linear system in this form, a summary is presented in the Appendix (Section 11.3). With the described algebraic development, the linear system can be expressed similarly to the model in Section 4.1.2 as $\underline{\underline{K}} \cdot \underline{x} = \underline{L}_{ther}$, where the thermal loading vector is equal to:

25

$$\underline{\boldsymbol{L}}_{ther} = \begin{bmatrix} (K_{A\_end} \cdot l_{end} - K_{A\_2} \cdot p_2)\alpha \\ -K_{B\_2} \cdot \beta \cdot p_2 \\ (K_{A\_2} \cdot p_2 - K_{A\_1} \cdot p_1)\alpha \\ (K_{B\_2} \cdot p_2 - K_{B\_1} \cdot p_1)\beta \\ K_{A\_1} \cdot \alpha \cdot p_1 \\ (K_{B\_1} \cdot p_1 - K_{B\_end} \cdot l_{end})\beta \\ K_{B\_end} \cdot \beta \cdot l_{end} \end{bmatrix} \Delta T$$

A generalized formulation for any number of fasteners is provided in the Appendix (Section 11.3). The model is equally applicable to double-lap joints by considering the appropriate value for the stiffness of the A plates with Eq.8. This also applies to K_{A_end}.

4.1.4 Fastener flexibility

The stiffness of the fasteners needs to be computed to compose the stiffness matrix for the uniaxial loading model of Section 4.1.2 and the thermal loading model of Section 4.1.3. Several models exist to account for fastener flexibility, equivalent to the inverse of the fastener stiffness in shear. These flexibility models are expressed in terms of plate thickness t_A and t_B. It should be noted that these correspond to the plate thickness values at the fastener location, which may not be the same for different fasteners, if the plate thickness is not constant.

The fastener flexibility formulations presented in this section were all experimentally derived. A comparison of the retained formulations is presented in Section 6.2.

- **Tate and Rosenfeld** [12]:

Single-lap:

$$\frac{1}{K_{\mathrm{F}}} = \frac{1}{t_A E_{x_A}} + \frac{1}{t_B E_{x_B}} + \frac{1}{t_A E_F} + \frac{1}{t_B E_F}$$
$$+ \frac{8(t_B^3 + 5t_B^2 t_A + 5t_B\, t_A^2 + t_A^3)}{5E_F \pi D^4} + \frac{32(t_B + t_A)(1 + \nu_F)}{9E_F \pi D^2} \quad (12)$$

Double-lap:

$$\frac{1}{K_{\mathrm{F}}} = \frac{1}{t_A E_{x_A}} + \frac{1}{2t_B E_{x_B}} + \frac{1}{t_A E_F} + \frac{1}{2t_B E_F}$$
$$+ \frac{8t_B^3 + 16t_B^2 t_A + 8t_2 t_A^2 + t_A^3}{3E_F \pi D^4} + \frac{8(2t_B + t_A)(1 + \nu_F)}{3E_F \pi D^2} \quad (13)$$

26

Where E_F and ν_F represent the fastener's modulus of elasticity and Poisson ratio. In both Eq.12 and Eq.13 the first two terms model the contribution to the flexibility from the bearing deformation for plates A and B. The third and fourth terms consider the bearing deformation of the fastener, while the fifth and sixth terms its deformation in bending and shear respectively.

- **Nelson** [13]:

Single-lap:

$$\frac{1}{K_F} = \frac{2(t_B + t_A)}{3G_F A_F} + \left[\frac{2(t_B + t_A)}{t_B t_A E_F} + \frac{1}{t_A \sqrt{E_{x_A} E_{y_A}}} + \frac{1}{t_B \sqrt{E_{x_B} E_{y_B}}} \right] (1 + 3\beta_N) \quad (14)$$

Double-lap:

$$\frac{1}{K_F} = \frac{2t_B + t_A}{3G_F A_F} + \frac{8t_B^3 + 16t_B^2 t_A + 8t_B t_A^2 + t_A^3}{192 E_F I_F} + \frac{2t_B + t_A}{t_B t_A E_F}$$
$$+ \frac{1}{t_B \sqrt{E_{x_B} E_{y_B}}} + \frac{2}{t_A \sqrt{E_{x_A} E_{y_A}}} \quad (15)$$

Where G_F, A_F and I_F represent the fastener's shear modulus, cross section area and section modulus. The last two are calculated from the nominal diameter of the fastener. Having the model proposed by Nelson been derived from the work of Tate Rosenfeld, the equations take a similar form. The first term on the right hand side of Eq.15 takes into account the effects of bolt deformation in shear, while bolt bending is accounted for by the second term. The term β_N represents the bending moment fraction which is reacted by non-uniform contact stresses in the laminates. It can range from 0.5 for countersunk fasteners to 0.15 for protruding head bolts.

- **Huth** [14]:

$$\frac{1}{K_F} = \frac{b}{\psi} \left(\frac{t_A + t_B}{2D} \right)^a \left(\frac{1}{t_A E_A} + \frac{1}{\psi t_B E_B} + \frac{1}{2t_A E_F} + \frac{1}{2\psi t_B E_F} \right) \quad (16)$$

Where the value of ψ is equal to 1 for single-lap joints and 2 for double-lap joints. The other coefficients depend on the materials of the connected members and are presented in Table 9.

Table 9: Coefficients for Huth's fastener flexibility formulation

Joint type	a	b
Bolted metallic	2/3	3
Riveted metallic	2/5	2.2
Bolted graphite-epoxy	2/3	4.2

- **Boeing** (as reported in [14]):

Single-shear:

$$\frac{1}{K_{\mathrm{F}}} = \frac{2^{\left(\frac{t_A}{D}\right)^{0.85}}}{t_A}\left(\frac{1}{E_A} + \frac{3}{8E_F}\right) + \frac{2^{\left(\frac{t_B}{D}\right)^{0.85}}}{t_B}\left(\frac{1}{E_B} + \frac{3}{8E_F}\right) \tag{17}$$

Double-lap:

$$\frac{1}{K_{\mathrm{F}}} = \frac{1.25^{\left(\frac{t_A}{D}\right)}}{t_A}\left(\frac{1}{E_A} + \frac{3}{8E_F}\right) + \frac{1.25^{\left(\frac{t_B}{D}\right)}}{t_B}\left(\frac{1}{E_B} + \frac{3}{8E_F}\right) \tag{18}$$

- **Douglas** (as reported in [14] and [37]):

Single-lap:

$$\frac{1}{K_{\mathrm{F}}} = \frac{5}{E_F D} + 0.8\left(\frac{1}{E_A t_A} + \frac{1}{E_B t_B}\right) \tag{19}$$

Double-lap

$$\frac{1}{K_{\mathrm{F}}} = \frac{5}{E_F D} + 0.8\left(\frac{1}{E_A t_A} + \frac{1}{2E_B t_B}\right) \tag{20}$$

4.1.5 Elastic method for shear loading

The model from Reilly [20], sometimes referred to as elastic method, was retained to predict bolt reactions in a joint subject to shear loading (LC3). The model was retained in the version presented in [38] to account for differently sized fasteners.

With the elastic method, a joint eccentrically loaded by a force P is assumed to rotate around the fastener group centroid (CG), as shown in Fig.17(a) for a joint

with 6 bolts. Considering infinitely rigid plates fastened by N bolts, the location of CG is calculated as:

$$x_{CG} = \frac{\sum_{j=1}^{N} A_j \cdot x_j}{\sum_{j=1}^{N} A_j} \qquad \text{and} \qquad y_{CG} = \frac{\sum_{j=1}^{N} A_j \cdot y_j}{\sum_{j=1}^{N} A_j} \qquad (21)$$

(a)   (b)
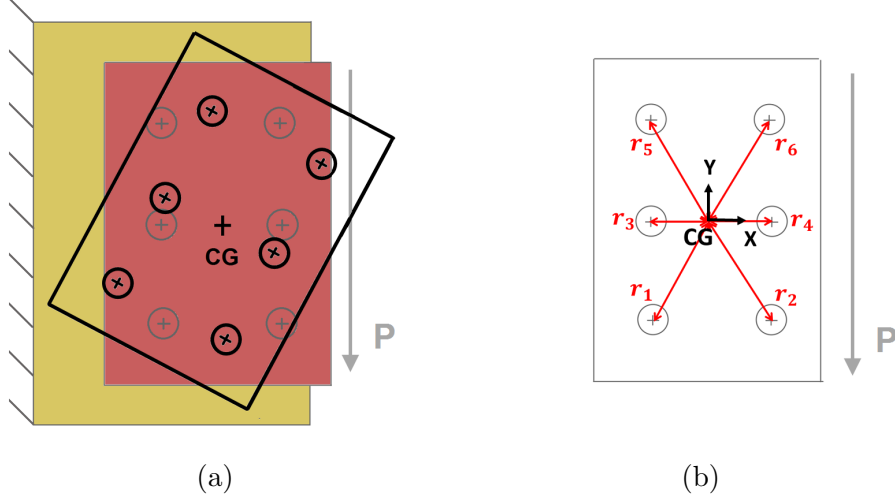
Figure 17: Joint deformation with elastic method (a) and definitions (b)

Where A_j is the section area of a generic fastener j, located at coordinates x_j and y_j at a distance r_j from CG, as shown in Fig.17(b).

A purely vertical load P applied at a point along the line at x_P from CG generates a counterclockwise moment around CG calculated as:

$$M_{CG} = -P \cdot x_P \qquad (22)$$

Once M_{CG} is known, the fastener reactions to the applied moment F_{M_j} can be calculated. It should be noted that the forces F_{M_j} are only the reactions generated by the moment around CG and are not in equilibrium with P along Y. These reactions are considered to act perpendicularly to r_j, so that:

$$F_{M\_j} = M_{CG} \frac{A_j \cdot r_j}{\sum_{j=1}^{N} A_j \cdot r_j^2} \qquad (23)$$

The horizontal and vertical components of the fastener reactions are then calculated considering the respective projections of F_{M_j} and the external load P:

$$F_{X\_j} = -P\frac{A_j}{\sum_{j=1}^{N} A_j} + \frac{(x_j - x_{CG})}{r_j}F_{M\_j} \,, \quad F_{Y\_j} = \frac{(y_{CG} - y_j)}{r_j}F_{M\_j} \qquad (24)$$

Knowing the horizontal and vertical components, the fastener reactions are easily obtained as:

$$F_j = \sqrt{F_{X\_j}^2 + F_{Y\_j}^2} \qquad (25)$$

4.1.6 Original instantaneous center of rotation method

While this model was not implemented in the tool, its description is necessary to understand the proposed modified model presented in Section 4.2.2.

Unlike with the elastic method, in the Instantaneous Center of Rotation (ICoR) method it is considered that an eccentric load P generates a rotation around CG as well as a translation of the joint. This is equivalent to a rotation around a certain Instantaneous Center (IC) shown in Fig.18(a).

(a) (b)
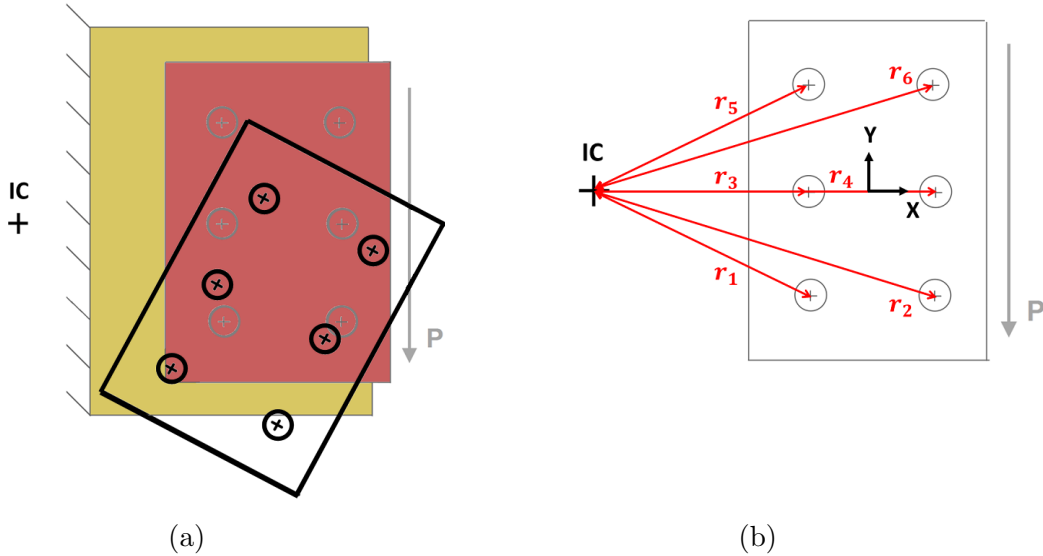
Figure 18: Joint deformation with ICoR method(a) and definitions (b)

The location of the IC depends on the bolt group geometry and load orientation. For a generic joint with N bolts, the original ICoR method assumes that joint failure is due to bolt failure in shear for the bolt furthest from the IC. The method is based on the work by Crawford and Kulak [21] in which, for a generic fastener j, an experimental relation between bolt deformation Δ_j and bolt force F_j was developed:

$$F_j = R_N(1 - e^{\tau \Delta_j})^\zeta \tag{26}$$

Where R_N is the bolt shear capacity, see Appendix (Section 11.5), while τ and ζ are regression coefficients. They are defined as $\zeta = 0.55$ and $\tau = 0.3937$ when Δ_j is expressed in millimeters. The relation was developed for ASTM A325 bolts and ASTM A36 steel plates but is applicable to various bolt sizes and steel grades [39]. The bolt deformation Δ_j is defined as the relative displacement between bolt head and nut, equivalent to δ_{F_j} or $\delta_{F_{j+1}}$ in Fig.13(a). The bolt force-deformation relation is shown in Fig.19, where the red dot indicates failure conditions, at Δ_j=8.636 mm, and the black dots the bolt deformations that will be considered in the investigations of Section 7.1.1.
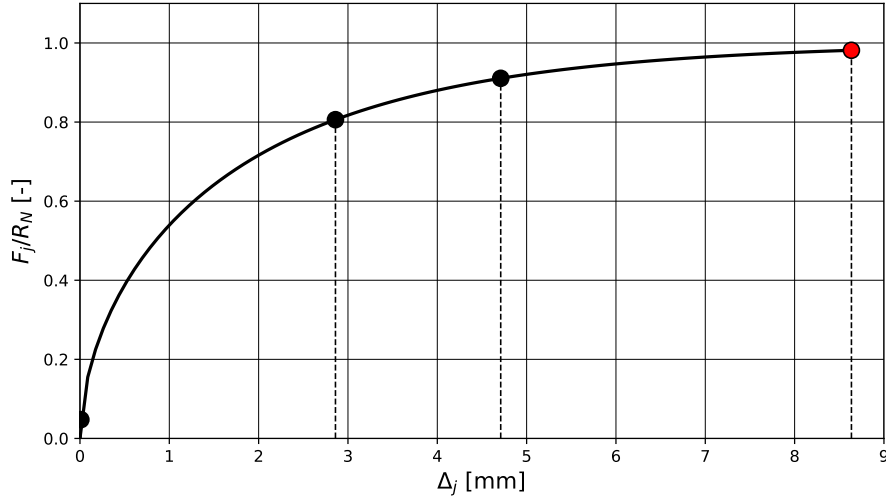
Figure 19: Load-deformation relation for ASTM A325 bolts

The method assumes that bolt failure arises at the bolt furthest from the IC, for which r=r_{far} and Δ_{far}=8.636 mm, while the bolt deformation for the other bolts is linearly proportional to the distance from the IC. The bolt forces, acting perpendicularly to the bolt-IC distance r_j, are calculated as:

$$\Delta_j = \frac{r_j}{r_{far}} \Delta_{far} = \frac{r_j}{r_{far}}(8.636) \tag{27}$$

To summarize, the method is based on four assumptions:

1. The fastener group rotates around the IC

2. Bolt failure takes place at the fastener furthest from the IC

31

3. Bolt forces act perpendicularly to the radius of rotation and are linearly proportional to the distance of the bolt from the IC

4. The connected parts remain rigid during the rotation

In other terms, it is assumed that, for a fixed geometry, at least one bolt deforms such that its Δ is equal Δ_{far} and the problem is solved to find a critical load P generating failure. Such a method can only be used to determine load distribution in a joint for bolt failure conditions.

In this formulation, Δ_{far} is known before starting the computation, while IC and P are to be found. The problem is solved iteratively by updating a guess for the IC position. At each guess, all r_{j} values are calculated with Eq.27 and the bolt forces with Eq.26. The force equilibrium equation in the Y direction is solved for the applied load P. With this value, the respect of the equilibrium of moments is verified for the IC guess. If the equilibrium of moments is respected within the defined tolerance, the IC guess is considered as correct, otherwise it is updated. Tolerance definition is presented in more detail in Section 4.2.2.

4.2 Modified methods and proposed approaches

Some models, while based on existing models in the literature, were modified as part of this thesis study and are presented in this section. Additionally, two approaches based on retained models are proposed to take into account biaxial loading and uniaxial loading of multi-column joints.

4.2.1 Bolt preload model for uniaxial loading

An extension to the uniaxial loading model to account for bolt preload was proposed by C.T. McCarthy in [3]. It was assumed that bolt preload variations among different fasteners were sufficiently small to consider equal preload conditions for all bolts.

In this model, a delay due to friction is introduced in the $\underline{\underline{K}} \cdot \underline{x} = \underline{L}$ system from Section 4.1.2, thus reproducing the load-deflection behavior already introduced in Section 1.2.

Since no bolt displacement can take place before the end of the quasi-linear region I, the bolts are not loaded in shear and the applied load is only transferred through friction between the plates. Being the plates and not the bolts subject to loading, the bolt stiffness K_{F} is replaced by a measure of the shear stiffness of the plates proposed by C.T. McCarthy. In this way, the $\underline{\underline{K}} \cdot \underline{x} = \underline{L}$ problem is solved with a modified $\underline{\underline{K}}$ matrix until slipping takes place. The sticking-to-slipping transition is enforced through Coulomb friction law:

$$F_{crit} = \mu F_N \tag{28}$$

Where F_N represents the bolt axial force due to preload and μ is the friction coefficient between the laminates.

When the reaction at a fastener F_j exceeds the critical friction force, slipping takes place. At that point, the shear stiffness of the plates is replaced by the bolt stiffness and the problem is solved as already described in Section 4.1.2.

To model the shear stiffness of the plates, C.T. McCarthy proposed a method based on the out-of-plane properties of the laminates. These properties cannot be calculated by assuming a purely 2D laminate behavior with CLT as described in Section 2.4.3. Being a simple laminate property derivation from CLT a requirement for the tool, a modification to this model was proposed in this thesis study to comply with these requirements.

With the proposed model modification, it is assumed that slipping takes place for all bolts when the applied load load P exceeds the slip resistance of the joint [40]:

$$R_s = \mu F_N \cdot N \cdot n_l \tag{29}$$

Where N is the total number of fasteners and n_l represents the number of slip surfaces, equal to 1 for single-lap joints and 2 for double-lap joints. With this model, the only reaction present in the joint before slipping is due to friction. After slipping is triggered, the load transferred by the joint in friction remains constant and the bolts start reacting part of the applied load at the same time. The bolt reactions are then calculated by solving the $\underline{\underline{K}} \cdot \underline{x} = \underline{L}$ problem, already described in Section 4.1.2 for a three-bolt joint. A modification to the last term of the loading vector is necessary to model the fact that only the part corresponding to the difference between the applied load and the slip resistance generates a load reacted by the bolts:

$$\underline{L} = \begin{bmatrix} -K_{F\_3} \cdot cl_3 \\ K_{F\_3} \cdot cl_3 \\ -K_{F\_2} \cdot cl_2 \\ K_{F\_2} \cdot cl_2 \\ -K_{F\_1} \cdot cl_1 \\ K_{F\_1} \cdot cl_1 \\ P - R_s \end{bmatrix}$$

The impact of such a modification is believed to be small since it does not affect the prediction of the total load transferred by the joint through friction. In fact, while with the formulation by C.T. McCarthy not all bolts reach F_{crit} simultaneously,

the sum of the friction forces when slipping has taken place at all bolts is equal to the slip resistance of Eq.29. To evaluate the validity of the modified model, it was implemented for the comparison of the tool results with the FEM in Section 6.2.

Any model to capture the effects of bolt preload is inevitably based on the knowledge of frictional interactions between the plates. Accurately estimating the friction coefficient is an important step in ensuring accurate results. A coefficient of 0.42 was employed in [3] for laminates with HTA/6376 45° plies in contact. The same value was used in the analyses of this thesis study, even though it might not be accurate in some cases. However, from this point of view, the FE models and the analytical model of the tool are equally affected by the uncertainty. While the considered friction coefficient might not be accurate, employing the same value for both models is sufficient to guarantee a fair comparison, which was the goal of the study.

4.2.2 Modified instantaneous center of rotation method

The original ICoR method was modified in this thesis study to allow load distribution calculation under LC3 for conditions other than bolt failure. Assumption 2 in Section 4.1.6 is no longer considered but it is still assumed that this bolt, indicated by the subscript *high*, has the highest Δ in the bolt group. Therefore, Eq.27 is re-derived as:

$$\Delta_j = \frac{r_j}{r_{high}}\Delta_{high} \tag{30}$$

With this formulation, Δ_{high} can have any value from 0 mm to failure conditions. Unlike with the original ICoR method, P is known and is an input for the calculation of the loads generated at all bolts. In order to simplify the solution to the problem, it is assumed that a load P with no X component is applied to the joint. When such a purely vertical load is considered, it is known a priori that the IC lies on the line passing through CG and perpendicular to P [19]. As a consequence, only the X component of the IC needs to be determined, while the Y position is known. An eventual X component of P could be taken into account with the model for uniaxial loading of Section 4.1.2. The study of the validity of a superposition of these effects is left for future studies.

The iterative approach for the modified formulation is more complex than with the original ICoR method. In fact, while Δ_{far} is known with the latter, Δ_{high} is unknown in the modified formulation. Therefore, both a guess for x_{IC} and Δ_{high} are made in this case, with r_j and F_j calculated with Eq.30 and Eq.26. As already mentioned, F_j is directed perpendicularly to the axis of rotation. The component along Y of this force is defined as F_{Y_j}. From the forces computed with the double guess, it is possible to define the following term:

$$F_{Y\_high}^{new} = P - \sum_{j \neq high} F_{Y\_j} \qquad (31)$$

Corresponding to the Y component of the force bolt *high* would need to have to respect the equilibrium of forces along Y. The total force at bolt *high*, F_{high}^{new}, can be calculated through simple trigonometry. By inverting the bolt deformation Eq.26, the bolt deformation corresponding to the calculated force can be expressed as:

$$\Delta_{high}^{new} = \frac{1}{\tau} ln\Big(1 - \Big(\frac{F_{high}^{new}}{R_N} \Big)^{\frac{1}{\zeta}} \Big) \qquad (32)$$

Lastly, the IC point that would generate equilibrium at these conditions is calculated:

$$x_{IC}^{new} = x_P - \frac{1}{P} \Big(F_{high}^{new} \cdot r_{high} + \sum_{j \neq high} (F_{Y\_j} \cdot r_j) \Big) \qquad (33)$$

Eq.32 and Eq.33 would give the same results of the guessed values Δ_{high} and x_{IC} if the guesses were perfectly exact. A solution for the modified ICoR method is therefore found by minimizing an error term based on the difference between the guessed and the "new" values:

$$err_\Delta = 2 \cdot \frac{\Delta_{high} - \Delta_{high}^{new}}{\Delta_{high} + \Delta_{high}^{new}} \qquad (34)$$

$$err_x = 2 \cdot \frac{x_{IC} - xIC^{new}}{x_{IC} + x_{IC}^{new}} \qquad (35)$$

The minimization is calculated through the SciPy optimize function in Python using Sequential Least SQuares Programming (SLSQP). SLSQP is an iterative method for constrained nonlinear optimization of a function of one or more variables. Within the main optimization process, the method solves a sequence of smaller optimization problems, with each of them optimizing a quadratic model of the objective based on a linearization of the constraints. In the calculation, Δ_{high} is limited between 0 mm and 8.636 mm, while x_{IC} can only assume negative values with the defined X axis orientation. The solutions from the optimization function are accepted if the fastener reactions respect both the equilibrium along Y and the equilibrium of rotations around IC within a certain tolerance defined as in Eq.36 and Eq.37.

$$Y_{check} = \frac{\sum_{j=1}^{N} F_j - P}{P} \qquad (36)$$

$$M_{check} = \frac{\sum_{j=1}^{N} F_j r_j - P(x_P - x_{IC})}{P(x_P - x_{IC})} \tag{37}$$

Both Y_{check} and M_{check} can be set to the desired value, equal to 10% in the case of this thesis study.

As will be further discussed in Sections 7.1.1 and 7.1.2, the modified ICoR method, not assuming bolt failure in the joint, can be used to estimate load distribution. In this sense, the applicability of the method is broader than with the original ICoR method, allowing studies that would not have been possible with the original method.

4.2.3   Limitations of the current method minimization

The current iterative approach to find load distribution with the modified ICoR model allowed to calculate the results analyzed in Sections 7.1.1 and 7.1.2. These results were obtained after brief computations, not exceeding 30 seconds. However, it should be noted that the programmed iterative approach with the SciPy minimization function has not been optimized. For some joint geometries and loading, no solution can be found. This is a limit of the optimization problem definition and not a physical phenomenon. The existence of a unique solution, or at least of a group of solutions satisfying the required tolerance, is always ensured, as long as no bolt force exceeds the maximum reaction possible from Eq.26. In that case no load distribution could be calculated as the joint would already be at failure conditions. Improving the minimization problem definition would ensure to always obtain a solution when existing, with the implication that the applied load exceeds the minimum value to generate bolt failure when no solution is found.

To guarantee a fast computation of the reactions with the tool for shear loading, the elastic method was implemented. The modified ICoR method was programmed in a separate Python script.

4.2.4   Uniaxial loading model for multi-column joints

The uniaxial loading model for single-column joints of Section 4.1.2 was defined to predict load distribution in single-column-multi-row joints subject to LC1 or LC2. With the goal of extending the applicability of the tool, an approach is proposed to also consider multi-column joints.

A uniaxial tensile load is applied to the top and bottom plates of a double-lap joint, while the central plate is held fixed. The former plates are colored in red and the latter in yellow in Fig.20.
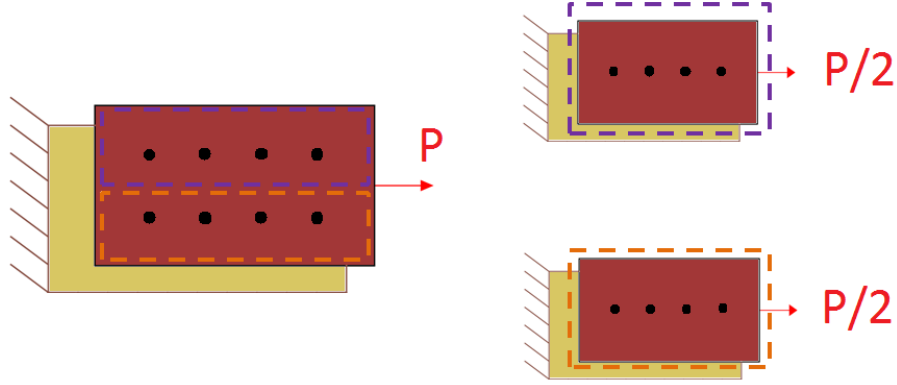
Figure 20: Single-column approach for a multi-column joint

While a double-lap joint is shown in the picture, the discussion of this section equally applies to single-lap configurations. It is considered that the bolt pattern is such that a division of the joint in different columns of equal width is possible. Each column has a width equal to w/n_{col}, where n_{col} indicates the number of columns in the joint. For this division to be applicable, the distance between fasteners in a same row needs to be the same for all rows. However, the spacing between rows does not need to be constant. The application of the tool is nonetheless restricted to cases where the spacing between rows, although not necessarily constant, is the same in all columns between the same two rows. Fig.21 shows an example of different spacing between rows which is however equal for all column between the same two rows.
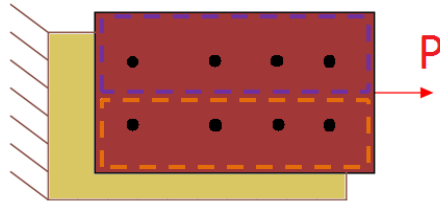
Figure 21: Example of admissible bolt spacings with the single-column approach

The approach shown in Fig.20 is to consider each column as independent, with an applied load of P/2 in the considered case. More generally, each column of a joint made of n_{col} columns would be subject to P/n_{col}. Each column is then analyzed through the models presented in Section 4.1.2 and 4.2.1. This was defined as the "Single-column approach".

The justification of the proposed approach on the basis of numerical investigations is presented in Section 7.2. Based on the findings of these studies, the uniaxial loading model for multi-column joints can be employed in the tool to also consider cases of non-zero bolt-hole clearance and non-zero preload.

4.2.5 Biaxial loading model of a joint

An approach to calculate the reactions in a joint subject to biaxial loading LC4 is also proposed. Two loads P_X and P_Y are considered to act on a joint as shown in Fig.22. The two loads are directed perpendicularly to the surface on which they are applied. The suggested approach, defined as "Superposition approach" is to consider a combination of the effects in the two spacial directions, first calculated independently.

As mentioned when presenting the models for uniaxial loading, the terms "row" and "column" are used to indicate a part of the geometry of a joint but also implicitly refer to the uniaxial nature of loading. For this reason, it was possible to refer to a "single-column approach" to calculate load distribution in a multi-column joint in the presence of a uniaxial applied load. In this section, biaxial loading of a joint is discussed. The terms "row" and "column" are therefore dropped to avoid confusion.
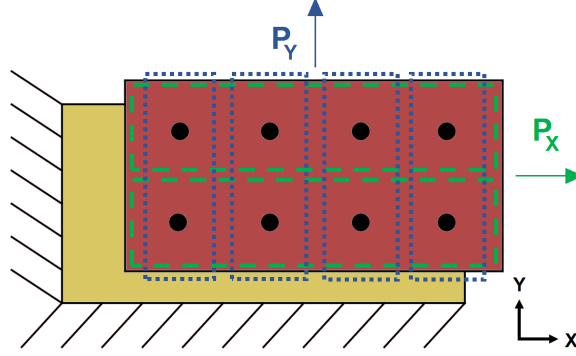
Figure 22: Superposition approach for a generic joint

A joint with constant bolt spacings in both directions, as in Fig.22, is considered. The fact that the distance between fasteners remains constant allows to consider that all the green strips in the X direction have equal width, as well as all the blue strips along Y have the same width. In the context of biaxial loading, "width" refers to the dimension of a strip in the direction perpendicular to the line of the fasteners in the strip. While the spacings are constant, they do not need to be equal along X and Y, so that the width of the green strips can be different from the width of the blue strips. The number of fasteners in the joint along the X direction is indicated by n_X, while n_Y is the number of fasteners along Y.

The effects of the load along the X direction are calculated at first. The load P_Y is ignored and the reactions $F_{X\text{-}j}$ solely due to P_X are calculated with the model for uniaxial loading of a joint presented in Section 4.2.4. To do so, the joint is divided in strips as shown in green in Fig.22 and by taking $n_{col} = n_Y$.

The reactions $F_{Y\text{-}j}$ along Y are calculated in a similar way by ignoring P_X and

employing the model for uniaxial loading from Section 4.2.4 with $n_{col} = n_X$. In this case, the division in strips is made as shown in blue in Fig.22.

In the two previous steps, the reactions along X and along Y due to P_X and P_Y were calculated separately for each fastener. The total fastener reactions due to the biaxial loads are calculated with the superposition approach by the combination:

$$F_j = \sqrt{F_{X\text{-}j}^2 + F_{Y\text{-}j}^2}$$

Which has been previously introduced as Eq.25 for a generic fastener j. Fastener numbering for multi-strip joints is provided when necessary. The biaxial loading model based on the superposition approach was implemented in the tool. The limits of its applicability and its accuracy are discussed in Section 7.3. No bolt-preload and no clearance can be specified in the analysis of biaxial loading with the tool.

5 Joint FE modelling

5.1 Definitions for FE modelling

All the FE models created in this thesis study were made of the same mechanical components: plates, washers, bolts and nuts. The term "component" will be used to refer to these mechanical entities. The number of these components or their dimensions in a joint vary depending on the considered case but they were always modelled with three parts created in Abaqus FEA. The term "part" refers to the virtual geometry modelling a fraction or an entire component. Part names will be indicated in italic to distinguish them from the components, which are written in normal characters. The three parts employed in the FE models are:

- *Plate*: This part corresponds to a single layer of elements to model a complete plate. More than one part is necessary to model an entire component, such as plate A or B as presented in Section 2.1. The number of parts depends on the plate thickness. *Plate* has a thickness of 1.04 mm, corresponding to 8 plies of nominal thickness 0.13 mm considered in this thesis study. The part is shown in Fig.23(a).

- *Bolt and nut*: As the name suggests, this part models at the same time a single bolt with the nut. This part is shown in Fig.26(a).

- *Washer*: Washers are modelled separately from the bolts and nuts. This part is shown in Fig.25b(a)

5.2 FE modelling of the components

This section presents how the components of the joints were modelled using the parts introduced in Section 5.1. Part partitioning for meshing and the considered edge seeding for the mesh sensitivity analysis are also discussed. Figures 27 and 28 show examples of two complete FE models for a single-lap and a double-lap joint.

5.2.1 Modelling of the plate components

A complete plate is modelled as a stack of *Plate* parts, see Fig.23. In a single *Plate* part, 8 plies are modelled in an 8-node quadrilateral continuum shell element SC8R. Three-dimensional solid elements C3D8 were also considered. The rationale for the element choice is presented in more detail in Section 5.7. As mentioned, more than 1 ply was modelled in a single SC8R element. While single-ply modelling was employed for similar loading conditions of single-lap joints, for example in [41], these studies focused on material damage and required finer mesh than for the investigation of load distribution. With the goal of obtaining a FE model with a reasonably low

computational time, and following the same approach of other studies in the relevant literature [2][3], single-ply modelling was discarded to model 8 plies in each element. Considering these relevant studies, the same ratio between the number of plies in an element and the element thickness was maintained.
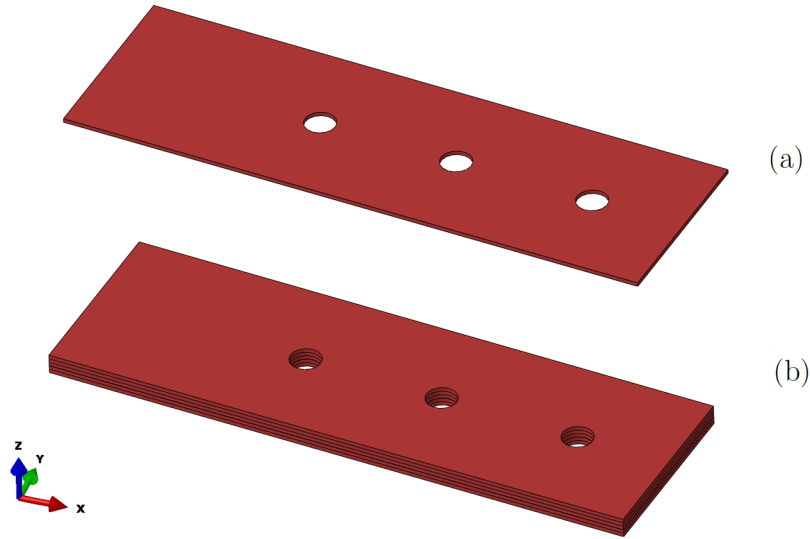
Figure 23: Plate modelling: (a) *Plate* part, (b) Stack of *Plate* parts

The part geometry of Fig.23 was partitioned as shown in Fig.24(a) to obtain the desired mesh. In the same picture, three edges were highlighted with different colors to indicate that the edge seeding along these edges was modified in the sensitivity analysis of Section 5.6. Table 12 presents the meshes that were employed and the corresponding seeding along the key edges. Fig.24(b) shows an example of a mesh for a plate in single-lap configuration. For all meshes, the region of finer mesh around the bolt was defined within a circle of diameter 18 mm, i.e. 2.25 times the nominal bolt diameter. This dimension was kept equal for all cases of the mesh sensitivity study.
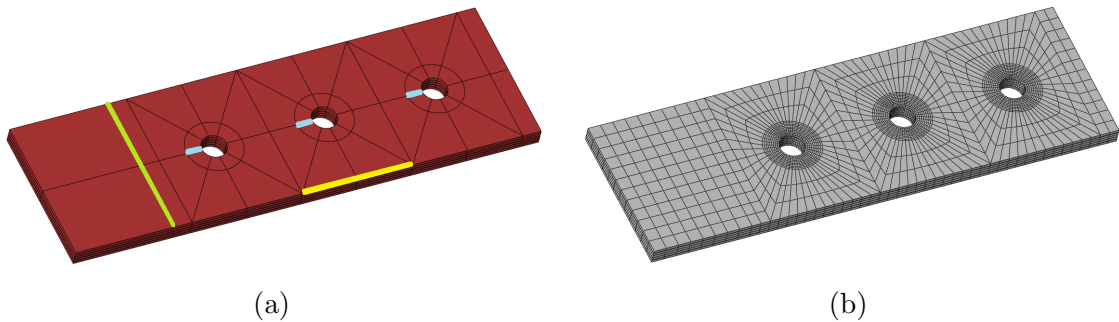
Figure 24: Plate mesh: Geometry partitions (a), Resulting mesh (b)

A similar mesh was employed in most of the studies found in the literature on numerical modelling of composite bolted joints, the first example being Ireman [26]. The number of divisions for edge seeding necessary for the mesh to capture the investigated phenomena was determined through the sensitivity study, which can be found in Section 5.6, as already mentioned.

5.2.2   Modelling of the washer components

Standard washers, as per ISO 7092 for M8 bolts, were modelled with a part called *Washer* having the following dimensions:

- Outer diameter: 15 mm

- Inner diameter: 8.4 mm

- Thickness: 1.6 mm

(a)   (b)
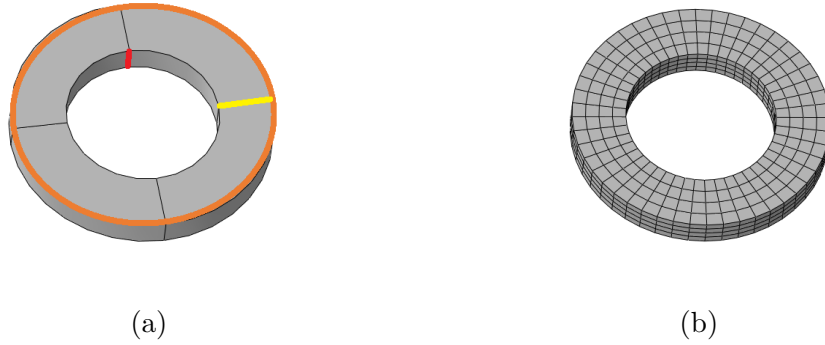
Figure 25: *Washer* mesh: (a) Geometry partitions, (b) Resulting mesh

Fig.25b shows the geometry partitions and the edges along which the mesh was modified, according to the divisions of Table 14, in the sensitivity analysis.

5.2.3   Modelling of the bolt and nut components

The bolts and the nuts were modelled as a single part called *Bolt and nut* and with a simplified geometry that considers the bolt head and the nut as cylinders of equal diameter and height. Only metric bolts with an 8 mm nominal diameter were numerically modelled in the thesis study. The portion of bolt extending beyond the nut was not modelled since it has no influence on the shear stiffness of the bolt or on its bending behavior.
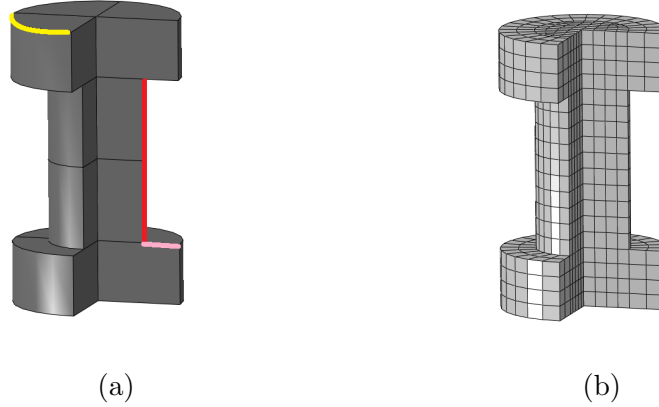
Figure 26: *Bolt and nut* mesh: (a) Geometry partitions, (b) Resulting mesh

Bolt and nut has the following dimensions:

- Bolt head diameter: 14 mm
- Bolt head height: 5 mm
- Bolt shank diameter: 8 mm

The bolt length is always set as equal to the sum of the thickness of the plates composing the joint. The seeded edges for this part are shown in Table 16.

5.2.4 Clearance modelling

As presented in Section 2.2, the bolts are assumed to be centered in the bolt hole in the thesis study. Different values of clearance were presented and considered. To account for the clearance λ_j at a certain bolt, the hole diameter in the plate is modelled as larger by λ_j than the nominal diameter of the bolt. The bolt is modelled with its nominal diameter independently of clearance.

5.3 Contact interactions

The FE models being composed of several parts, contact interactions needed to be defined. They apply equally to all the numerical models created in the thesis study and can be grouped on the basis of the contact surfaces:

- *Plate* parts: As described in Section 5.2.1, a complete plate is modelled as a stack of *Plate* parts. At the surfaces where the parts meet, tie constraints were imposed.

- <u>Washer - Bolt</u>: For every washer, one face is in contact with a plate, while the other face is in contact with a bolt head or a nut. At the latter surface, tie constraints were imposed to ensure equal displacements of the two parts. No condition was imposed at the internal surface of the washer which is not in direct contact with the bolt. No contact would be possible through deformation for the considered loadings and no interaction was defined.

- <u>Washer - Plate</u>: At the washer face in contact with the plate, hard contact was imposed in the normal direction. Displacement was allowed in the tangential direction with penalty friction formulation and a friction coefficient of 0.3, the washer surface having been defined as slave. This value was reported in [8] for steel washers in contact with composites. It was assumed that the orientation of the ply in contact with the washer has a negligible effect on the friction coefficient and the same value was taken for all simulations.

- <u>Bolt - Hole</u>: When a load is transferred from one plate to another through a bolt, contact takes place between the bolt itself and the hole surface in the plate. Throughout the length of the bolt, at the contact surface, a hard contact was defined for the normal behavior. Tangential sliding was allowed with friction coefficient 0.1 also taken from [8] for bolt-composite contact and accounting for the reaming of the hole surfaces. Also due to the effects of reaming, the same coefficient was also used when modelling metal plates. Friction was modelled with penalty friction formulation with the bolt surface selected as slave.

- <u>Plate - Plate</u>: The contact interaction between plates was modelled through the penalty method and hard contact in the normal direction. Considerations regarding the friction coefficient for this interaction have already been presented in Section 4.2.1.

For all these cases, surface-to-surface contact is employed as discretization method. A finite sliding formulation was used in the modelling of the three sliding interactions, thus avoiding the limitations of a small-sliding assumption.

As already mentioned, the tangential behavior of the sliding interactions was modelled with the penalty friction method [42]. This method models contact between two surfaces by allowing penetration of one into the other. From penetration, contact pressure is calculated through a specified penalty stiffness. The default stiffness value was not modified in the study and the method allowed for a reasonably rapid convergence of the solutions.

5.4 Boundary conditions

The boundary conditions for the FE models with the different forms of loading are presented in this section. No symmetry was imposed on the model alongside

the boundary conditions. It should be noted that the double-lap model could have been modelled with only half the elements by imposing a symmetry with respect to the central plane of the joint. This would be possible since the protruding-head bolts were also considered as symmetric with respect to this plane. Originally, also countersunk fasteners, which do not show this symmetry, were to be investigated. With the goal of developing a numerical model that could be easily adapted to different bolt geometries, a model with no symmetry was created. Countersunk fasteners in the end were not considered but the numerical model was not modified to include symmetry, given the already reasonably short computational time.

5.4.1   Bolt preload implementation

For all numerical simulations, some level of bolt preload was considered. The possible values were introduced in Section 2.3.

Bolt preload was defined as a "Bolt load" in Abaqus FEA by applying an axial force at the central cross section along the bolt length. Also the alternative approach to define preload employed by McCarthy [2] was considered. With this approach, orthotropic thermal expansion properties are defined for the washers so that only a deformation in the direction of the bolt axis is possible. Applying a certain temperature increase generates an expansion of the washer, which induces an axial force in the bolt, thus generating clamping of the plates. No significant difference was observed between the two preload implementations, at least for finger-tight torque conditions. Since the "Bolt load" command allowed for a more straightforward definition, it was used in the numerical models.

Bolt preload was always defined at the first step of the solution, with all the other loads being applied at later steps.

5.4.2   Uniaxial load application (LC1-LC2)

Uniaxial loads were imposed in the numerical model by specifying a displacement of the end surface of a plate. Displacement-controlled modelling was also employed in the studies retained from the literature for comparison, see Section 5.7. Figures 27 and 28 show the boundary conditions for a single-lap and double-lap joint respectively. On the surfaces defined as "Pinned End" no displacement was possible in any direction, while rotations were allowed. On the opposite side of the joint, on the surface defined as "Loaded End", a displacement along X was imposed.

By defining a displacement of one end of the joint, a load was applied indirectly on the corresponding surface. A zero displacement was imposed in the other two directions but rotations were not constrained. A positive X displacement was specified for tensile loadings, while a negative displacement was imposed to generate joint

45

compression. The load was applied in the second step of the solution, after bolt preload.
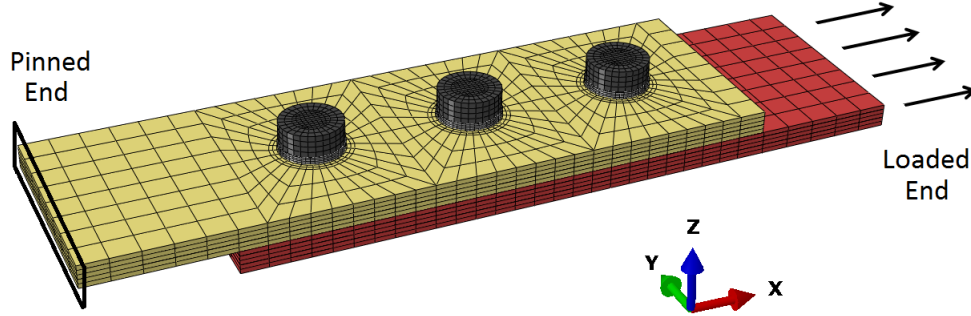
Figure 27: Boundary conditions for tensile load application with a single-lap joint
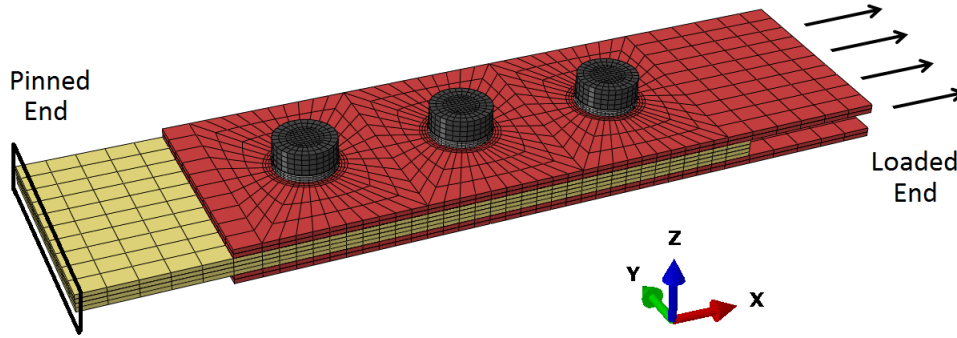
Figure 28: Boundary conditions for tensile load application with a double-lap joint

The same approach was used for all considered cases of uniaxial loading, independently of the joint geometry or number of columns.

5.4.3 Shear load application (LC3)

Similarly to uniaxial loading, displacement was restricted in the three spacial directions on one end of the central plate. The shear load is implemented with a "Concentrated force" command in Abaqus, with the force being applied on the end surface of the A plates. The shear load was applied in the second step of the solution, after bolt preload. Shear loading was studied for a double-lap joint geometry as shown in Fig.45 in Section 7.1, where further details about boundary conditions are provided.

5.4.4 Biaxial load application (LC4)

Since boundary condition formulation was observed to play a vital role in the study of biaxial loading, a detailed discussion on the topic is presented in Section 7.3.1, while here only a brief summary is given. An example of a joint subject to biaxial loading is shown in Fig.52.

Similarly to uniaxial loading, biaxial loading was modelled by imposing joint displacement while constraining two edges of the plates. The loads were applied at two successive steps of the solution. Therefore, bolt preload was modelled in the first step, the load along X was applied in the second and in the third and last step a load was generated by imposing a displacement along Y. The FE models are linear both in terms of material deformation and of geometry, being only a zero clearance considered with biaxial loading. The load application order is considered to have no influence in this case and the loads were applied separately to verify the load distribution after the application of the first uniaxial load. The load application order should be carefully considered in cases of non-zero clearance in which it could significantly influence load distribution.

5.4.5 Thermal load application (LC5)

Joints subject to thermal loads were modelled by imposing a zero displacement in all directions on the "Pinned End" surface. Temperature differences were imposed on the parts composing a joint when defining a temperature step with the "Predefined field" command. Fig.29 shows an example of a numerical model of joint subject to thermal loading, with the parts subject to the temperature step indicated in orange.
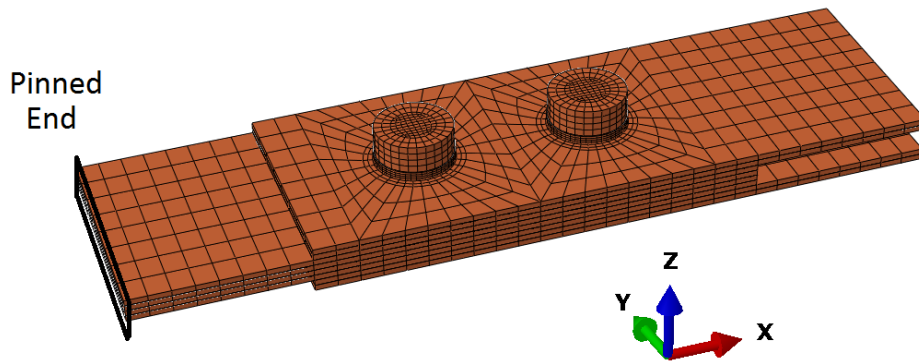
Figure 29: Boundary conditions for thermal load application with a double-lap joint

Bolt preload was applied in the first step of the analysis and the temperature step in the second, while the cooling between curing and assembly conditions was not included in the model, following the approach by Santiuste [25]. Ignoring cooling is equivalent to assume a stress-free state of the laminates at joint assembly conditions, which may be inaccurate in some cases. These effects should be taken into account if a precise estimation of bolt reactions were to be calculated with the FE models. It should be noted that such effects could not be captured with the analytical model for thermal loading. In this study, cooling was ignored to verify if, at least for favorable comparison conditions, reasonable agreement could be found between numerical and analytical models.

5.5   Extraction of the forces

The first step of the post-processing phase was the extraction of the monitored forces from the FE model. The forces were extracted through "Free Body Cuts", which display the resultant forces transmitted across a selected surface of the FE model. Resultant forces are calculated as the integral of the internal forces in an element over a selected section.

The total applied load is known in case of LC3, since it is directly applied as a concentrated force. However, with displacement-controlled modelling, as with LC1, LC2 and LC4, the applied load was not known before the numerical calculation. In these cases, the applied load value was extracted from the FE model with a free body cut by selecting the surface on which the displacement had been imposed.

The internal face of a plate hole was selected as integration surface to calculate the shear force acting on each bolt. Fig.30 shows how the surface was selected at the central plate B for a double-lap joint. Due to the equilibrium of the forces applied on the bolt by the plates, selecting the two hole surfaces of the A plates would lead to the same force value. For the same reason, in the case of single-lap joints, the hole surface of plate A or of plate B can be indifferently selected.

(a)   (b)
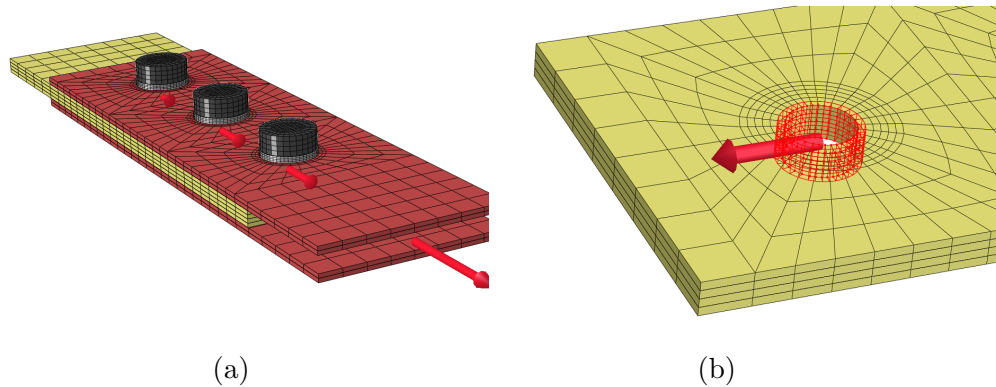
Figure 30: Extracted forces (a) and surface selection for bolt reactions (b)

Since some level of bolt preload was modelled as already discussed, the joint models reacted to external loads also through friction and not only with bolt reactions. The friction force was calculated as the difference between the total applied load and the sum of the bolt reactions, therefore assuming the absence of any forces other than friction and bolt reactions.

5.6 Mesh sensitivity study

A mesh sensitivity study was carried out to demonstrate the independence of the numerical results from the meshing of the parts. The results obtained with the converged meshes were then compared to relevant studies from the literature. The mesh convergence study was therefore conducted for the same joint design as in [2] and [3] for comparison purposes.

Considering the large number of simulations carried out in this thesis study, the indications about meshing drawn from the sensitivity study were applied to the following simulations. In this way, such a study did not need to be repeated for each case.

5.6.1 Approach and joint geometry

The study was carried out for both a single-lap and and a double-lap joint, with layups H-SL-Q-C and H-DL-Q-C respectively. The joint geometries are summarized in Tables 10 and 11. Both for double-lap and single-lap configurations, $\lambda = \{80, 10, 10\}$ conditions were considered. This way, the effects of a longer delay in load take-up at bolt 1, where a larger clearance was defined, could be monitored. As in the retained studies, finger-tight torque conditions were modelled.

Table 10: Single-lap joint geometry for mesh sensitivity study

N [-]	D [mm]	w [mm]	p_1 [mm]	p_2 [mm]	l_{end} [mm]	t_A [mm]	t_B [mm]
3	8	48	36	36	56	5.2	5.2

Table 11: Double-lap joint geometry for mesh sensitivity study

N [-]	D [mm]	w [mm]	p_1 [mm]	p_2 [mm]	l_{end} [mm]	t_A [mm]	t_B [mm]
3	8	48	36	36	56	2.08	4.16

Independent mesh refinements were applied to each of the three previously introduced parts. It was thus determined the minimum level of refinement needed to capture the relevant phenomena.

At first, four different meshes for *Plate* were considered, from P1 to P4 according to Table 12. While the mesh for *Plate* was refined, the meshes for *Bolt and nut* and *Washer* were kept unchanged at BN2 and W2 respectively, see Table 14 and Table 16. Once a suitable mesh for *Plate* had been identified, it was used for all the following simulations. The second step was to only modify the mesh for *Washer* and select a suitable one. Lastly, the meshes for *Plate* and *Washer* were not modified while a satisfactory *Bolt and nut* mesh was identified. The approach to the mesh sensitivity study can be summarized as follows:

I. Identified suitable *Plate* mesh while keeping *Bolt and nut* and *Washer* meshes unchanged.

II. Identified suitable *Washer* mesh while keeping *Bolt and nut* and *Plate* meshes unchanged.

III. Identified suitable *Bolt and nut* mesh while keeping *Washer* and *Plate* meshes unchanged.

To evaluate the suitability of a mesh through successive refinements, the change in applied load P, bolt reactions, load distribution and computational time were monitored. The bolt reactions F_1, F_2 and F_3 were not individually reported in the results, however they were monitored through a term defined as $F_{\text{sum}} = \sum_{j=1}^{N} F_j$, the sum of the reactions F_j. The difference between P and F_{sum} corresponds to the load transferred by the joint through friction, which is small in the considered cases because of the finger-tight torque conditions. The load fraction at a bolt j was defined as:

$$f_j = \frac{F_j}{F_{sum}} \tag{38}$$

Tables 13, 15 and 17 show the monitored values for the double-lap case. The same approach was adopted to evaluate the results with a single-lap joint, which are presented in the Appendix (Section 11.6).

5.6.2 Mesh sensitivity study for a double-lap joint

The four meshes employed for *Plate* in the refinements of point I are presented in Table 12.

Table 12: Meshes for *Plate* employed in the sensitivity analysis

	Divisions green edge	Divisions yellow edge	Divisions blue edge	Number of elements	Refine. factor
Mesh P1	6	6	4	546	
Mesh P2	8	8	6	920	1.68
Mesh P3	10	10	8	1390	1.51
Mesh P4	12	12	9	1812	1.3

The predictions obtained with P2, P3 and P4 were all reasonably close, as shown in Table 13. The coarsest mesh, on the other hand, led to a significantly higher F_{sum} prediction, as well as rather different load distributions.

Table 13: Monitored variables for *Plate* mesh refinements in double-lap

Mesh	P [kN]	F_{sum} [kN]	f_1 [%]	f_2 [%]	f_3 [%]	Simulation time [min]
P1-W2-BN2	21.5	20.8	23.2	34.9	41.9	11.5
P2-W2-BN2	19.6	18.9	16.5	39.7	43.9	12.5
P3-W2-BN2	19.9	19.2	17.6	38.9	43.4	22.7
P4-W2-BN2	19.5	18.5	17.1	39.3	43.6	72.9

To extend the evaluation of mesh convergence for *Plate* beyond the study of load distribution, the evolution of the bypass stress at the central bolt was monitored. Fig.31 shows the curves for σ_{11} as a function of the distance from the hole center. The plate surface is shown in grey for clarity. The values for the curves were extracted from the top surface of the top plate of the joint. These curves confirm the observations drawn from the load distribution study, with P2, P3 and P4 leading to similar estimations and P1 showing sensibly different results for any point along Y. At the plate edge, y=24 mm, the stress with P1 is 1.18 times larger than with P2, while the curves for meshes P2, P3 and P4 predict very similar values.

Based on the conclusions of the load distribution and bypass stress analyses, P2 was chosen as a suitable refinement for the mesh of *Plate*, because of its accuracy and low computational time. The relative F_{sum} change between the chosen mesh and the successive refinement is of 1.56%. With this mesh, 32 elements are used around the plate holes to capture plate deformation and contact with the bolt.
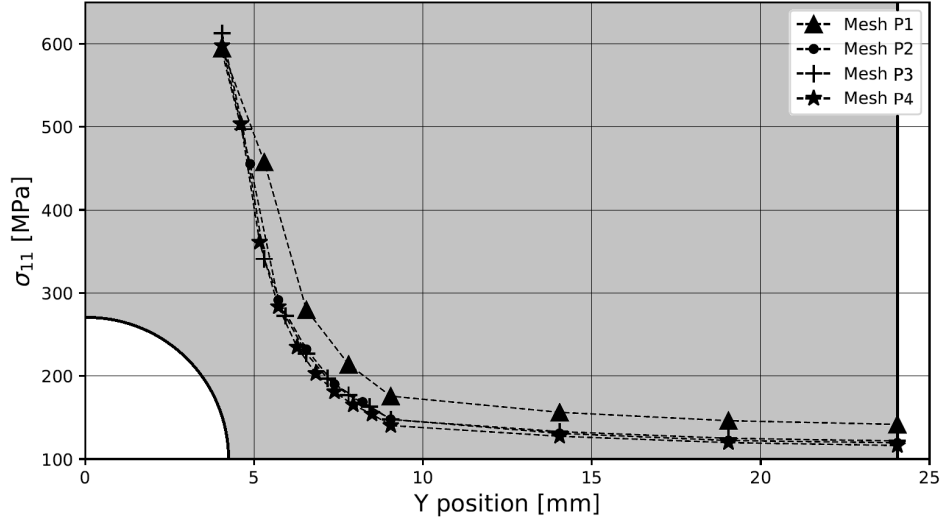
Figure 31: σ_{11} as a function of the Y position on the top plate at bolt 2

The meshes employed in the second refinement, concerning only *Washer*, are described in Table 14. The results with the refinements of step II are presented in Table 15.

Table 14: Meshes for *Washer* employed in the sensitivity analysis

Mesh	Divisions yellow edge	Divisions red edge	Divisions orange edge	Number of elements	Refine. factor
W1	2	2	32	128	
W2	4	4	48	768	6
W3	5	5	60	1500	1.95

All the predictions were extremely close, showing that the mesh of *Washer* does not affect significantly the load distribution. It is however to be noted that, despite a refinement factor of 6 between P2-W1-BN2 and P2-W2-BN2, the computational time remained almost unchanged. The expected increase in computational time due to the increase of mesh elements was balanced by a better definition of the washer-laminate contact surface. Mesh W2 was chosen for the successive simulations because of the equivalent computational time with respect to W1 and the superior contact modelling it ensured.

Table 15: Monitored variables for *Washer* mesh refinements in double-lap

Mesh	P [kN]	F_{sum} [kN]	f_1 [%]	f_2 [%]	f_3 [%]	Simulation time [min]
P2-W1-BN2	19.6	18.9	16.5	39.7	43.9	12.1
P2-W2-BN2	19.6	18.9	16.5	39.7	43.9	12.5
P2-W3-BN2	19.6	18.9	16.5	39.7	43.9	17.8

The third and last step of the sensitivity analysis was to refine *Bolt and nut*, previously defined as point III. The three meshes that were employed are presented in Table 16[iv].

Table 16: Meshes for *Bolt and nut* employed in the sensitivity analysis

Mesh	Divisions red edge	Divisions yellow edge	Divisions pink edge	Number of elements	Refinement factor
BN1	8	5	2	1024	
BN2	10 (8)	7	2	1816 (1667)	1.77 (1.63)
BN3	10 (8)	10	4	3728 (3456)	2.05 (2.07)
BN4	(8)	(12)	(4)	(4352)	(1.26)

Table 17 presents the results obtained with the refinements of *Bolt and nut*. The predictions obtained with BN1, BN3 and BN4 differed from the results of BN2. This difference is observable both for load distribution and F_{sum}. After analyzing the results for the considered case, as well as those for other clearance conditions, mesh BN2 was selected because of its superior agreement with the relevant literature. This comparison is presented in Section 5.7. The relative F_{sum} change between the chosen mesh and the successive refinement is of 3.57%.

Table 17: Monitored variables for *Bolt and nut* mesh refinements in double-lap

Mesh	P [kN]	F_{sum} [kN]	f_1 [%]	f_2 [%]	f_3 [%]	Simulation time [min]
P2-W2-BN1	20.3	19.5	19.6	37.9	42.6	15.1
P2-W2-BN2	19.6	18.9	16.5	39.7	43.9	12.5
P2-W2-BN3	20.3	19.6	19.7	37.7	42.6	27.4
P2-W2-BN4	20.8	20.1	20.1	37.6	42.2	25.8

[iv]The values in brackets indicate the number of divisions with the double-lap joint, if the value is different from the divisions with the single-lap joint. The difference was made to always satisfy the constraints on mesh density of master and slave surfaces at the bolt-hole contact regions. It should be noted that the total joint thickness with single-lap and double-lap configurations is not equal, see Tables 10 and 11. Mesh BN4 was only considered for double-lap configurations

5.7 Finite element comparison with literature

After the mesh sensitivity analysis, the FE models for double-lap and single-lap joints were compared to the results obtained in [2] and [3] respectively. While joint geometry and material properties were the same for both studies, finger-tight conditions were modelled in the former and torque-tight conditions in the latter. The preload was therefore modified in the FE models to allow comparison with the literature. Tables 18 to 21 summarize the comparison of the results.

As previously mentioned, both SC8R and C3D8 elements were considered for modelling composite plates. Therefore, simulations for double-lap joints were conducted by replacing SC8R elements with C3D8 for modelling the composite laminates. It was assumed that the refinements that led to convergence of the models with SC8R elements would also be suitable for C3D8 elements. It should be noted that the results from [2] were obtained with continuum composite elements with MSC.Marc (Element 149), while C3D8 elements available in Abaqus were employed in [3].

Table 18: Double-lap FEM comparison for $\boldsymbol{\lambda} = \{10, 10, 10\}$ [2] (Finger-tight)

	$\mathbf{F_{sum}}$ [kN]	Rel. difference literature [%]	$\mathbf{f_1}$ [%]	$\mathbf{f_2}$ [%]	$\mathbf{f_3}$ [%]
Literature	21.1		36.7	26.6	36.7
SC8R	20.9	-1.41	37.0	26.4	36.6
C3D8	20.7	-2.18	37.1	26.3	36.7

Table 19: Double-lap FEM comparison for $\boldsymbol{\lambda} = \{80, 10, 10\}$ [2] (Finger-tight)

	$\mathbf{F_{sum}}$ [kN]	Rel. difference literature [%]	$\mathbf{f_1}$ [%]	$\mathbf{f_2}$ [%]	$\mathbf{f_3}$ [%]
Literature	18.8		16.3	39.8	43.9
SC8R	18.9	0.12	16.5	39.7	43.9
C3D8	18.8	-0.24	16.3	39.5	43.8

The comparison with the results from the literature for double-lap configuration, also obtained through displacement-controlled loading, was carried out for an imposed displacement of 0.4 mm. Good agreement between literature and FE models can be observed in Tables 18 and 19. The relative difference with respect to [2] in terms of total load transferred by the bolts is 1.41% and 2.18%, both considered reasonably close. Load distributions are also close, with a largest difference of 0.4% at bolt 1 with C3D8 elements.

Table 20: Single-lap FEM comparison for $\boldsymbol{\lambda} = \{10, 10, 10\}$ [3] (Torque-tight)

	$\mathbf{F_{sum}}$ [kN]	Rel. difference literature [%]	$\mathbf{f_1}$ [%]	$\mathbf{f_2}$ [%]	$\mathbf{f_3}$ [%]
Literature	39.5		37.0	27.6	35.4
SC8R	40.2	1.82	37.6	26.4	35.9

Table 21: Single-lap FEM comparison for $\boldsymbol{\lambda} = \{10, 160, 10\}$ [3] (Torque-tight)

	$\mathbf{F_{sum}}$ [kN]	Rel. difference literature [%]	$\mathbf{f_1}$ [%]	$\mathbf{f_2}$ [%]	$\mathbf{f_3}$ [%]
Literature	36.1		46.5	7.8	45.6
SC8R	36.2	0.36	47.8	6.6	45.5

The comparison with the literature for single-lap configuration was carried out for an imposed displacement of the loaded end of 1 mm. Also these results were obtained through displacement-controlled loading. Only SC8R elements were employed in the numerical models with single-lap configuration but, once again, the results retained from the literature had been obtained with C3D8 elements.

Also in this case, the models showed a good agreement with the retained literature, with variations of F_{sum} smaller than 2%. The load distributions were also similar, the largest discrepancy being 1.3% at bolt 1 in Table 21.

5.8 Conclusions on numerical modelling approach

Based on the results of the sensitivity study for double-lap joints, a suitable mesh was identified. Although not discussed in this chapter, a similar approach was applied to the selection of the P2-W2-BN2 mesh for single-lap joints, which was deemed as suitable for load distribution evaluation. The retained meshes for single and double-lap joints were also evaluated through comparison to relevant numerical studies.

Regarding the element choice for the laminates, SC8R elements showed better agreement with the literature compared to C3D8 elements, which might be partially due to the fact that the sensitivity analysis was carried out with SC8R elements. The former were chosen for modelling all the composite plates in the thesis study. The fully metal plates of Sections 7.1.1 and 7.2 were modelled with solid elements. SC8R elements were employed to model both single-lap and double-lap joints. While with the latter configuration no out-of-plane plate deformation takes place, the eccentricity of the load lines with single-lap joints induces plate bending. SC8R elements,

assuming plane stress state, cannot account for through-the-thickness stresses, which may limit their application to cases in which out-of-plane effects are significant. It should be noted that the comparisons of Table 20 and Table 21 were made with a source in which plates for single-lap joints had been modelled with solid elements C3D8, observing good agreement. In those cases, the out-of-plane effects showed to have small impact on load distribution.

It is worth mentioning that SC8R are the only elements in Abaqus FEA with a built-in progressive damage model for composites, which might prove useful if the numerical models created for this study were used in the future with a need to extract such information. However, since the sensitivity analysis was not carried out to evaluate the mesh accuracy in modelling progressive damage, further evaluations of mesh suitability would first be necessary. It should also be carefully noted that SC8R are susceptible to hourglassing when damage is triggered, making them unsuitable for modelling near-failure behavior, especially when delamination is involved [23]. Employing solid elements in this case can avoid the issues deriving from the use of SC8R elements.

When joint geometries other than those considered in this section were modelled, the same number of mesh divisions was reproduced to guarantee suitability of the mesh. While the thickness of the plates considered in the sensitivity study was not modified in successive studies, it would be possible to adapt the mesh to thicker or thinner laminates. Suitability is assumed not to change if the same ratio of plate thickness to though-the-thickness divisions were ensured. The same proportionality should be ensured for bolt divisions.

Finally, while axial tension was considered in the sensitivity study, it is believed that the mesh suitability would not be affected in cases of compression due to loading similarity, at least when no structural instability is investigated. Additionally, having the mesh sensitivity analysis proven the capability of the selected meshes to capture the plate deformation around bolts, the indications derived from the analysis were applied when modelling shear and biaxial loading.

However, mesh suitability was not directly assumed for thermal loading and different numerical models were compared to evaluate whether the refinements were sufficient to capture thermally induced material deformation. Further considerations were made as discussed in Section 6.3.2.

6 Investigations on the retained models

6.1 Validation study for fastener flexibility

Several fastener flexibility formulations were considered in this thesis study and were implemented in the tool. In this section, the analytical model for uniaxial loading is used to predict load distribution with different flexibility formulations. To evaluate the accuracy of each formulation, the load distribution prediction is compared to experimental data retained from the literature. Only the accuracy of the flexibility formulations is discussed, while the validation of the analytical model itself is carried out separately in Section 6.2.

First, the load distribution in a single-lap joint was computed. The prediction was compared to experimental results from [3], obtained through instrumented bolts for finger-tight torque conditions and $\boldsymbol{\lambda} = \{10, 10, 10\}$. The layup of the composite plates is H-SL-Q-C, while the joint geometry is summarized in Table 22.

Table 22: Single-lap joint geometry for fastener flexibility validation

N [-]	D [mm]	w [mm]	p_1 [mm]	p_2 [mm]	l_{end} [mm]	t_A [mm]	t_B [mm]
3	8	48	36	36	56	5.2	5.2

The results of the comparison are presented in Fig.32. To compare the analytical predictions to the experimental measures, only the portion of graph in between 12 kN and 15 kN is shown for clarity, as all the curves are rather close. It should be noted that the linearity of the deformation, together with the considered case of equal clearance at all bolts, ensure that the load fractions f_1, f_2 and f_3 are independent of the applied load. Comparing the results at any applied load value would lead to equal results.
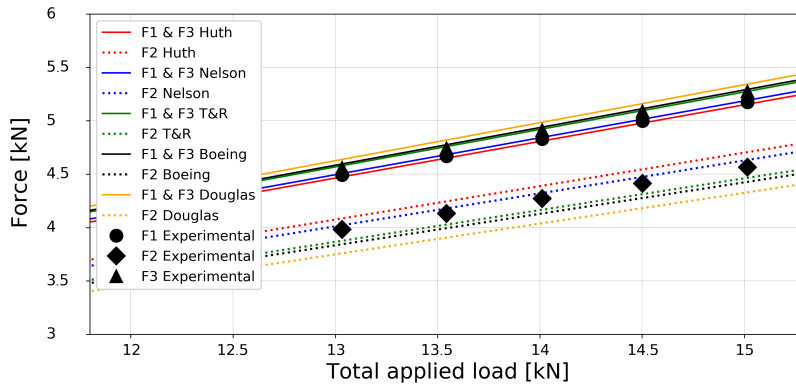
Figure 32: Fastener flexibility comparison to experimental data for single-lap

The comparison of the different flexibility formulations shows that Huth and Nelson lead to the most accurate results. The latter formulation, with the bolt shape factor β_N set to 0.15, is the closest to the experimental values. This is in good agreement with the conclusions by Nelson [13], who identified 0.15 as the optimal value of the coefficient for protruding-head bolts for similar plate thickness to bolt diameter ratios. All the other flexibility formulations lead to less even load distributions, with overpredictions of the reactions at the external bolts. The relative difference between experimental data and the curve for the most loaded bolt with the formulation by Nelson is -1.62%, the difference having been normalized over the analytical value from Nelson. For the central bolt 2, the relative difference is 1.44%.

The same comparison was carried out for a double-lap joint with geometry as presented in Table 23. Finger-tight torque was also considered here, with clearance conditions $\boldsymbol{\lambda} = \{0, 0, 0\}$. While these values are only theoretically possible, Lawlor [43] approximated these conditions by imposing a high quality hole tolerance H6, obtained with especially manufactured reamers. The laminate layup for the joint is H-DL-Q-C.

Table 23: Double-lap joint geometry for fastener flexibility validation

N [-]	D [mm]	w [mm]	p_1 [mm]	p_2 [mm]	l_{end} [mm]	t_A [mm]	t_B [mm]
3	8	48	36	36	56	2.08	4.16

Through the comparison of the curves in Fig.33, it is possible to observe that all fastener flexibility formulations predict a more even load distribution than the experimental curves. The closest prediction is observed with Huth, for which the relative difference at the highest loaded bolt is -4.3%, while it is 10.8% at the central bolt. Also here the relative difference was normalized over the analytical value. The formulation by Boeing leads to results very close to Huth, while the other formulations show less accurate predictions.

In the case of single-lap joints, the two most accurate flexibility formulations were observed to overpredict the reaction at the central bolt and underpredict the reactions at the external bolts. This resulted in more even load distributions compared to the experimental data. The opposite behavior was observed with all the flexibility formulations for the double-lap configuration. If the largest reaction is considered for joint design, a tendency to predict excessively even load distributions can lead to non conservative predictions of the largest reaction. A discussion on the conservatism of the overall analytical approach is presented in Section 6.2.
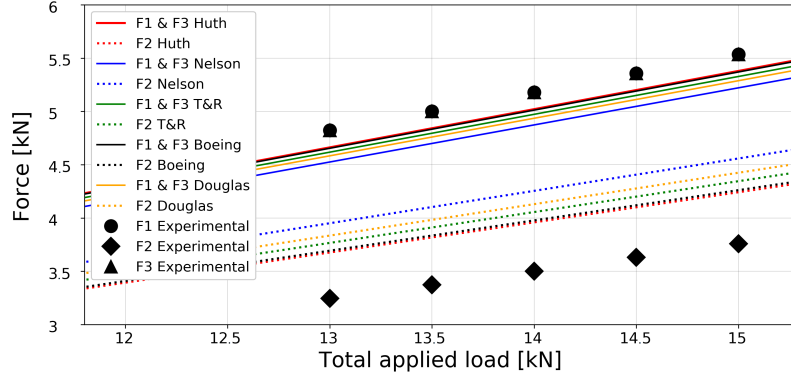
Figure 33: Fastener flexibility comparison to experimental data for double-lap

The fastener flexibility formulation by Huth was employed in the analytical studies presented in other sections because of the good agreement with experimental data, both with single-lap and double-lap joints.

6.2 Analytical model evaluation for axial loading

A very high level of detail can be reproduced with the 3D FE models, modelling factors such as washer-laminate contact or bolt head shape. All these details cannot be kept into account in the analytical models. Of course, an accurate prediction of complex phenomena can be achieved only if the details the analytical model neglects have little impact on load distribution.

To evaluate the accuracy of the analytical model, therefore ensuring that the ignored aspects are of secondary importance compared to bolt flexibility, preload and clearance, load distribution predictions were compared to results from numerical models.

The retained model for uniaxial loading of single-column joints, presented in Section 4.1.2 was considered in this section in connection with the proposed method to account for bolt preload, introduced in section 4.2.1. Load cases LC1 and LC2 were therefore investigated in the case of a single-column joint, while an extension to multi-column joints under these loadings is discussed in section 7.2.

6.2.1 Comparison study for double-lap joints under tensile loading

A double-lap joint with three bolts was considered in the comparison studies. The joint dimensions are summarized in Table 24, while the FE model's geometry can be found in the Appendix (Fig.62). Intermediate torque was considered to evaluate the capability of the analytical model to predict joint forces in presence of non-negligible bolt preload. Three different clearance conditions were investigated: $\lambda =$

$\{40, 40, 40\}$, $\boldsymbol{\lambda} = \{40, 100, 40\}$ and $\boldsymbol{\lambda} = \{100, 40, 40\}$. With the first case of clearance conditions, the analyses were carried out for two different layups: M-DL-D-C and M-DL-Q-C. Only the former was employed in the second and third cases. It should be noted that these conditions are all within the tolerance limits for the f7/H10 fitting.

Table 24: Double-lap joint geometry for model evaluation in tensile loading

N [-]	D [mm]	w [mm]	p_1 [mm]	p_2 [mm]	l_{end} [mm]	t_A [mm]	t_B [mm]
3	8	48	36	36	36	2.08	4.16

Being the thickness of the A plates exactly double that of the central plate B, and being the layup properties identical in orientation and material, the stiffness of plates A combined is equal to the stiffness of B. Moreover, in the considered joint geometry p_1 and p_2 are equal, with a constant plate width w. As a consequence, the reactions predicted by the model at bolt 1 and 3 are exactly the same for all the considered cases.

The study was carried out through a comparison of the force predictions from FE models and the analytical models. The fastener flexibility formulation by Huth was employed in this study. The definitions introduced in Section 1.2 are used in the analysis of the phenomena. Unlike in Fig.1, the friction component of the joint reaction is plotted separately from the bolt forces. The friction curve is calculated from Eq.29 considering that friction reaches a maximum when joint slipping is triggered and that it remains constant afterwards.

It is important to note that a direct comparison of force-displacement curves from the different models would be impossible, since they adopt different definitions of displacement. In the analytical model, as presented in Section 4.1.2, the joint displacement is calculated by summing for all fasteners the difference between top and bottom node displacement. There is no equivalent displacement in the FE models, in which displacement was imposed at the free edge of the plates. To allow a comparison between models, force-applied load curves are studied. The applied load, previously defined as P, in the tool is equal to the sum of all the bolt reactions plus the fraction of load reacted by friction. Broadly speaking, these could be interpreted as force-displacement curves which have been normalized to the same displacement. While never explicitly mentioned, it is believed the same approach was adopted by other studies in the literature [2][3].
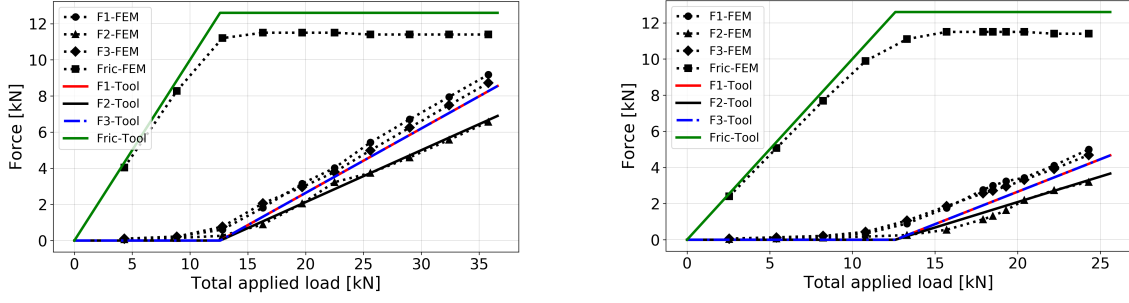
Figure 34: Force prediction comparison for $\boldsymbol{\lambda} = \{40, 40, 40\}$ with M-DL-D-C (left) and M-DL-Q-C (right)

Fig.34 shows the comparison for the case of equal clearance $\boldsymbol{\lambda} = \{40, 40, 40\}$. Good agreement between the models can be observed, especially regarding the slope of the curves in the bolt load transmittal region. The analytical model overpredicts the largest friction reaction by 8.7%. While the knowledge of this force is not directly relevant if only bolt forces are of interest, the modelling of joint friction indirectly affects the load distribution when bolt reactions appear. In fact, an accurate prediction of load distribution can only be ensured if the critical load initiating slipping is correctly estimated. It should be noted that friction is modelled through the Coulomb model, only taking into account bolt preload and laminate friction, which were considered equal for all cases in the comparison study. Therefore, the applied load at which slipping appears is always the same, about 12 kN. If the analytical model predicted a late slipping compared to reality, for some values of applied load the bolts would be assumed to carry no load while reactions would in fact be present.

For the considered clearance conditions and with both layups, the prediction of the applied load at which bolt reactions appear is reasonably accurate. Since the slope of the curves after the transition region is also well captured by the implemented fastener flexibility, the prediction remains consistent for all applied loads. At the highest considered applied load value, the largest relative difference between the results from the two models was observed for bolt 1 to be roughly 7% with both layups, the difference having been normalized over the prediction from the FE model. Since no significant difference in behavior between the two layups was observed, the following analyses were carried out only for M-DL-D-C.

The graph for the $\boldsymbol{\lambda} = \{40, 100, 40\}$ case is shown in Fig.35. Also for these conditions, the critical load initiating plate slipping is rather well predicted, with a slight delay of the analytical model with respect to the FE model. The analytical prediction for the first two bolts to react the applied load, bolts 1 and 3, follows closely the FE model's results. Bolt 2 shows an interesting behavior, which can be understood by investigating the bolt-hole contact and looking back at the early discussion presented for a single-lap joint in Fig.1.

61
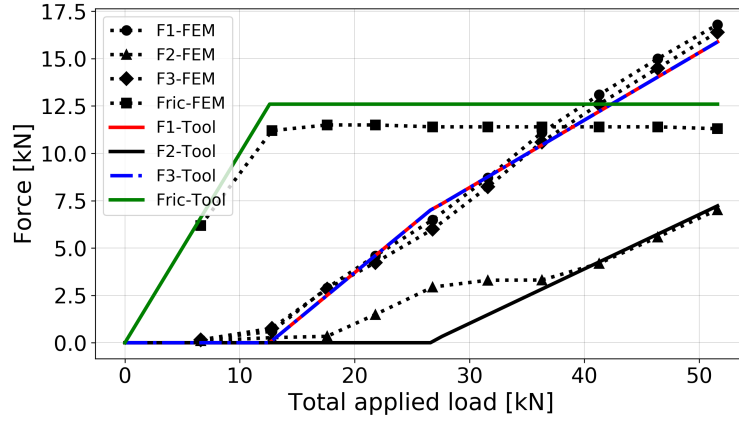
Figure 35: Force prediction comparison for $\boldsymbol{\lambda} = \{40, 100, 40\}$ with M-DL-D-C

The analytical model is defined to assume that in the transition region II, the transferred load remains the same. In other terms, when slipping starts at point 1, a bolt cannot transfer any additional load until contact is established with both plates as shown in the picture for region III. In reality, even with a contact with just one plate as in the picture for region II, the bolt can transfer loads in shear. In fact, due to the clamping of the plates and frictional contact between the washers and the plates, a resistance opposes a relative motion of the bolt towards the yellow plate. Since this motion does not take place immediately because of friction, the bolt can transfer load in shear until the transferred load is sufficient to overcome these frictional effects. Therefore, in Fig.35, the FE model's curve shows an early load take-up at bolt 2 compared to the analytical model because the bolt starts transferring load in shear before completing a 100 μm displacement. Section views of the joint are presented in large size in the Appendix (Section 11.7) to illustrate the different stages of bolt contact in the considered case. Around 27 kN of applied load, bolt 2 is only in contact with the central plate B, while at 42 kN, the bolt is in contact with all plates.

To summarize the behavior of bolt 2, at about 18 kN of applied load, a first contact between the bolt and the central plate is established. Until the applied load reaches 27 kN, bolt 2 is capable of transferring the load in shear without being in contact with the A plates. At 27 kN, the applied load is large enough to induce the relative motion of the bolt towards the A plates. Until this second contact is established, no additional load can be transferred and the FE model's curve remains flat. At contact, the 100 μm displacement is completed and the numerical and analytical curves adhere very closely. At 50 kN, the largest discrepancy between models is observed for bolt 1, with the analytical model underpredicting the reaction by 5.4%. The fact that also in this case, after full contact has taken place, the slopes of the curves are in good agreement, is proof that Huth's flexibility formulation can capture accurately the bolt reaction deformation.
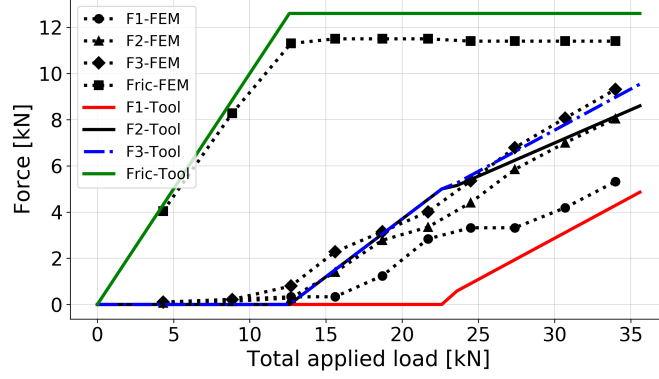
Figure 36: Force prediction comparison for $\boldsymbol{\lambda} = \{100, 40, 40\}$ with M-DL-D-C

Generally, the considerations for the previous clearance conditions apply to the case of $\boldsymbol{\lambda} = \{100, 40, 40\}$ shown in Fig.36. Comparing the two models at an applied load of 16 kN, allows to observe once again the slight delay in load take-up of the analytical model. After this point, the curve from the FE model for bolt 1 shows a behavior already described for bolt 2 in the previous analysis. For large applied loads, the curves from the FE model are in good agreement with the analytical model in terms of slope. At 34 kN of applied load, bolt 1 shows the largest discrepancy, 18.2%, while the underprediction of the largest joint reaction at bolt 3 by the analytical model is 3.2%.

The fact that a reaction takes place at bolt 1 here before a full 100 μm displacement, leads the analytical model to give a highly non-conservative prediction for that bolt. This equally applies to bolt 2 in the previous analysis. It should however be noted that this early take-up only takes place at bolts where a large clearance introduces a delay in comparison to the most loaded bolts. Therefore, if only the largest reaction in the joint were considered for design, a good level of accuracy of the analytical prediction would be ensured even when the load at bolt 1 is underpredicted.

The accuracy of the analytical model heavily relies on how much the assumptions made in its formulation hold for a real joint. The accuracy of the assumptions can of course vary for different clearance conditions or applied load. The study in this section underlines the need to respect the fundamental assumptions in order to closely predict load distribution.

The first assumption is that no slipping of the plates can take place until a certain critical load is applied. An underestimation of this load would lead to the prediction of an early load take-up by the bolts, thus overpredicting the bolt reactions. On the other hand, an overestimation of the critical friction load would lead to an underprediction of the bolt reactions. This point was rather well respected by the analytical model through Coulomb friction law, with a tendency to overestimate the critical friction force.

63

The second assumption is that reactions in bolts appear at the end of the transition region when a sufficient difference in displacement between top and bottom nodes is ensured. The fact that the reaction is zero until that moment leads to a modelling of clearance as a simple source of delay in load take-up, which applied well to $\boldsymbol{\lambda} = \{40, 40, 40\}$. However $\boldsymbol{\lambda} = \{40, 100, 40\}$ and $\boldsymbol{\lambda} = \{100, 40, 40\}$ show a more complex frictional behavior. Having the assumption been validated for the first case, it should be possible to generalize that the assumption would hold equally well with similar cases where $\lambda_1 = \lambda_2 = \lambda_3$. As long as no contact is established at any bolt, it is possible to safely consider all bolt reactions to be zero, the amount of delay due to clearance not influencing this conclusion. For cases of very diverse clearance at different bolts, this assumption could be less accurate. Generally, the more homogeneous the clearance, the more safely the assumption can be considered to hold.

The third critical point is that it is possible, when bolt-hole contact has been established, to reduce the problem to a simple 1D model accounting for stiffness properties of plates and fasteners in the loading direction. In this sense, the results have shown to confirm the assumption through the correct prediction of the slopes in the bolt transmittal region. They also indicate that the estimation of the global stiffness properties of the laminates with CLT was accurate.
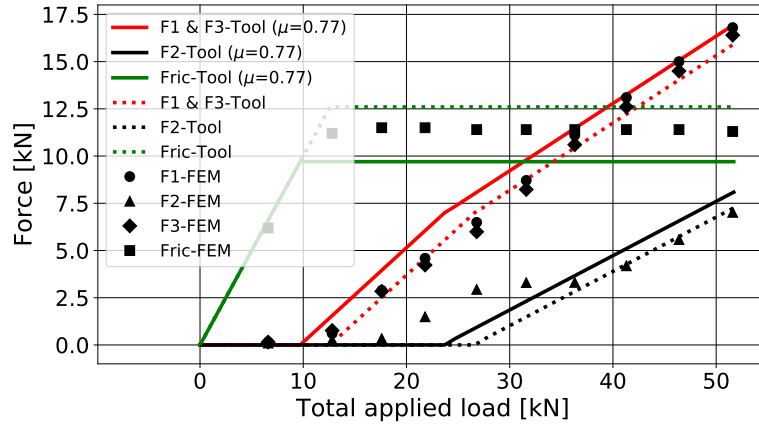
Figure 37: Friction coefficient influence on load distribution for $\boldsymbol{\lambda} = \{40, 100, 40\}$

Finally, a consideration on conservatism is necessary. As discussed, the analytical model was capable of predicting the bolt reactions with good accuracy at times, with larger discrepancies in other cases. However, the prediction has always proved to be non conservative compared to the results from the FE model. As already mentioned, the delay introduced by the overestimation of the critical friction load led to an underprediction of the bolt reactions. A measure to compensate this inaccuracy could be to take the friction coefficient to be smaller than its actual value. This would lead to an early load take-up by the bolts thus compensating

for friction model's inaccuracy. Such an approach could be justified only because the slopes in the bolt load transmittal region are correctly predicted. An example of how the delay induced by the friction coefficient influences load distribution is shown in Fig.37. The graph, for a case already shown in Fig.35, shows that, with a reduction of the friction coefficient, load take-up at all bolts takes place earlier. The prediction for the most loaded bolt is conservative for all the considered applied load values and could also be the case beyond 50 kN thanks to the good prediction of the slopes in the bolt load transmittal region.

By adopting such an approach and taking the friction coefficient to be 77% of the value implemented in the numerical models, the analytical model would give conservative predictions at the most loaded bolt for all the previously presented cases at the highest considered applied load. From a visual study of the numerical curves, and considering the fact that the correct slope in the bolt load transmittal region is predicted, it is possible to approximate that reducing the friction coefficient to 77% of its value should also be close to guarantee conservatism for all applied loads.

Adapting the plate-plate friction coefficient could then be a way to compensate the delay introduced by the imprecisions of the Coulomb model. The limit is intrinsic in the friction law, attempting to model the complexity of frictional interactions with a simple relation. To avoid these uncertainties, it is sometimes assumed that no preload is present, as done by Esp [4], thus ensuring conservative predictions. Such an approach is also possible with the tool but the sacrifice in terms of accuracy would be considerable. If, through detailed investigations on sticking-to-slipping transition in bolted joints, a more precise definition of the friction coefficient to be employed were obtained, the tool could lead to a compromise between the needs for accuracy and conservatism.

6.2.2   Comparison study for single-lap joints under tensile loading

In Section 6.1 the prediction obtained with the analytical model for a single-lap joint was compared to experimental data for different fastener flexibility formulations. Good agreement was found, especially with formulations by Nelson and Huth. This experimental comparison serves as a first validation of the analytical model but only low bolt preload and no clearance were considered. A comparison between analytical model and FE models was carried out for two additional cases: $\boldsymbol{\lambda} = \{0, 40, 0\}$ with finger-tight and intermediate torque. These conditions allow to also take into account the effects of clearance and preload. Huth's fastener flexibility formulation was implemented in the analytical model.

The joint geometry presented in Table 25 is considered in both cases, with a M-SL-D-C layup and $\boldsymbol{\lambda} = \{0, 40, 0\}$ clearance conditions. In the first comparison, whose results are shown in Fig.38, finger-tight torque conditions were modelled.

Table 25: Single-lap joint geometry for model evaluation in tensile loading

N [-]	D [mm]	w [mm]	p_1 [mm]	p_2 [mm]	l_{end} [mm]	t_A [mm]	t_B [mm]
3	8	48	36	36	36	4.16	4.16
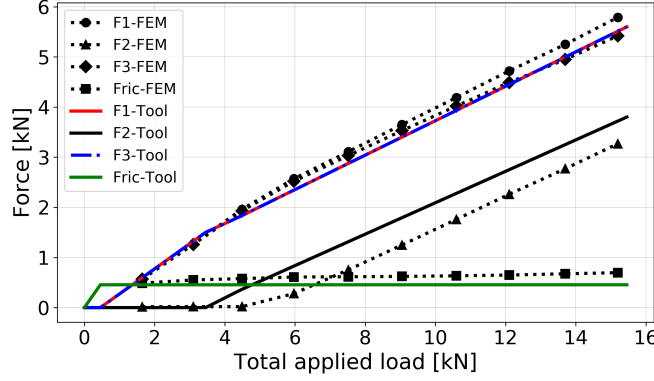
Figure 38: Force prediction comparison for $\boldsymbol{\lambda} = \{0, 40, 0\}$ with M-SL-D-C and finger-tight torque

For this case, the two models lead to similar predictions. The curves of the most loaded bolts are in good agreement and also the slopes for the three bolts are very similar with the two models. The biggest discrepancy is found at the central bolt 2, for which the analytical model predicts an early load take-up, thus leading to an about 15% relative difference at 15 kN. As already mentioned, when a discrepancy between models for a curve is introduced by a difference in the load take-up moment, the relative error is maximum for small forces. It then becomes smaller as the force, in this case F_2, increases, since the slopes are correctly predicted. The last aspect worth mentioning is a slight overestimation of the FE model prediction for the friction curve with respect to the analytical model. This is further analyzed in light of the results of the second analysis of this section for intermediate torque conditions. The comparison between models is presented in Fig.39.

The graph shows all the trends that were observed for the finger-tight torque case: accurate predictions for the most loaded bolts, early take-up at bolt 2 and friction curve overestimation with the FE model. The magnitude of the variations, however, appears to be larger. To correctly interpret the results, the first aspect to consider is the critical friction force. According to the FE model, around 6 kN of applied load, bolts 1 and 3 start reacting in shear, since the critical friction load has been overcome. This is in good agreement with the analytical model, which predicts the critical friction value to be 6.3 kN. It was already observed for double-lap joints

in Section 6.2.1 that the Coulomb model leads to a slight overprediction of the critical friction which, in a way, poses an upper bound to loads transferable by static friction. However, in Fig.39, the curve for the friction force from the FE model keeps increasing after shear reactions have appeared at bolts 1 and 3. This is probably a limit of the strategy for force extraction from the numerical model rather than the actual behavior of friction forces, as there is no reason to believe they would increase further. In fact, the frictional curve is calculated as the difference between the applied load and the fastener reactions. The reactions themselves are extracted as the forces the plates are exerting on the bolts. This approach is reasonably accurate with double-lap joints, since only the plates transfer a significant load to the bolts, but is more prone to inaccuracies with single-lap joints. In fact, while for a double-lap joint an applied load generates a purely in-plane plate deformation, a single-lap joint also deforms in bending because of the eccentricity of the load lines.
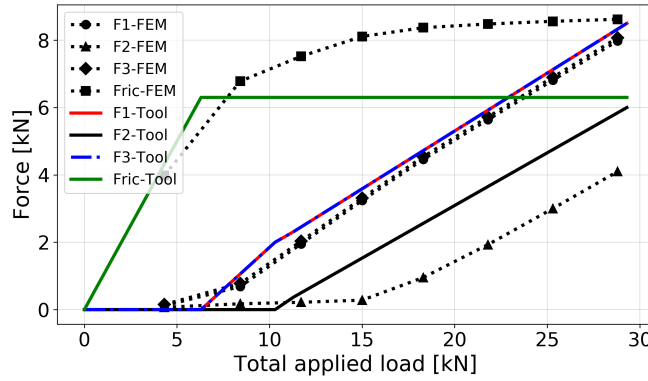
Figure 39: Force prediction comparison for $\boldsymbol{\lambda} = \{0, 40, 0\}$ with M-SL-D-C and intermediate torque

Fig.40 shows an example of single-lap joint deformation for the considered boundary conditions. This difference in deformation leads to the appearance of reactions along the loading direction at the plate-washer interface. These forces are not accounted for in the fastener reactions with the current force extraction approach and end up contributing to the friction force, which appears to be still growing, even if the critical friction value has already been reached. The fact that these forces are transferred by friction at the washers explains why these effects are negligible for small preload and larger for intermediate torque conditions.
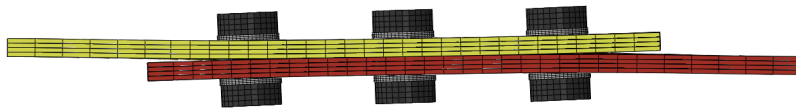
Figure 40: Typical single-lap joint deflection for uniaxial tensile loading

Coming back to the evaluation of the analytical model and just looking at the fastener reactions at low preload, reasonable agreement can be found between the two models, especially for bolts 1 and 3. It is important to keep in mind that the analytical model for single-lap joints was evaluated by comparison with experimental data in Section 6.1 but for finger-tight torque conditions. To extend the evaluation of the single-lap model to also large preload conditions, and without applicable experimental data, the force extraction from the FE model needs to be improved. Due to a lack of time, no further numerical studies on single-lap joints with highly torqued bolts were carried out so that no alternative force extraction method was investigated. It should however be possible to improve the extraction method by directly extracting frictional effects through integration of the tangential forces at the contact surfaces. The shortcomings of the current approach, based on the difference with the total applied load, could then be avoided.

6.2.3 Compressive loading modelling justification

The tool was designed to predict load distribution in a joint for both uniaxial compression and tension. The only distinction made by the tool in the two cases is in the global stiffness properties of the laminates.

To evaluate if it is possible to model the two different cases by simply adapting the material properties, the tool prediction for a single-column joint with 3 fasteners is compared to numerical results for the same joint. The joint geometry was already introduced in Table 23, while the layup of the plates is M*-DL-D-C. Finger-tight torque conditions were defined for the three bolts. Since the frictional behavior of the joint is not dependent on the displacement direction, the conclusions for high bolt preload with tension loading equally apply here. The fastener formulation from Huth was employed with the analytical model.
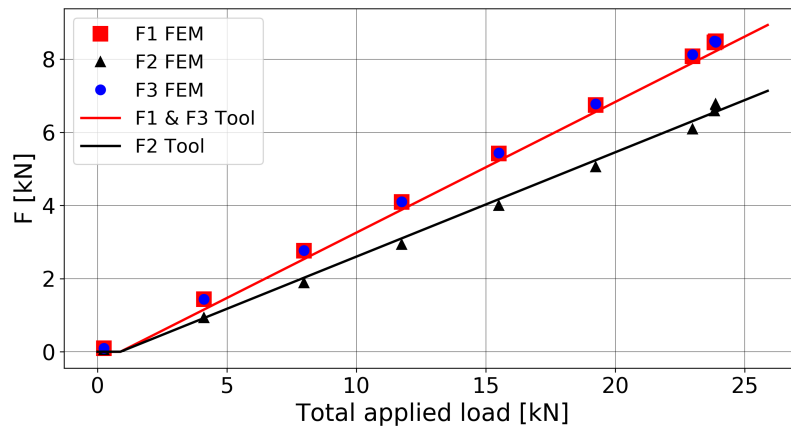
Figure 41: Force prediction comparison for $\boldsymbol{\lambda} = \{0, 0, 0\}$ with M*-DL-D-C

68

The first considered case is with $\boldsymbol{\lambda} = \{0, 0, 0\}$ clearance conditions and the force prediction comparison is shown in Fig.41. For equal clearance conditions at all bolts, the curves obtained from the two models show very good agreement. The similarity of the slopes confirms the accuracy of the fastener formulation and of the global stiffness calculation approach. At about 20 kN of total applied load, the load distribution obtained with the FE model is f_1=36.3%, f_2=27.2%, f_3=36.5%, while with the tool is f=35.7% at bolts 1 and 3 and f_2=28.5%. The relative differences are -2.2% at the most loaded bolt and 5.6% at the central bolt. The relative differences here are smaller than in a case of equal clearance in the experimental validation of tensile loading previously discussed.

The second considered case is $\boldsymbol{\lambda} = \{0, 40, 0\}$ and the corresponding results are shown in Fig.42. Also in this case, the slopes of the curves are similar, which leads to a rather good agreement in terms of load distribution. At about 20 kN, the load fractions predicted by the tool are f=41.8% at bolts 1 and 3 and f=16.5% at bolt 2. The forces extracted from the FE model lead to a load distribution of f_1=42.3%, f_2=15.0% and f_3=42.7%. The relative difference between numerical and analytical models is of -1.2% at the most loaded bolts and 9.1% at the central bolt.
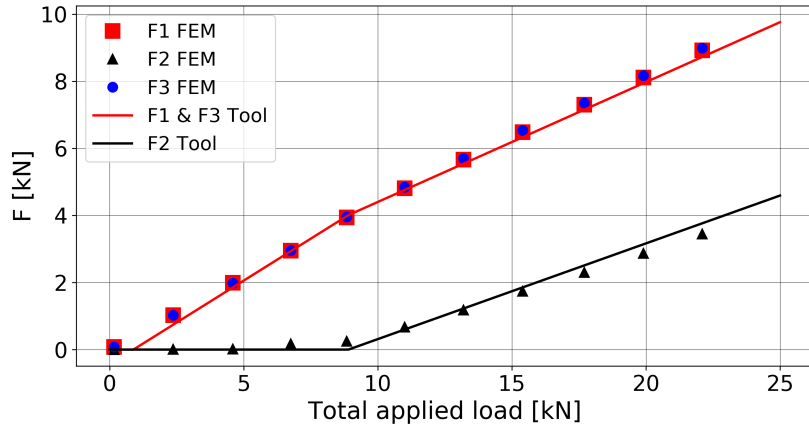
Figure 42: Force prediction comparison for $\boldsymbol{\lambda} = \{0, 40, 0\}$ with M*-DL-D-C

The differences between the two models are comparable to what was observed for tensile loading in the study on fastener flexibility of Section 6.1. In that case, the analytical model was observed to predict a more even distribution than the experimental data, as is the case here with respect to a numerical model.

Considering these results, it was concluded that the adopted approach for compressive loading shows an accuracy comparable to what was previously evaluated for tensile loading. Due to the similarity of the two loadings, only the latter is considered in the next sections, as it is believed that the two would show similar trends, both for single-lap and double-lap joints. It should however be noted that when modelling compression loading, unlike with tension, structural instability can be

triggered before the connected members or the bolts reach material non-linearity. The onset of buckling would influence load distribution but the tool would not be able to keep this phenomenon into account.

6.2.4   Conclusions on uniaxial loading modelling

Considering the achieved level of accuracy, reasonable for preliminary design, it was concluded that the details not accounted for by the analytical model can be neglected in a first approximation. A rigorous approach to quantify the impact of these neglected factors would be to carry out extensive parametric studies with numerical models. The influence of each parameter could be investigated individually to assess when phenomena that are ignored by the analytical model become relevant. Through these studies it would then be possible to set precise applicability limits of the assumptions underlying the analytical model.

6.3   Thermal loading modelling

In this section, investigations are presented to identify the factors influencing load distribution in presence of thermal loading and to quantify their impact. Being aware of the importance of these factors is especially relevant in the case of the analytical model for thermal loading. In fact, the model cannot account for some of the aspects that showed to have a fundamental impact on load distribution in other loading scenarios, such as bolt preload or the presence of clearance at a certain fastener. Moreover, a purely one-dimensional deformation due to thermal loading is considered by the analytical model, thus ignoring any other in-plane deformations. Another potentially relevant factor neglected by the analytical model is the expansion or contraction of washers and bolts, with only plates considered as thermally deformable.

Through the numerical investigations, the impact of the aforementioned factors was evaluated. For some relevant cases, a comparison between the results from the numerical models and the prediction from the model implemented in the tool is presented and discussed. The analytical model for the considered load case was presented in Section 4.1.3.

Considering the intended application of the tool, the most severe conditions for thermal loading correspond to a temperature decrease from 25° C to -55° C and an increase from 25° C to 110° C. These scenarios correspond to temperature differences of ΔT=-80 K and ΔT=85 K respectively. The studies carried out for the case ΔT=85 K, presented in this section, were deemed sufficient to evaluate the retained model.

6.3.1   Numerical modelling of CFRP plates with thermal loading

When computing load distribution under thermal loading, the computations of the FE models are based on the unidirectional properties of the prepreg material. An accurate estimation of the expansion properties for the entire laminate is fundamental to accurately predict load distribution under thermal loading. A suitable mesh of the composite plates is therefore necessary.

The numerical studies on thermal loading were carried out with a mesh as described in Section 5.6 with continuum shell elements. The modelling choice could not be directly compared to similar studies from the literature since no source specifically dealing with load distribution with composite joints under the considered loading was identified. However, Santiuste [25] numerically investigated the variation of the axial force due to preload in case of thermal loading in a composite joint. The modelling approach in the study was considered to be relevant to the case for thermal loading treated in this section.

Each ply in the composite plates was modelled by Santiuste individually with C3D8 elements. Adopting this kind of single-ply modelling would have required to completely re-evaluate mesh convergence and to compare the model against other relevant results. Such an approach was not possible due to time constraints. However, before proceeding with any study employing SC8R elements, a comparison of the two approaches was made in terms of global laminate CTE.

Two laminates were considered with both approaches. The laminates are rectangular plates of length l_0=100 mm and 10 mm of width. The plate thickness varied depending on the layup. The comparison between the two approaches was made by estimating the global CTE of the laminates from the plate deformation due to thermal expansion. A ΔT=60 K temperature increase[v] was applied to the plates, pinned at one end as shown in the Appendix (Fig.65). The laminate average displacement along X at the free end Δl_X was measured to estimate from the numerical models a global expansion coefficient along X, CTE_X:

$$\Delta l_X = l_0 \cdot CTE_X \cdot \Delta T \qquad \rightarrow \qquad CTE_X = \frac{\Delta l_X}{l_0 \cdot \Delta T} \tag{39}$$

This extraction of CTE_X was not intended to provide an accurate estimation of the value for the considered laminates but it rather served as a mean to evaluate the differences between the two approaches when modelling thermally induced deformation.

---

[v]This arbitrary value was used in the early numerical studies on thermal loading. The comparisons between numerical and analytical models were carried out with the relevant temperature differences

Part of the side view of the rectangular plate is shown in Fig.43 for the two approaches. The 0° ply direction was oriented along X, while Z was used to specify the stacking direction.

(a)   (b)
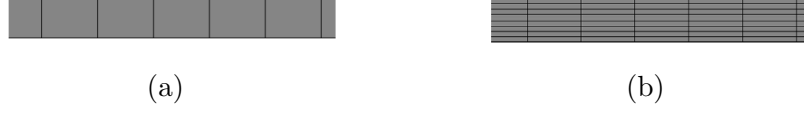
Figure 43: Partial side view of the plate for CTE comparison: (a) Continuum shell element, (b) Single-ply modelling

With both FE models, two hybrid M21/T700GC layups were considered. The material properties, among which CTE_1 and CTE_2, have already been introduced in Section 2.4. Taking advantage of part of the code introduced in Section 2.5, the laminates can be defined as:

- Q-H: $[45/m/-45/0]_s$

- D-H: $[0/45/0/-45/0/0/m/0]_s$

Where "m" indicates a metal sheet of thickness equal to that of composite plies in a hybrid laminate.

A temperature increase was applied to the rectangular plate as previously described. The values of CTE_X resulting from the extracted Δl_X displacements are presented in Table 26. With both the SC8R and the C3D8 models, the results for a quasi-isotropic laminate were calculated with three gradually refined meshes. For refinement factors between 1.5 and 2, no relative change of Δl_X larger than 1.5% was observed. The reported results were all calculated with the most refined meshes.

Table 26: Comparison of CTE_X with the two considered models

	$CTE_X \cdot 10^6 [K^{-1}]$	
	FEM SC8R	FEM C3D8
Q-H	8.55	8.75
D-H	3.99	3.86

The CTE_X values computed with the two approaches are fairly close, as shown in Table 26. A 2.3% relative difference is present for the Q-H laminate, while a slightly larger relative difference, equal to 3.4%, is observed for the D-H laminate. Interestingly, the CTE_X prediction with SC8R elements is larger than with C3D8 elements for the Q-H laminate but smaller for the D-H laminate. Additionally, by modifying the layups, the two models were observed to equally predict $CTE_X = CTE_1$ with only 0° plies and $CTE_X = CTE_2$ with all 90° plies.

Without a comparison with other relevant sources, it is not possible to draw a conclusion regarding which approach is more accurate. Nonetheless, it is possible to observe that the differences in terms of CTE_X prediction are small in the considered cases. Laminates such as Q-H and D-H were employed in the analyses of Section 6.3.5.

Before these numerical calculations, a brief mesh sensitivity study was also carried out for the mesh of a joint with SC8R elements to further increase the confidence on the numerical approach. The sensitivity analysis is presented in Section 6.3.2.

According to the Composite Materials Handbook [44], as reported by Esp [4], the analytical approach is "relatively accurate for [...] CTE properties". To evaluate the level of accuracy of this model, a comparison was carried out with FE models. In the comparison, constant material properties corresponding to ambient temperature conditions were assumed with both analytical and numerical models. In reality, expansion properties, and material properties in general, are temperature-dependent. If constant properties are assumed, values should be defined to represent as closely as possible the properties over the entire temperature range. While considering constant properties corresponding to ambient temperature may lead to inaccurate reaction predictions, the conclusions regarding model comparison are unaffected. In fact, the same properties are used as input for the analytical and the numerical models. It should be noted that in a FE model it would be possible to define different material properties for different temperature values, thus better capturing the physics of the entire temperature range. In this sense, detailed FE modelling shows clear advantages over an analytical approach.

6.3.2 Mesh suitability for thermal loading modelling

As mentioned in Section 5.8, mesh suitability was not directly assumed for thermal loading. Based on the findings of the mesh sensitivity analysis for uniaxial loading, a simplified approach to evaluate the independence of the results of simulations for LC5 was adopted.

To model a double-lap joint as described in Table 27, two levels of refinement were considered in the sensitivity study for thermal loading. The mesh for *Plate* and *Bolt and nut* was refined, while it was left unchanged for *Washer*, which showed to have very little relevance in earlier investigations. The divisions for edge seeding of the two meshes correspond to P2-W2-BN2 and P3-W2-BN3 and the meshes are shown in the Appendix (Figures 66 and 67).

Titanium A plates and steel B plate were considered in the joint[vi]. The sensitivity analysis was carried out with a 50 N preload for each bolt. Imposing a very small

---

[vi]The CTEs for titanium and steel were taken as equal to $2 \cdot 10^{-6}$ K^{-1} and $1 \cdot 10^{-6}$ K^{-1} here. Since convergence, and not the reactions, was of interest, the correctness of the properties was not relevant. In the comparison with the analytical model, the values from Section 2.4.2 were used

bolt preload was observed to facilitate the convergence of the numerical solutions. It was thus kept in all cases where nominally no preload was considered and, being the axial force about a sixth of the force in case of finger-tight torque conditions, this preload was believed to negligibly affect the behavior of the joint. The boundary conditions with LC5 were presented in Section 5.4.5.

Table 27: Double-lap geometry for mesh sensitivity study with LC5

N [-]	D [mm]	w [mm]	p_1 [mm]	l_{end} [mm]	t_A [mm]	t_B [mm]
2	8	40	32	56	2.08	4.16

A 60 K temperature increase was applied to the joint, leading to equal reactions, but of opposite direction, in the two bolts. With the coarser mesh, a 2.91 kN reaction was observed, while the force was 2.89 kN with the finer mesh. A small -0.7% change of the monitored variable was therefore observed for a significant refinement and the results were considered as independent of the mesh. P2-W2-BN2 was therefore employed in the following numerical studies.

Having identified an appropriate level of mesh refinement, comparison studies between the results from the tool and from the numerical model were carried out.

6.3.3 Comparison study for different bolt spacings

A first comparison was made for different bolt spacings. The key parameters of the double-lap geometry considered in the comparison study are summarized in Table 28.

Table 28: Double-lap geometry for comparison study of Section 6.3.3

N [-]	D [mm]	w [mm]	t_A [mm]	t_B [mm]
2	8	48	2.08	4.16

The spacing p_1 between the two bolts was varied, taking values of 3D, 7D and 9D. A spacing between fasteners of 3D corresponds to the smallest spacing considered in joint design at DLR with hybrid laminates, as reported by Fink [45].

In the study presented in this section, metal plates composing the joint were modelled, with titanium A plates and a steel central B plate. The material properties correspond to those described in Section 2.4. Considering isotropic plates allowed to only compare the results from the tool to the predictions of the numerical models for

cases in which the global laminate CTE_X was exactly known. No uncertainty due to CTE_X estimation by the tool is present for such a case. The influence of laminate layup on bolt reactions, and the accuracy of the CTE_X prediction by the tool, is analyzed separately in Section 6.3.5. Also, no preload or bolt-hole clearance were considered in the study of this section. These represent the conditions for which the tool is the closest to the numerically modelled joint and for which the highest agreement between the models was expected to be observed.

The bolt reaction prediction from the tool and from the numerical models are presented for the three bolt spacings in Table 29 for a temperature increase ΔT=85 K. Only F_1 is indicated since, for the considered conditions, equal reactions appear at the two bolts. The reaction F_2, while being equal in magnitude to the reaction F_1, is, of course, oriented in the opposite direction.

Table 29: FEM-Tool comparison under LC5 for different spacings

	$\mathbf{F_1}$ [kN]	
	FEM	**Tool**
$\mathbf{p_1=3D}$	1.05	1.27
$\mathbf{p_1=7D}$	2.70	2.55
$\mathbf{p_1=9D}$	3.27	3.07

Looking at the results of the comparison, a moderate agreement between models can be observed. For the smallest considered bolt spacing p_1=3D, the reaction predicted by the tool is 21.4% larger than the reaction from the numerical model. However, the prediction of the tool is not always conservative. For p_1=7D, the reaction calculated with the tool is 5.9% smaller than the reaction extracted from the numerical model. Also for the largest considered spacing p_1=9D, the analytical prediction is not conservative, in this case by 6.5%.

Overall, the predictions from the two models are fairly close. Both models indicate that the bolt reactions generated by thermal loading increase with bolt spacing. This was expected since, considering a linear thermal expansion as modelled in Eq.26, the elongation or contraction of the portion of plate between the fasteners is dependant on the bolt spacing. The larger the spacing, the larger the plate deformation, which in turn generates larger bolt reactions.

It is important to note once again that the conditions considered in these section were such that the factors neglected by the tool could not influence load distribution. For these favorable conditions, the agreement between models is moderate and the predictions by the tool not always conservative.

6.3.4 Comparison study for different clearance conditions

With the joint considered in Section 6.3.3 for p_1=3D, a study on the effect of bolt-hole clearance was carried out. A temperature increase of ΔT=85 K was implemented also in this comparison study.

Four different clearance conditions were implemented in FE models and compared to the prediction from the tool. All the defined clearance values are within the limits of the f7/H10 fit. Being the tool unable to take into account clearance, the same prediction is given by the tool for all possible clearance conditions. The bolt reactions for the comparison study are shown in Table 30.

Table 30: FEM-Tool comparison under LC5 for different clearance conditions

	FEM		Tool	
	$\mathbf{F_1}$ [N]	$\mathbf{F_2}$ [N]	$\mathbf{F_1}$ [N]	$\mathbf{F_2}$ [N]
$\boldsymbol{\lambda} = \{0, 0\}$	1050	-1050		
$\boldsymbol{\lambda} = \{40, 40\}$	10.3	-10.3	1270	-1270
$\boldsymbol{\lambda} = \{0, 40\}$	13.5	-31.9		
$\boldsymbol{\lambda} = \{0, 100\}$	13.7	-31.9		

By looking at the comparison between the two models, the tool is observed to provide very inaccurate predictions for any joint in which a non-zero clearance is present.

By not taking into account clearance, the tool translates any plate deformation into a source of bolt shearing. In presence of a temperature difference, the plates composing the joint deform differently and push, or pull, on the bolts. In reality, clearance allows the plates to deform, at least partially, without being in contact with the bolts. Therefore, not all plate deformation induces a shear load on the bolt since, as long as no bolt-plate contact is established, the plates deform freely. By not taking this phenomenon into account, the tool is unable to accurately predict bolt reactions. The bolt forces from the FE models are two orders of magnitude smaller than the predictions of the tool. As was already observed for uniaxial loading of a joint, clearance has the potential to greatly influence load distribution. It should be noted that the difference in reaction between F_1 and F_2 with $\boldsymbol{\lambda} = \{0, 40\}$ $\boldsymbol{\lambda} = \{0, 100\}$ corresponds to the load transferred by the joint through friction. A roughly 40 N friction load is in agreement with Eq.29 for the considered axial force.

By looking at the results of Table 30, it is clear that the case of zero clearance represents the case with highest reaction prediction for a 2-bolt joint, since the entire plate deformation generates bolt loads. Any type of clearance will reduce these loads. Assuming no clearance in a 2-bolt joint, however, is not sufficient to guarantee conservatism of the tool, as was already seen in Table 29 for bolt

spacings of 7D or 9D. Moreover, the fact that the reactions in a joint are maximum when considering no clearance cannot be generalized for joints with any number of fasteners.

Table 31: Double-lap geometry for comparison study of Section 6.3.4

N [-]	D [mm]	w [mm]	p [mm]	t_A [mm]	t_B [mm]
5	8	48	24	2.08	4.16

Let us consider a 5-bolt-double-lap joint as described in Table 31, where an equal spacing p is present between all fasteners. The joint is shown in Fig.44(a). The plate is composed of titanium A plates and a central plate B made of steel. If for some fasteners clearance were larger than for others, some fasteners would enter into contact with the plates sooner than others. If the difference in clearance between fasteners were sufficiency large, some of them would not be in contact with the plates altogether. The results of Table 30 have already shown that, for clearance values within f7/H10 tolerances such as $\lambda = \{40, 40\}$, it is possible for the interaction between bolts and plates to be so moderate that almost no loads appear. This was observed in a numerical model also accounting for bolt expansion. Two of such cases were considered with no contact assumed to take place at bolt 2, case (b), and bolts 2, 3 and 4, case (c). If no bolt-plate contact is present, the joint can be modelled, in first approximation, as if the fasteners with large clearance were missing. The two cases are shown in Fig.44(b) and (c). The loads arising in such joints were calculated with the tool for a temperature increase ΔT=85 K.
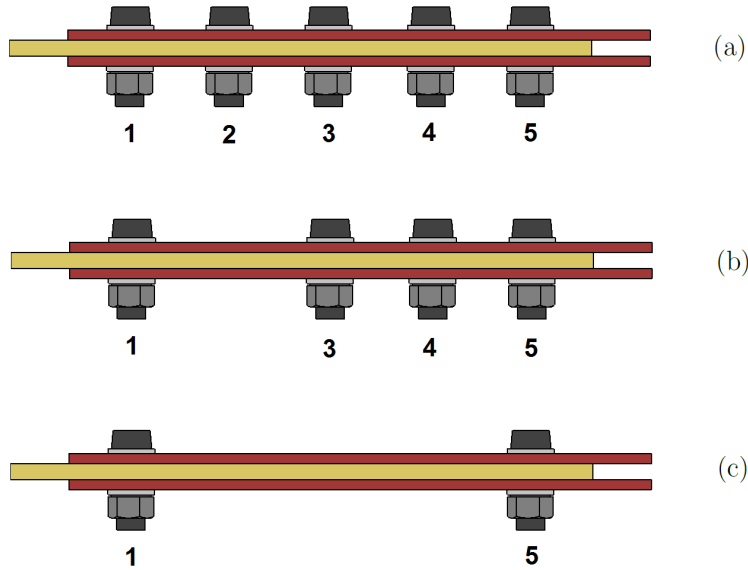
Figure 44: Joint geometry for the analytical investigation on clearance with LC5

It was already observed in Table 29 how increasing the distance between fasteners could increase the reactions due to thermal loading. The goal of the study was to evaluate if a similar behavior could be observed in cases (b) and (c), where the large clearance at some bolts led the actual distance between two adjacent bolts in contact with the plate to be increased. The interest was to better understand the physical behavior of the joint rather than correctly estimating the loads and the tool was deemed capable of providing this kind of insight. The results of the analytical calculations are summarized in Table 32.

Table 32: Results of the analytical investigation on clearance with LC5

	$\mathbf{F_1}$ [kN]	$\mathbf{F_2}$ [kN]	$\mathbf{F_3}$ [kN]	$\mathbf{F_4}$ [kN]	$\mathbf{F_5}$ [kN]
Case (a)	3.46	1.53	0	-1.53	-3.46
Case (b)	4.02		0.441	-1.23	-3.23
Case (c)	3.73				-3.73

The results of the analytical investigation confirm the assumption that an increase of the distance between adjacent fasteners in contact with the plates can in fact lead to an increase of bolt loads. In case (a), bolts 1 and 2 are separated by a distance of 3D. If the clearance at bolt 2 were such that contact were not established with the plate despite thermal expansion, bolts 1 and 3 would actually be the two adjacent bolts, separated by 6D. In this case, the maximum reaction in the joint increases by 14%. Similarly, in case (c) the largest bolt load in the joint increases by 7.2%.

Once again, the analytical study was carried out with the goal of improving the understanding of the physical behavior of the joint, rather than to precisely quantify loads. The findings of the study underline the dangers of neglecting the effect of clearance to predict bolt loads in thermal loading.

6.3.5 Comparison study for different laminate layups

For the study on the effects of laminate layup on bolt reaction, the joint presented in Section 6.3.3 for p_1=3D was considered again. The joint was subject to a ΔT=85 K temperature increase. The joint is composed by both metal plates and composite laminates.

The central B plate was modelled as a laminate and four different layups were considered. They are M-DL-D-C, M-DL-D-H, M-DL-Q-C and M-DL-Q-H. As described in Section 2.5, the hybrid layups differ from their purely composite counterparts for the 90° plies replaced by steel sheets. The top and bottom A plates were modelled as made of titanium. The results of the comparison between tool and numerical models are shown in Table 33.

Table 33: FEM-Tool comparison under LC5 for different layups

	F_1 [kN]		$CTE_X \cdot 10^6$ [K^{-1}]
	FEM	Tool	Tool
M-DL-D-C	-1140	-399	4.98
M-DL-D-H	-745	-470	4.71
M-DL-Q-C	-897	431	13.8
M-DL-Q-H	-23.7	229	10.6

The agreement of the two models is very bad. The FE models always predict a negative reaction at bolt 1, meaning that the expansion of the titanium plates is larger than for all the four laminates. However, this is not the case with the analytical model implemented in the tool. This difference of bolt reactions is largely due to the difference of the CTE_X prediction.

For M-DL-Q-H, a rough estimation of the equivalent CTE_X considered by the FE model was given in Table 26 for plates modelled with SC8R elements. The analytically computed CTE_X of $10.6 \cdot 10^{-6}$ K^{-1} is 19.3% larger than the estimation for the FE model. When evaluating CTE with an analytical method based on CLT, a discrepancy of this order of magnitude was already observed by Raghava [46] with experimentally measured values. This level of discrepancy leads to a very different reaction prediction from the two models. Being the CTE of titanium $8.6 \cdot 10^{-6}$ K^{-1}, the difference in CTE estimation between tool and FEM leads the former to consider the laminates to expand more than titanium with the quasi-isotropic laminates. This is not the case with the numerical models.

With the laminates for which the two models predict equally directed bolt reactions, the prediction by the tool would be non-conservative, if the numerical models were to be validated. It should be noted that the prediction from the analytical tool for small bolt spacings p_1=3D and metal plates, see Table 29, was larger than the prediction from the FE model. While more studies would be necessary to verify if this would always be the case for isotropic plates, the results from Table 33 show that a smaller prediction from the tool is given with the two composite layups M-DL-D-C and M-DL-D-H.

The results from Table 33 can also provide useful insight on laminate hybridization. Due to the highly questionable accuracy of the analytical results, only the bolt reactions from the FE model are considered in this discussion.

Hybridization can be used to reduce thermal loads in case of a joint composed by plates with different thermal expansion coefficients. In this sense, the potential of hybridization can be observed in the force reduction witnessed by replacing a M-DL-D-C laminate with M-DL-D-H. In this case, a 34.6% reduction of the bolt loads is calculated by the numerical models. By hybridizing the quasi-isotropic layup

M-DL-Q-C, the reduction of the thermal loads is even larger, with the M-DL-Q-H laminate leading to almost no bolt load due to thermal deformation. This result can be interpreted by looking at the CTE_X estimation with SC8R elements for such a laminate in Table 26. This value is very close to the CTE of titanium, so that all the plates in a joint with the M-DL-Q-H laminate deform almost equally.

While the beneficial effect of hybridization was shown, it is important to note that, in some cases, it could lead to larger bolt loads than with a purely composite laminate. This is due to the fact that the material of plates A, titanium here, has a smaller CTE than the steel used for layup hybridization. For moderate fractions of steel in the layup, as in M-DL-Q-H, hybridization can almost nullify thermally induced bolt loads. However, increasing the steel fraction beyond would only lead to larger loads. For small steel fractions, the laminate would expand less than the titanium plates, while the opposite would take place at large steel fractions.

6.3.6 Effect of bolt preload

Bolt preload was expected to have a beneficial effect in reducing bolt reactions due to thermal loading. In fact, if friction is sufficiently high to avoid, or at least reduce, plate deformation, a smaller reaction in shear takes place at the bolts. To verify this, a double-lap joint was numerically modelled with the dimensions as summarized in Table 34. In this case, a three-bolt joint was considered to also discuss the dependence of load distribution on the fastener number. Plates A were modelled with titanium, while the central plate with steel[vii].

Table 34: Double-lap geometry for investigation on bolt preload with LC5

N [-]	D [mm]	w [mm]	p_1 [mm]	p_2 [mm]	l_{end} [mm]	t_A [mm]	t_B [mm]
3	8	48	36	36	36	2.08	4.16

Applying a temperature increase of 60 K led to 1.85 kN reactions when a negligible bolt preload was applied, as shown in Fig.35. For intermediate torque conditions, the reactions at the external bolts were reduced, as anticipated, by 35%.

Table 35: Effect of preload on bolt reactions under LC5

Preload [kN]	F_1 [kN]	F_2 [kN]	F_3 [kN]
0.05	-1.85	0.00009	1.85
5	-1.37	0.00087	1.36

[vii]The same remark of footnote v applies here

These results show an agreement in terms of behavior of the analytical and numerical models. In fact, the analytical model is designed in such a way that a zero reaction always appears at the central bolt if N is odd. The numerical results also show the reaction at bolt 2 to be several orders of magnitude smaller than the reactions at bolts 1 and 3. For an even number of bolts, the analytical model predicts the reactions to be symmetrically increasing, in magnitude, with respect to the central point of the joint. Of course, they are oriented in opposite directions. All the numerical models investigated for N=2 showed this kind of symmetry and it is therefore believed that it would be equally observed with FE models for even N values larger than 2. As already observed in Section 6.3.4, these considerations apply to cases in which no bolt-hole clearance is present.

These findings underline how neglecting preload can be considered a conservative assumption, representing the worst case scenario in terms of bolt forces. Additionally, even if a precise estimation of bolt preload could be ensured for assembly conditions, preload could change greatly and in unpredictable ways in case of thermal loading. Ignoring preload could be a conservative approach allowing to ignore the uncertainties generated by temperature differences.

6.3.7   Conclusions on thermal loading modelling

When neglecting clearance and bolt preload, the investigations on a double-lap joint with two bolts and isotropic plates showed the analytical model to provide moderately accurate predictions. Conservative and non-conservative results were both obtained for cases of different bolt spacings, with predictions becoming less conservative as spacing increased, with the considered geometries.

The presence of clearance in a joint was observed to greatly influence bolt loads. The tool, being incapable of accounting for this effect, inaccurately predicted the bolt reactions. The inaccuracy nonetheless led to conservative reaction calculation for a joint with two bolts. Through an analytical investigation, the risks of a non-conservative prediction deriving from neglecting clearance for a joint with more than two bolts were underlined.

The above conclusions were drawn for joints composed of isotropic metal plates. The presented limits do not, therefore, take into account the accuracy of CTE estimation for the laminates. The uncertainty in the estimation of thermal expansion laminate properties was observed to greatly affect the agreement of the tool with the numerical models.

The beneficial effect of bolt preload was also stressed. Models not accounting for bolt preload with thermal loading give non-accurate but conservative predictions.

In conclusion, the investigated model for computing thermal loading is not considered sufficiently accurate, nor conservative, for joint design. The main factors

affecting both accuracy and conservatism of the model were observed to be clearance and the laminate global expansions property estimation. Due to the inaccuracy of the analytical model, no approach for modelling a combination of thermal and mechanical loadings was investigated. Also, the conclusions on the inaccuracy of the analytical model drawn for a temperature difference of ΔT=85 K rendered useless an investigation on the case ΔT=-80 K.

Finally, the potential of laminate hybridization to reduce bolt loads due to thermal loading was highlighted. Care should however be taken when considering hybridization of joints composed of both metal and composite laminates. If the metal sheets used for laminate hybridization have expansion properties different from those of the metal plates, hybridization can increase bolt loads due to thermal loading in some cases.

The lack of comparable studies in the available literature prevented the validation of the numerical models for thermal loading. The independence of the results from the level of refinement of the considered meshes was nonetheless demonstrated.

7 Investigations on the modified models

The numerical and analytical studies on the modified models presented in Section 4.2 are collected in this chapter.

7.1 Investigation on the models for shear loading analysis

Two models were considered to predict the load distribution in a bolted joint subject to shear loading (LC3) and were presented in Sections 4.1.5 and 4.2.2. To evaluate their applicability to joint design, a comparison study with the results from a FE model was carried out. Since both models do not take into account bolt preload, the comparison was made for finger-tight torque conditions. For the same reason, clearance conditions of $\boldsymbol{\lambda} = \{0, 0, 0, 0\}$ were considered.

7.1.1 Comparison for steel plates and bolts

The joint geometry and shear loading considered in the comparison study of this section is shown in Fig.45. It is a double-lap joint composed of ASTM A36 steel plates with thickness t_A=2.08 mm and t_B=4.16 mm.
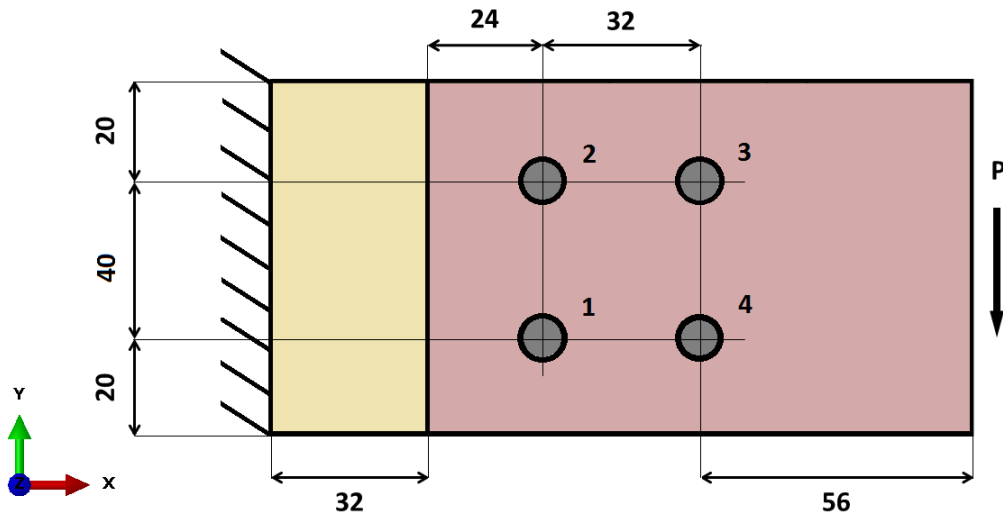
Figure 45: Joint geometry and bolt numbering for studies with shear loading

The four bolts employed in the connection, of 8 mm nominal diameter, are modelled with ASTM A325 bolt properties as described in Section 2.4. In the same section, the properties of the plates were presented. Such material properties correspond to the conditions for which the experimental data the original ICoR method relies on were derived. This material choice was made to allow for a fair comparison of the models.

Again, with the goal of allowing comparison between models, plastic deformation of the bolts was allowed in the FE model, since the modified ICoR method takes into account plastic deformation of the bolts. Plate deformation is considered to remain linear. The applicability of the modified ICoR method to composite structures is discussed in Section 7.1.2.

The comparison of the predicted loads between models was carried out for different values of the applied load P. The load only has a component along Y and is applied on the edge of the two A plates at a distance of 56 mm from bolts 3 and 4. Half the load is applied to the top A plate and half to the bottom A plate, so that the overall force P in the four considered cases was equal to 2 kN, 35 kN, 40 kN and 47.7 kN. They correspond to the dots shown on the curve of Fig.19, with Δ_{high} values of 0.01 mm 2.86 mm, 4.71 mm and 8.636 mm. Different stages of bolt deformation were thus kept into account.

The results at a generic location j are analyzed through the total bolt reaction as defined in Eq.25. The results for the Δ_{high}=4.71 mm case are presented in Table 36. The complete results for the other cases can be found in the Appendix (Section 11.9), while key points are summarized in Table 37 and Fig.47.

Table 36: Bolt loads comparison for Δ_{high}=4.71 mm (P=40 kN)

	FE model		Modified ICoR		Elastic	
	F [kN]	**f [%]**	**F [kN]**	**f [%]**	**F [kN]**	**f [%]**
Bolt 1	28.9	23.9	30.4	23.5	26.2	20.3
Bolt 2	28.6	23.6	30.4	23.5	26.2	20.3
Bolt 3	32.0	26.4	34.2	26.5	38.3	29.7
Bolt 4	31.7	26.2	34.2	26.5	38.3	29.7

The results in Table 36 show a good agreement between the modified ICoR method and the FE model in terms of load distribution, with maxima at bolt 3 of 26.5% and 26.4% respectively. The elastic method leads to slightly less accurate results, with variations of about 3.5%, both for the minimum and maximum f values. Both the elastic and the modified ICoR models give conservative predictions of the maximum fastener reaction. In this regard, the modified ICoR method is more accurate than the elastic method.

Looking at the results from the FE model in Table 36, it can observed how the reactions at the bolts close to the applied load P, bolt 1 and 2, are very close. They are respectively 28.9% and 28.6%. The same can be observed for bolts 3 and 4, which are further away from the load application point and have load fractions of 32.0% and 31.7%. This is not only true for Δ_{high}=4.71 mm but is confirmed by the data from all other cases reported in the Appendix. This aspect is of great

importance, since both the analytical models were defined in such a way that the reaction prediction is the same for all bolts at the same distance from the center of the considered rotation. These numerical results show that it can be reasonably assumed that the instantaneous center of rotation for a joint loaded in shear as shown in Fig.45 is located along the line passing through the fastener group's centroid and perpendicular to P. The assumption of rigid rotation of the joint is further investigated in Section 7.1.2. A typical von Mises stress contour plot for the four bolts is shown in Fig.46. The largest stresses in the picture correspond to the locations where the external load is mostly being transferred from the external A plates to the constrained central plate. The joint rotation induced by the eccentric load is discussed in Section 7.1.2 and with Fig.48 for CFRP plates but it can already be witnessed here. In fact, looking at bolts 3 and 4, the stress fields look rather similar but show an angular offset indicating that the bolt reactions are not oriented in the same directions for the two bolts.
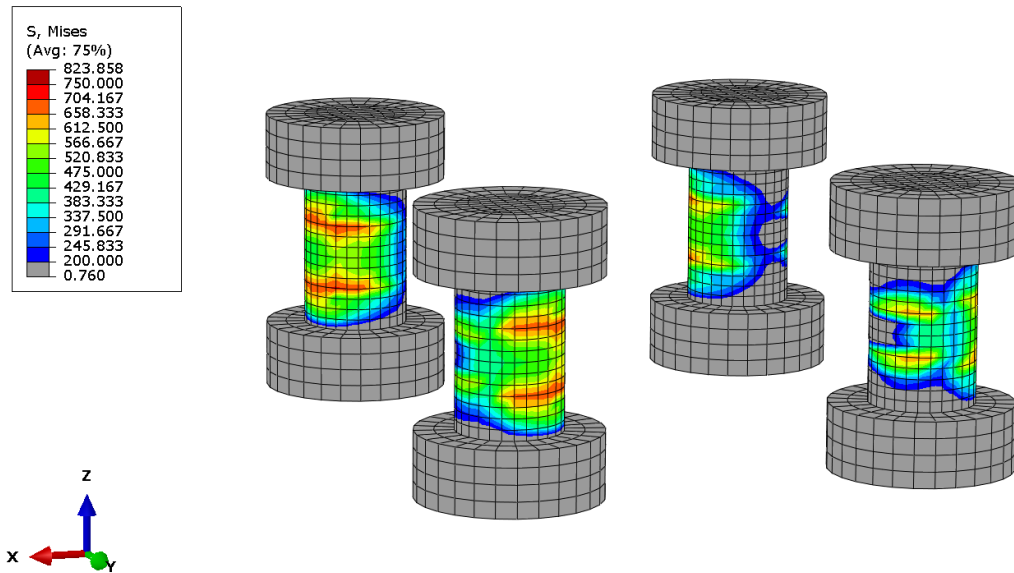
Figure 46: Von Mises stress contour plot for bolts 4,3,1 and 2 from left to right

Table 37 presents a summary of the results for all cases of load P which can be used to discuss accuracy and conservatism of the analytical methods. The ratios between the largest reaction extracted from the FE model and the largest reaction predicted by the modified ICoR method are reported in the second column. Similarly, the third column reports the maximum load from FE model divided by the maximum reaction calculated with the elastic method. Lastly, the largest reaction predicted by the ICoR method was divided by the largest reaction calculated with the elastic method and was reported in the fourth column.

The second column shows the accuracy of the modified ICoR method to increase

as the bolt deformation becomes larger. The method leads to mostly conservative predictions, with the only exception for the bolt failure case Δ_{high}=8.636 mm, with a discrepancy with the FE model of 1%. Apart from this underprediction, the method shows remarkable accuracy in predicting bolt failure. With the exception of this case, the modified ICoR method showed to conservatively predict the reactions at all bolts and for all Δ_{high} values.

Table 37: Ratios of the maximum predicted reactions

Δ_{high} [mm]	$\dfrac{\text{FEM}_{\text{max}}}{\text{Mod. ICoR}_{\text{max}}}$ [-]	$\dfrac{\text{FEM}_{\text{max}}}{\text{Elastic}_{\text{max}}}$ [-]	$\dfrac{\text{Mod. ICoR}_{\text{max}}}{\text{Elastic}_{\text{max}}}$ [-]
0.01	0.804	0.806	1.00
2.86	0.924	0.834	0.903
4.71	0.928	0.829	0.893
8.636	1.01	0.816	0.807

When only considering the highest reaction in the joint, the predictions obtained from the elastic method are always conservative, with quite significant overpredictions between 16.6% and 19.4%. It should however be noted that, while the elastic method has shown conservatism when looking at the most loaded bolt, it also underpredicts the load at the least loaded bolts. An example of such underprediction can be found in Table 36, where the load at bolt 1 extracted from the FE model is 28.9 kN against 26.2 kN calculated from the elastic method. As previously mentioned, the modified ICoR method was observed to lead to conservative predictions for the least loaded bolts at every Δ_{high} value.

The fourth column quantifies how much the reactions calculated with the modified ICoR method are smaller than those from the elastic method. For very small bolt deformation, Δ_{high}=0.01 mm, the two models provide almost identical maximum reaction estimations. This is no longer the case for larger bolt deformations, with an about 10% difference already at Δ_{high}=2.86 mm, reaching almost 20% at bolt failure conditions Δ_{high}=8.636 mm.

These results have great importance when considering the use of the tool for joint design. In fact, even in the case of a joint for which bolt shear failure is not critical, with bearing failure of the plate for example, the highest accuracy of the modified ICoR method would have a significant potential for better joint design. If the plate were expected to fail when the bolt deformation is still very small, the elastic method or the modified ICoR method could be used almost interchangeably to predict the largest reaction. However, for an intermediate bolt deformation, such as Δ_{high}=2.86 mm, a 10% smaller load could be considered thanks to the modified ICoR method, leading to a more lightweight design.

While the prediction of the largest reaction is almost equal with the two methods at small bolt deformation, the two methods being almost interchangeable in this sense,

the differences in terms of load fractions are always quite significant, as shown in Fig.47. The continuous lines indicate the evolution of the maximum of the four f values, $f_3=f_4$, as a function of Δ_{high}, while the dashed lines represent the minimum values, $f_1=f_2$. Based on these results, the analytical models were compared to the FE model.
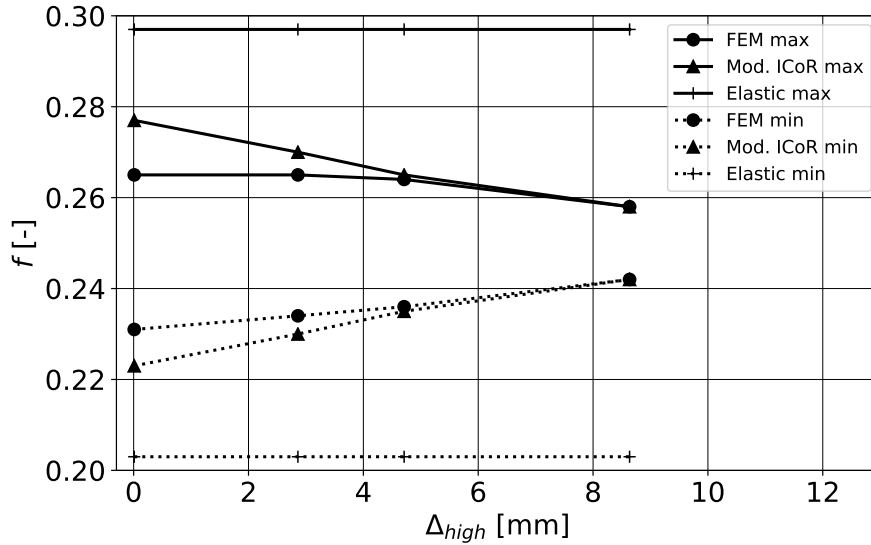
Figure 47: Comparison of load fraction evolution for the shear loading models

Looking at the curves for the elastic method in Fig.47, no change in load distribution is observable, with f=20.3% at bolts 1 and 2 and f=29.7% at bolts 3 and 4. This is a consequence of the fact that with the elastic method the load fraction at a certain fastener is dependent on the joint geometry and load application point but not on the load magnitude. Therefore, increasing P does not affect the load distribution, as Fig.47 shows. The model always overpredicts the load fraction at the most highly loaded bolts and underpredicts it for the least loaded ones. These inaccuracies are about 14% for small bolt deformation and increase as Δ_{high} gets closer to the bolt failure value of 8.636 mm. This increase in inaccuracy is dependant on the appearance of load re-distribution due to plastic deformation of the bolts, which cannot be taken into account by the elastic method.

Similarly to the elastic method, the modified ICoR method tends to overpredict the load fraction at the most loaded bolts and underpredict it for the least loaded fasteners. Unlike the elastic method, however, this method can account for load re-distribution due to plastic deformation of the bolts. For increasingly deformed bolts, the load distribution from the modified ICoR method gets closer to the prediction from the FE model. At Δ_{high}=8.636 mm, the two distributions are almost identical, the largest discrepancy being 0.1% at bolts 2 and 4, see Table 59.

A 4-bolt-double-lap joint was considered for the study of this section. An extension to single-lap joints of the conclusions drawn above is justifiable by the fact that, both the elastic method and the original ICoR method are formulated indifferently for single or double-lap joint configurations, the bolt allowable in shear being the only parameter influenced by such a distinction. The original ICoR method can also be equally employed for different bolt patterns, thus not limiting the conclusion of this section to 2-by-2 joints. Generally, the respect of the assumptions underlying the ICoR method, presented in Section 4.2.2, is of higher importance than joint configuration and bolt group geometry.

Finally, although omitted in this section, the AISC Manual of Steel Construction [19] suggests the use of safety factors[viii] with both the elastic method and the original ICoR method. If the modified ICoR method were to be employed for joint design in the future, further studies would be necessary to first establish suitable factors of safety.

7.1.2 Applicability of the modified ICoR method to CFRP

The analyses of Section 7.1.1 showed that the modifications to the original ICoR method allow to extend its applicability to predicting load distribution in steel joints at conditions for which bolt failure is not assumed. In this section, the applicability of the modified ICoR method to other plate materials, specifically CFRPs, is discussed. It is particularly important to verify the respect of the assumption that the connected parts remain rigid also for materials with moduli of elasticity smaller than steel.

It should be noted that the method is not directly dependent on the material properties of the plates. However, the empirical data for bolt deformation of Fig.19 are indirectly influenced by the plate deformation. Evaluating the magnitude of this influence is a key point of this section.

No information about the original ICoR method's applicability to materials other than steel was found in the literature, having the method been developed for civil engineering applications. Segui [39] mentions that it can be used with little error for steels of different grades. However, the stiffness properties of steels of different grades are rather similar and this consideration cannot be directly extended to the case of CFRPs.

To investigate the effects of reducing the plate modulus of elasticity, a series of FE studies were carried out as shown in Table 38. These studies were repeated only modifying the plate modulus of elasticity for the same joint geometry presented in Fig.45 and for an applied load P=35 kN. Also in this case, $\boldsymbol{\lambda} = \{0, 0, 0, 0\}$ conditions were modelled. These analyses considered fictitious plate materials with moduli

---

[viii]Two different approaches (ASD and LRFD) are possible to evaluate strength allowables, see Specification for Structural Steel Buildings [47]

of elasticity equal to 90%E_{A36}, 75%E_{A36} and 40%E_{A36}, where E_{A36} is the Young's modulus for ASTM A36 steel plates presented in Section 2.4.

The results presented in Table 38 indicate that the fastener reactions seem to be only slightly affected by the variation of the plate modulus of elasticity. The largest change in load distribution takes place at bolts 1 and 2, with a variation of 0.3%. Overall, the reactions at the least loaded bolts increase while the reactions at the most loaded bolts become smaller.

Table 38: Influence of the modulus of elasticity of the plates on load distribution for Δ_{high}=2.86 mm (P=35 kN)

	FEM 90%E_{A36}		FEM 75%E_{A36}		FEM 50%E_{A36}	
	F [kN]	f [%]	F [kN]	f [%]	F [kN]	f [%]
Bolt 1	25.3	23.8	25.4	23.9	25.6	24.1
Bolt 2	25.0	23.5	25.1	23.6	25.4	23.8
Bolt 3	28.1	26.4	28.1	26.4	28.0	26.3
Bolt 4	27.9	26.3	27.9	26.2	27.7	26.0

Reducing the Young's modulus of the plates, despite obviously influencing the overall joint displacement, seems to have very little impact on the load distribution. The applicability of the method to CFRPs was then evaluated through a comparison of the model prediction with results from FE models. Two layups were considered to investigate if the difference in modulus of elasticity of composite materials in different directions could influence the accuracy of the analytical prediction.

The plate geometry of Fig.45 was considered once again. A 15 kN shear load was modelled, corresponding to a bolt deformation prediction by the modified ICoR method of Δ_{high}=0.409 mm. Two laminate layups were considered in the study, M-DL-D-C and M-DL-Q-C, with the 0° ply orientation aligned with X and Z as stacking direction. The global stiffness properties of the plates, derived through CLT, are presented in the Appendix (Table 60). The in-plane moduli of elasticity of the quasi-isotropic laminate are about a quarter of the value for A36 steel plates. A comparison of the results is presented in Table 39.

The load distribution from the numerical models for the two composite layups is shown in the second and third column of the table. The modified ICoR method cannot account for different plate properties and its load prediction is presented in the fourth column. Additionally, the results from the elastic method for equivalent conditions were reported in the Appendix (Table 61).

Table 39: Bolt loads comparison with CFRP plates for Δ_{high}=0.409 mm (P=15 kN)

	FEM [M-DL-D-C]		FEM [M-DL-Q-C]		Modified ICoR	
	F [kN]	**f [%]**	**F [kN]**	**f [%]**	**F [kN]**	**f [%]**
Bolt 1	10.9	24.0	11.2	24.2	10.5	22.2
Bolt 2	10.8	23.8	11.1	24.0	10.5	22.2
Bolt 3	11.8	26.1	11.9	25.8	13.2	27.8
Bolt 4	11.8	26.1	12.0	25.9	13.2	27.8

According to the results from the FE models, the load distribution with a quasi-isotropic laminate M-DL-Q-C is more homogeneous than with M-DL-D-C, which has higher stiffness along the X direction. The variations with the two layups were, however, very slight, never exceeding 0.2%. The largest reaction appears at bolt 4 for the M-DL-D-C layup. The modified ICoR method conservatively overpredicts this load by 10%, while the overprediction is of 11.9% with the quasi-isotropic layup for the same fastener. The reactions at bolt 1 are underpredicted by -3.7% and -6.25% with M-DL-Q-C and M-DL-D-C respectively. Overall, a rather good agreement of the prediction from the modified ICoR method and the numerical results was observed. It should be noted that, while also leading to a conservative estimation of the largest reaction, the elastic method is less accurate than the modified ICoR method in estimating the largest reaction, with a 20% overprediction for the quasi-isotropic layup.

To further investigate the applicability of the method to CFRPs, the bolt displacement was monitored. In fact, the ICoR method assumes the rigidity of the connected parts in order to justify a rotation around a point defined as the IC. To verify that the assumption of rigid rotation is respected for a considered CFRP joint, the displacement for all bolts was extracted from the FE model for M-DL-D-C. Considering the bolt displacement as the hole surface average displacement at the central plate, the displacement values shown in Table 40 were extracted.

Table 40: Bolt displacement from FE model with M-DL-D-C

	Bolt 1	Bolt 2	Bolt 3	Bolt 4
X displacement [mm]	-0.139	0.133	0.179	-0.171
Y displacement [mm]	-0.457	-0.442	-0.806	-0.822

A representation of the displacement vectors is shown in Fig.48, where proportionality between vector components was maintained. Considering the vector directions, perpendicular lines were drawn to evaluate if the four bolts were rotating around a common center. The lines corresponding to bolts 1 and 2, the closest to the rotation

center, meet at x=-66 mm, y=20.1 mm, while the intersection for bolts 3 and 4, the two further away from the center of rotation, is at x=-61 mm, y=19.3 mm.

The difference in prediction for the Y coordinate of the center of rotation is of 0.8 mm, only 2% of the bolt group height. This small discrepancy justifies in this case the assumption that, for an applied load P with no component along X, the center of rotation is located on a line perpendicular to P and passing through the bolt group centroid. For the bolt pattern of the modelled joint, the centroid is located at x=16 mm, y=20 mm.

The difference between the two intersections over X is of 5 mm. This variation is also rather small, about 8% of the distance between either one of the two intersections and the fastener group centroid.

Overall, for the considered laminate material and layup, the results show that it is possible to assume with little error the existence of a common center of rotation of the joint. It is important to note that the material properties considered in this case are significantly different from those of steel plates, with which the experimental data for the ICoR method were derived.
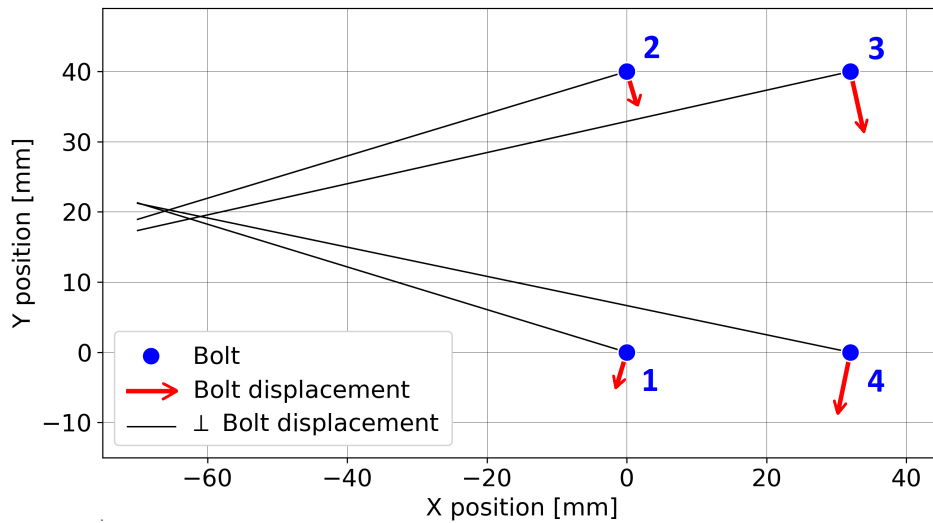
Figure 48: Joint rotation under shear loading with M-DL-D-C

The comparison with FE models, as well as the considerations regarding the rigidity of the connected plates, indicate that CFRP joints behave similarly to steel joints, at least as long as the fundamental assumptions are respected. With the considered geometry and loading, the modified ICoR method could be used to conservatively estimate the largest reaction in the joint. Given the similarities between CFRP and steel joints, the accuracy of the prediction with the former can be expected to increase in cases of more relevant bolt deformation. In fact, as the results of Section 7.1.1 showed, the agreement of the modified ICoR method with numerical

results increased with bolt deformation, which here was considered as very low, with Δ_{high}=0.409 mm. The best agreement was observed at bolt failure conditions, with almost identical load distribution predictions. Already for small bolt deformation considered here, the method allowed for a significantly more accurate prediction compared to the elastic method.

The analyses of this section consider linear deformation of the plates and no damage modelling in the laminates was implemented in the FE models. The applicability of the modified ICoR method to bearing critical joints at failure conditions, where the material non-linearity could affect the rigidity assumption for the plates, was not investigated. Further studies on the matter could provide significant insights while, as an approximation, it may be assumed that the joint deforms rigidly until failure arises.

It was demonstrated that, when respecting the hypothesis of plate rigidity, the modified ICoR method could be used with the experimental data from [21] to analyze load distribution in joints with A325 or metric 8.8 bolts. The applicability of the original method was extended to different plate materials. For the material and geometric conditions considered for comparison, the influence of laminate layup showed to be negligible. These considerations are of primary importance if the model were to be employed with different bolt materials or grades. In fact, after having derived similar empirical relations for fasteners other than metric 8.8, it would not be necessary to derive several relations for different plate materials or laminate layups. The small relevance of these factors when plate rigidity is ensured would allow the application of a relation for one fastener material to different plates and laminates.

7.2 Single-column approach justification for uniaxial loading

The analytical model evaluated in Section 6.2 was shown to provide a good prediction of the load distribution in multi-row-single-column joints subject to uniaxial loading. With the goal of broadening the applicability of the tool, a strategy for the analysis of multi-column joints is proposed in this study as presented in Section 4.2.4. Based on the results of numerical studies, considerations regarding the applicability of the proposed approach, also in presence of clearance and bolt preload, are presented in this section.

7.2.1 The case of perfectly tight bolt holes

A uniaxial tensile load was considered to be applied to a double-lap joint. Such a joint has identical columns with equal spacings between fasteners in the loading direction. Moreover, for all bolts, the bolt shank diameter is exactly equal to the

bolt hole diameter, so that $\boldsymbol{\lambda} = \{0, 0, 0, 0\}$. Lastly, all the bolts share the same preload value. Such a joint is perfectly symmetric, both in geometry and loading conditions, with respect to the center line along which the load P is applied.

With the single-column approach, the two columns would be analyzed independently. This approach would be justified not only if the stress distribution in the two columns were equal but if the stress distribution generated around a hole in a single-column joint by an applied load P/2 were equal to the stress distribution generated by P in a two-column joint.

This condition is assumed to be verified if the columns are sufficiently distanced for the stress distribution around the holes not to influence each other. In order to verify this assumption for highly distanced columns, a numerical study was carried out. Such a study also had the goal of verifying if the no-influence assumption is applicable for the smallest fastener spacings commonly considered in joint design.

Based on the work by Fink [45], typical minimum values of column width to bolt diameter ratios of 4 are employed at DLR for CFRP joints. Values of 3 would be possible in case of hybrid laminates. A factor of 4 is then considered for minimum bolt pitch.

A double-lap joint with top and bottom generic steel plates and a composite central plate was considered in the numerical study. The plates are assembled with 4 titanium bolts with a nominal diameter of 8 mm. Two different laminate layups were modelled for the central plate: M-DL-D-C and M-DL-Q-C. Finger-tight torque conditions were modelled for all the bolts. The geometry of the central plate is shown in Fig.49(a). It should be noted that the load P is a graphic representation and not an actual boundary condition of the model. The load is indirectly generated by imposing a displacement of the plate edge, as described in Section 5.4.2.
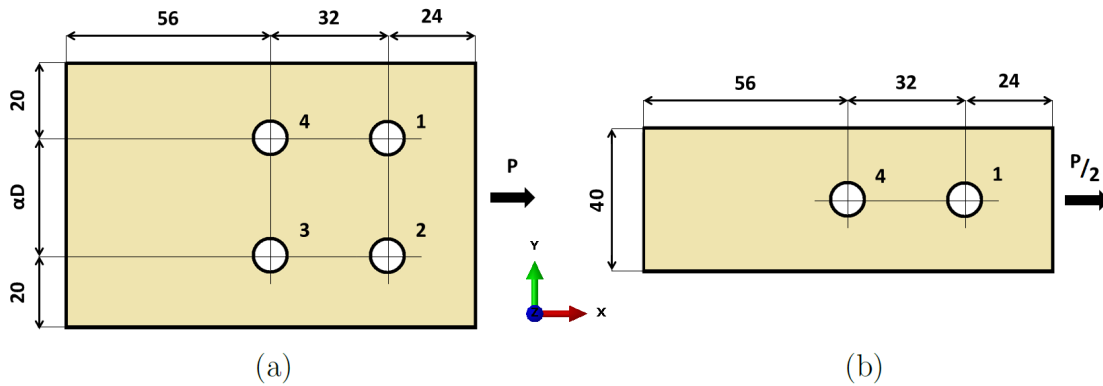
Figure 49: Two columns or *2-col* approach (a) and single-column or *1-col* approach (b) for $\boldsymbol{\lambda} = \{0, 0, 0, 0\}$

The distances of bolts 1-2 from the left plate edge and of bolts 3-4 from the right

plate edge were taken as equal to the geometry from the mesh sensitivity study for consistency and given the similarity in dimensions. The bolt pitch along X was set to the minimum value indicated by Fink for M8 bolts.

For both layups, the numerical study was carried out by modelling the joint in Fig.49(a) for different values of the parameter α. The load distributions for these two-column models were compared to those obtained by a single-column numerical model as in Fig.49(b). To verify the no-influence assumption with the numerical study, the loads F_1 and F_2 in the two-column models were expected to be equal and close to F_1 obtained in the single-column joint. Similarly, F_3 and F_4 in the two-column models were expected to be equal and close to F_4 in the single-column joint.

The results of the numerical studies are presented In Tables 41 and 42, where F_{sum} indicates the sum of the fastener reactions. As was the case for the mesh sensitivity study, the fraction of load transferred by friction is small due to low preload, which is reflected in the small difference between P and F_{sum}. For the two-column joints the values f_1, f_2, f_3 and f_4 indicate the fastener reactions as a percentage fraction of F_{sum}. The values reported with brackets refer to single-column joints. These values were divided by two to facilitate the load distribution comparison with the two-column joints.

Table 41: Load distribution with M-DL-D-C and $\boldsymbol{\lambda} = \{0, 0, 0, 0\}$

Joint	P [kN]	F_{sum} [kN]	f_1 [-]	f_2 [-]	f_3 [-]	f_4 [-]	u_x [-]
1-col	18.4	17.9	(28.1)			(21.9)	
2-col $\alpha = 4$	34.3	33.4	28.3	28.3	21.7	21.7	0.2
2-col $\alpha = 5$	36.8	35.9	28.1	28.1	21.9	22.0	0.2
2-col $\alpha = 7$	40.6	39.7	27.9	27.9	22.1	22.1	0.2
2-col $\alpha = 12$	43.9	43.1	27.9	27.9	22.1	22.1	0.2

Table 42: Load distribution with M-DL-Q-C and $\boldsymbol{\lambda} = \{0, 0, 0, 0\}$

Joint	P [kN]	F_{sum} [kN]	f_1 [-]	f_2 [-]	f_3 [-]	f_4 [-]	u_x [-]
1-col	14.0	13.5	(30.1)			(19.9)	0.2
2-col $\alpha = 4$	26.0	25.0	30.7	30.7	19.3	19.3	0.2
2-col $\alpha = 5$	28.2	27.3	30.1	30.1	19.9	19.9	0.2
2-col $\alpha = 7$	32.2	31.2	29.3	29.3	20.7	20.7	0.2
2-col $\alpha = 12$	37.3	36.4	28.7	28.7	21.3	21.3	0.2

The applied load was obtained by imposing a displacement at the free end of the plates u_x of 0.2 mm. It should be noted that, since the two-column joints do not

all have exactly the double of the joint stiffness of the single-column joint, imposing the same displacement does not generate a load P in the two-column cases which is exactly the double of the single-column case. A rigorous approach would have been to apply to each case a u_x such that P in the double-column joint were precisely the double of P in the single-column joint. However, considering the linearity of the material deformation and the absence of clearance, the load distribution was expected to be almost independent from the applied load, once the slip-critical force had been overcome. Therefore, the applied loads were considered sufficiently close to the desired values to be acceptable. A stricter modelling approach was observed in the analysis of Section 7.2.2, where imprecisions in the applied load would greatly affect the results.

For both layups and for all column spacings, the results validate the no-influence assumption. Looking at f_1 in Table 41, very small variations between single-column and two-column can be observed, the maximum deviation being +0.2% for $\alpha = 4$ and -0.2% for $\alpha = 7$ and $\alpha = 12$. Equal variations can be observed for f_4. The symmetry of the problem is reflected in the symmetry of the results, with f_1 equal to f_2 and f_3 equal to f_4. It is therefore not necessary to focus on f_2 and f_3 for both tables. The variations in Table 42 are larger, with a maximum of 1.4% at $\alpha = 12$.

In both tables, particularly good agreement was observed between the single-column case and the two-columns case for $\alpha = 5$. Firstly, this is due to the fact that, for such an α value, the column spacing is still large enough for the stress distributions of the two columns not to influence each other. In addition to this, the load P for the considered α is almost exactly the double of the load in the single-column case, thus rendering the two cases as precisely comparable as possible.

It is of great importance that, for the smallest spacing between columns considered $\alpha = 4$, the load fractions f_1 and f_4 are very similar to the single-column case, with a maximum discrepancy of 0.6% with M-DL-Q-C. Considering the load distribution in the two columns separately would lead to a reasonably accurate prediction even for the smallest spacing considered in joint design.

In both tables can also be observed how the variation between single-column and two-columns models increases for an increase of columns spacing. This is considered to be a consequence of the modelling imprecisions linked to the imposed displacement, not an actual phenomenon. An additional factor that could justify this increase in variation is the influence of the plate edge on the stress distribution. In fact, for an increase of α, the 20 mm distance in Fig.49(a) was not modified, so that the bolt holes get relatively closer to the lateral edge of the plates. The influence of these effects could have been avoided by scaling this distance together with α, thus keeping the same ratio for all cases. Such an approach would have made the modelling more complex and, since the results were only slightly influenced, the modelling approach was not changed.

7.2.2 The case of different bolt-hole clearance

In the analysis of Section 7.2.1, an ideal scenario was considered. Together with equal preload conditions, no bolt-hole clearance was assumed to exist at every fastener location. A numerical study was performed to evaluate the shortcomings of the single-column approach in case of a non-zero clearance in the joint. The same joint geometry was considered, with the only exception of a 100 μm bolt-hole clearance modelled at fastener 2. The clearance conditions in this study were therefore $\boldsymbol{\lambda} = \{0, 100, 0, 0\}$. The previously introduced approach of repeating the analysis for different α values was adopted.
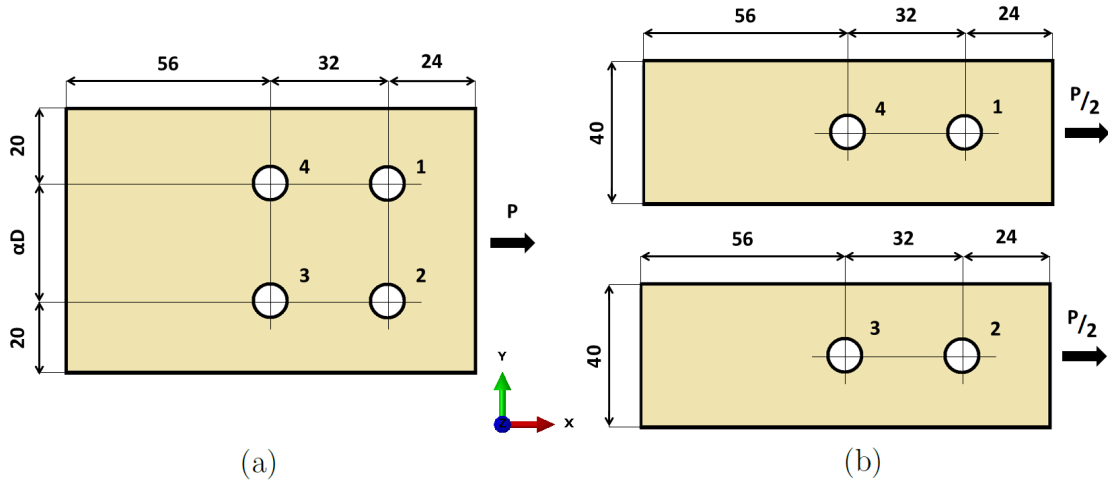
Figure 50: Two columns or *2-col* approach (a) and single-column or *1-col* approach (b) for $\boldsymbol{\lambda} = \{0, 100, 0, 0\}$

Introducing the clearance as described could potentially lead to serious inaccuracies with the single-column approach shown in Fig.20. In fact, in a real 4-bolt joint, as soon as the load P is large enough to overcome the friction effects due to preload, reactions appear at bolts 1,3 and 4. However, no reaction takes place at bolt 2 until the applied load is sufficient to generate a joint displacement such that the bolt-hole clearance is taken-up. Unlike the scenario considered in Section 7.2.1, such a load distribution introduces a moment in the joint, which is then reacted by the same three bolts through force components along the Y axis of Fig.50. The FE model is capable of capturing this effect but that would not be the case for a tool modelling each column as individual. The goal of the numerical analysis was to quantify the inaccuracy of the single-column approach for a pessimistic scenario, in which a large clearance is present at one of the bolts.

Tables 43 and 44 show the results of the numerical investigation. Two single-column FE models as shown in Fig.50(b) were employed to obtain the reactions at bolts 1 and 4 separately from 2 and 3. These two numerical models were equal in geometry

96

and loading, with the only exception of the clearance at bolt 2 in one FE model. The results of these simulations were reported in the Appendix (Section 11.10). From these results, the first line of the tables was calculated. The additional information in the Appendix provides clarification about how the load distribution for the single-column approach was calculated. Based on those results, the reader can simply interpret the values f_1 to f_4 as the load fraction at the respective fastener for an applied load of about 42 kN in Table 43 and 32 kN in Table 44. For the *1-col* cases, these values should not be intended as fractions of F_{sum}, which was indicated in brackets to avoid possible misinterpretations.

Table 43: Load distribution with M-DL-D-C and $\boldsymbol{\lambda} = \{0, 100, 0, 0\}$

Joint	P [kN]	F_{sum} [kN]	f_1 [-]	f_2 [-]	f_3 [-]	f_4 [-]	u_x [-]
1-col	21.3	(20.8)	28.1	11.3	38.7	21.9	0.3
2-col $\alpha = 4$	42.2	41.3	33.8	6.5	33.8	25.9	0.28
2-col $\alpha = 5$	41.8	40.9	33.0	6.5	34.7	25.9	0.26
2-col $\alpha = 7$	42.2	41.3	32.4	6.7	35.1	25.9	0.24

Table 44: Load distribution with M-DL-Q-C and $\boldsymbol{\lambda} = \{0, 100, 0, 0\}$

Joint	P [kN]	F_{sum} [kN]	f_1 [-]	f_2 [-]	f_3 [-]	f_4 [-]	u_x [-]
1-col	15.9	(15.5)	30.1	8.9	39.6	19.9	0.3
2-col $\alpha = 4$	31.8	30.8	38.1	3.9	33.8	24.2	0.28
2-col $\alpha = 5$	31.8	30.9	36.1	4.4	35.4	24.2	0.26
2-col $\alpha = 7$	31.0	30.0	34.8	3.3	36.9	25.0	0.225

As anticipated, the introduction of a clearance breaking the horizontal symmetry of the joint can have a significant impact on the load distribution.

For the highly directional laminate of Table 43, the two-column models showed the reaction along the X direction at bolt 3 to be the largest, followed by bolt 1, 4 and 2. The single-column approach manged to predict correctly this order of importance.

In the case of the quasi-isotropic laminate of Table 44, for $\alpha = 4$ and $\alpha = 5$, the reaction at bolt 1 is larger than at bolt 3. This effect was not predicted by the single-column approach, which always predicted the largest reaction at 3. It should be noted that, in both Table 43 and 44, the reaction at bolt 1 can be observed to become less prominent when increasing α, while the reaction at 3 showed the opposite trend.

Generally, the single-column approach tended to underestimate the reactions at bolt 1 and 4 and overestimate the reactions at 2 and 3. Considering both composite

layups, the largest difference in prediction between single and multi-column approach was 8% for $\alpha = 4$ at bolt 1 with the quasi-isotropic laminate.

It is of great importance to note that, despite larger inaccuracies with respect to Section 7.2.1, the largest reaction predicted by the single-column approach was always larger than the largest reaction extracted from the multi-column models. This aspect, together with the quite pessimistic clearance conditions in the considered joint, could qualify the single-model approach as conservative.

As mentioned, the clearance conditions of the joint were considered as pessimistic. This is partly due to the fact that the 100 μm clearance corresponds to the largest possible value for typical joint fitting tolerances, as presented in Section 2.2. In addition to that, unlike in the considered case $\boldsymbol{\lambda} = \{0, 100, 0, 0\}$, bolts 1, 3 and 4 would also have a non-zero clearance in reality. The presence of bolt-hole clearance at other locations would generate a beneficial delay in load-take up at those bolts too, not just at 2. The more similar the clearance at the four bolts, the more accurate the prediction of the single-column approach. In fact, if the exact same clearance value were present at every bolt, the rotational effects considered in this section would not appear. The discussion of Section 7.2.1 would equally apply to such a case, with a simple delay in load take-up, equal for all bolts.

Table 45: Y reactions with M-DL-D-C and $\alpha = 5$

Joint		$\mathbf{F_1}$ [kN]	$\mathbf{F_2}$ [kN]	$\mathbf{F_3}$ [kN]	$\mathbf{F_4}$ [kN]
1-col	**X**	11.7	4.7	16.1	9.13
	Y				
2-col $\alpha = 5$	**X**	13.5	2.65	14.2	10.6
	Y	0.247	0.426	-0.736	-0.0761

It has already been mentioned that the rotational effects generated by the non-symmetric clearance were reacted by the bolts through forces along the Y direction. Such forces cannot be kept into account by the single-column approach. Table 45 shows an example of the predicted reactions by single and multi-column approaches. The reactions along Y can be easily observed to be of a smaller order of magnitude compared to the reactions along X. A factor of about 20 separates these reactions at bolt 3, where the largest loads were observed. These effects can be ignored, at least in a first approximation, and do not influence the considerations on conservatism of the single-column approach.

7.2.3 Conclusions on single-column approach

On the basis of the results of Section 7.2.1, the single-column approach is considered suitable to model multi-column joints subject to uniaxial loading in case of perfectly tight bolt holes. Satisfactory accuracy was observed for all values of bolt spacing commonly considered in joint design.

Similarly, the use of the single-column approach with clearance, investigated in Section 7.2.2, showed to give conservative results if joint design is made considering the reaction at the most loaded bolt. The appearance of reactions to balance rotational effects was observed to be of negligible importance. This kind of study was therefore allowed with the tool.

Lastly, the effects of bolt preload were not investigated. If preload were the same in every column, then using the single-column approach would pose no problem as every column would behave exactly in the same way. If preload were different at different bolts, the sticking-to-slipping transition behavior could be affected. However, this is equally true for single-column and multi-column joints subject to uniaxial loading. The assumption of equal preload at all bolts made in the preload model for single-column joints was extended to the multi-column case. Thus, the analysis of multi-column joints was defined in the tool with equal preload at all bolts.
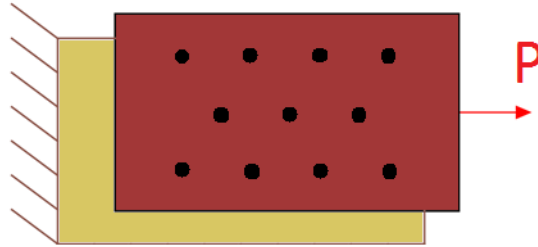
Figure 51: Example of bolt pattern not investigated for tool analysis

The joint considered in the numerical studies had four bolts but the conclusions are believed to be applicable to cases of different number of rows and columns. In fact, it was shown that, even with the minimum spacings in the two directions considered in joint design, the no-interference assumption of the stress states holds. This conclusion does not depend on the number of fasteners but on the fact that the bolts are sufficiently far not to influence the stress distribution around each other. It is worth mentioning again that equal bolt spacings in the loading direction were assumed in every column.

Fig.51 shows an example in which this assumption is not respected. The applicability of the tool to this kind of load pattern was not investigated. It is possible

that the single-column approach would lead to predictions with a level of accuracy comparable with the case of equal spacings, at least if a minimum distance between all fasteners were ensured. Once again, it is important to ensure the non-influence of stress distributions around the bolts. Symmetry of the bolt pattern with respect to the line along which P is applied could also play a role in the validity of the no-influence assumption. However, without sufficient data, it is impossible to draw a conclusion regarding these speculations. Having uniaxial loading of such a joint not been sufficiently investigated, it was not included in the cases handled by the tool.

7.3 Biaxial loading modelling

As introduced in Section 4.2.5, the tool is capable of predicting load distribution in joints subject to biaxial loading through a superposition of the reactions for two uniaxial loadings.

In this section a discussion of the results for load distribution obtained with superposition is presented. For all cases, tension loading was considered in both loading directions. On the basis of the discussion in Section 6.2.3, it is assumed that different combinations of compression loading can be equally modelled by superposition. Therefore, the discussion for tension loading in both directions is assumed to apply, at least in first approximation, to cases of compression-compression loading and to tension loading in one direction and compression in the other.

With the goal of evaluating the feasibility and accuracy of the superposition approach, only cases of zero bolt-hole clearance and no preload were considered. A discussion on their effects on load distribution with biaxial loading is presented in the end of this section.

7.3.1 The importance of boundary conditions definition

Fig.52 shows the mesh for a FE model of a joint subject to biaxial loading. The geometry was adapted from the joint considered for shear and uniaxial loading, such as in Fig.45. The plates were modified to allow for the introduction of a tensile load P_Y and boundary conditions at the central plate BC_Y. As in previous studies, the central plate was modelled with M-DL-Q-C layup, with the 0° ply orientation aligned with X and Z as stacking direction. The titanium top and bottom plates were modelled with an isotropic elastic material behavior. The four titanium bolts have a nominal diameter of 8 mm.

The considered cross geometry does not correspond strictly to the geometry of the entire joint, as it was considered that the plate portion surrounding the fasteners does not need to be fully represented. The arms of the cross were introduced for the

application of boundary conditions. A similar approach was used by Kapidžić [23] for modelling thermal loading perpendicular to the axial loading direction.

It is important to note that the presence of boundary conditions along two different surfaces, BC_X and BC_Y, introduced a fundamental difference with respect to cases of uniaxial loading. A zero displacement along X and Y was imposed on a single edge for uniaxial loading, as shown in Fig.28. Any point of the yellow central plate not belonging to the surface where these boundary conditions had been applied was free to move in any direction. If also in the biaxial loading case no displacement along X and Y were imposed on both BC_X and BC_Y in Fig.52, the plate deformation along a single direction would be significantly different from the case of uniaxial loading. This effect clearly has an impact on the accuracy of any prediction based on superposition.
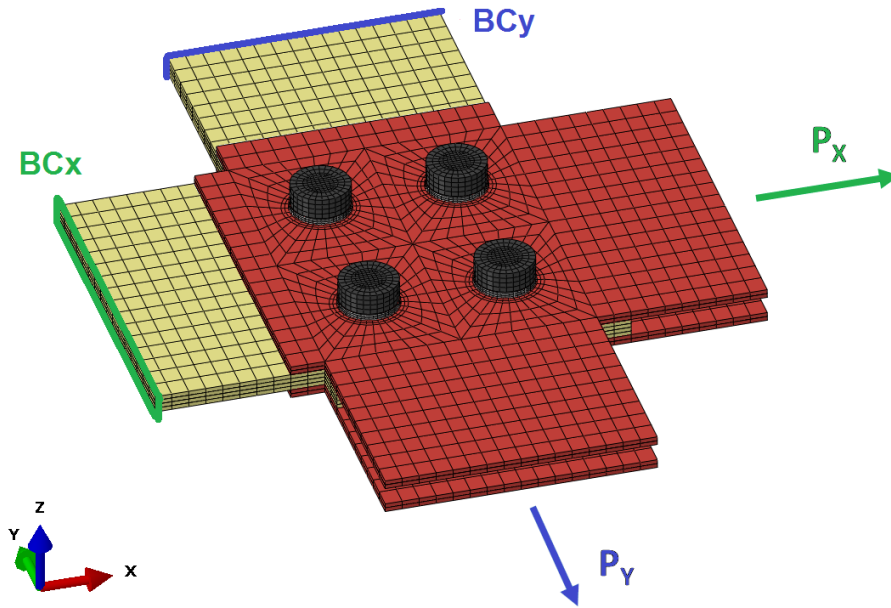
Figure 52: Boundary conditions definition and mesh for FE model of a joint under biaxial loading

To evaluate the impact of the boundary conditions definition on load distribution, two FE models with the two different definitions were compared. Both have a geometry as shown in Fig.53 and were subject to the same tensile loads, with $P_Y=0.78P_X$. Only these loads were considered in this analysis but the effects of the applied load on load distribution are discussed in detail in Section 7.3.3. The edge length s is equal to 40 mm for all cases considered in this section unless otherwise specified.

In the first FE model, whose results are presented in Table 46 under the name *1D BCs*, the boundary conditions on the surfaces BC_X and BC_Y were different. On the former surface, no displacement along X and Z was imposed, while on the latter only

the displacement along Y was set to zero. As a consequence, only on BC_X a force reaction in the X direction was present, while a reaction along Y could only take place at BC_Y. Since on each boundary condition surface reactions could appear in only one direction, these conditions were named *1D BCs*.
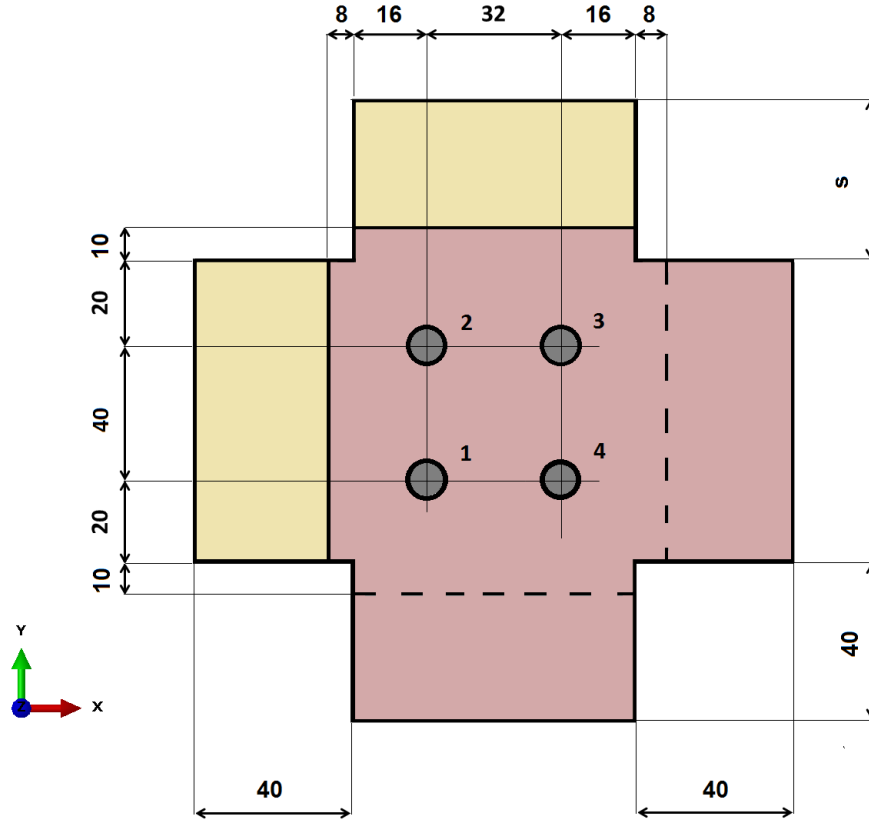
Figure 53: Joint geometry and bolt numbering for a joint under biaxial loading

The other FE model similarly had boundary conditions at both BC_X and BC_Y, but with no displacement possible along X and Y on both surfaces. Additionally, on the former surface no displacement along Z was also imposed to avoid rigid body motions. In Table 46, the load distribution with this FE model is indicated as *2D BCs* since, on both surfaces, reactions appeared in two directions with the implemented boundary condition formulation. The reaction forces along X and Y were extracted both from BC_X and BC_Y and compared to the applied loads P_X and P_Y. The terms X_{re} and Y_{re} are used to indicate the fractions of the P_X and P_Y loads respectively which were reacted on a surface where boundary conditions had been applied. The definition of load fraction f_j from Eq.38 was maintained, bearing in mind that a fastener reaction F_j can have components $F_{X\text{-}j}$ and $F_{Y\text{-}j}$ in the two spatial directions and that the total reaction is given by Eq.25.

Looking at Table 46, the largest variation in terms of load fraction takes place at

bolt one, with a variation of 1.8%. The variation at bolts 2 and 3 is roughly 1%, while bolt 4 is almost unaffected. As already mentioned, the boundary conditions definition in *2D BCs* changes the central plate displacement and the location where it reacts the applied loads. It should be noted that in the considered geometry the plate edge is located at a distance from the fasteners roughly equivalent to the bolt spacing.

Table 46: Load distribution with different boundary conditions

	f_1	f_2	f_3	f_4	$\mathbf{BC_X}$		$\mathbf{BC_Y}$	
	[%]	[%]	[%]	[%]	$\mathbf{X_{re}}$ [%]	$\mathbf{Y_{re}}$ [%]	$\mathbf{X_{re}}$ [%]	$\mathbf{Y_{re}}$ [%]
1D BCs	27.6	25.4	27.1	19.9	100	0	0	100
2D BCs	29.4	24.7	26.1	19.8	84.5	30.4	15.5	69.6

Only load fractions and not force reactions were reported in the table. It is important to note that a direct comparison of the two cases is possible since, for the same applied loads P_X and P_Y, the load transferred by the bolts is the same and does not depend on the definition of the boundary conditions. The sum of the fastener reactions in any of the two directions is the same in both cases. However, the boundary conditions have an influence on how the central plate deforms, which can have an impact on how the same transferred load is distributed among the fasteners. A comparison of the central plate displacement with the two modelling approaches is shown in Fig.54.
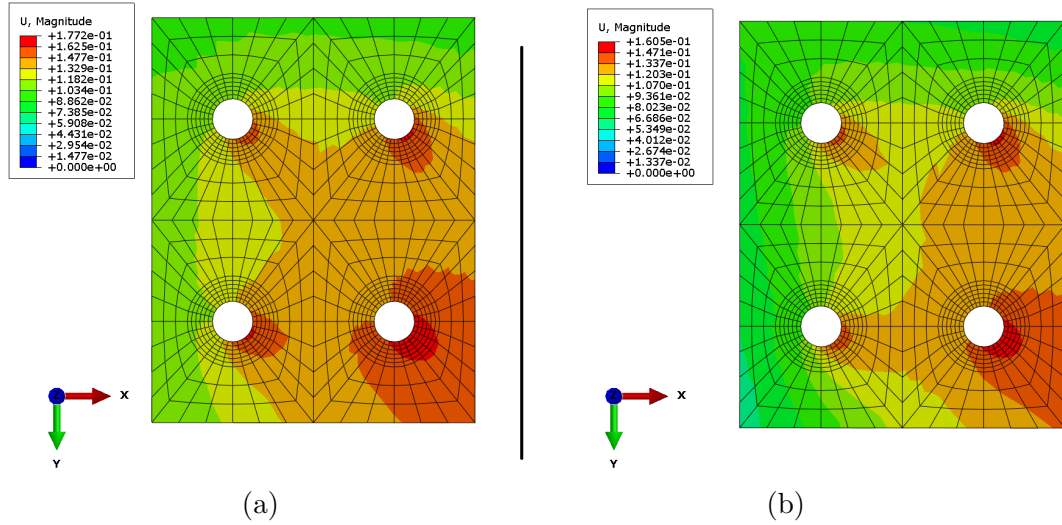
Figure 54: Central plate displacement with *1D BCs* (a) and *2D BCs* (b)

2D BCs boundary conditions correspond to the reality of a joint which is pinned at the considered locations. However, the effect on plate displacement from boundary

conditions definition cannot be captured by a model based on superposition. In the studies of the next sections, boundary conditions as in *1D BCs* are considered, to evaluate feasibility and accuracy of the superposition approach without the influence of additional effects. Boundary conditions as in *1D BCs* correspond to a case in which the plate edges are sufficiently distant from the fasteners not to greatly influence load distribution. For sufficiently far away edges, the two approaches are expected to lead to the same results. A parametric study on the impact of edge distance is presented in the Appendix (Section 11.11)

7.3.2   Superposition approach evaluation

A joint with four bolts was considered in the previous section for a numerical study. The same joint was considered again for comparison of the tool's prediction obtained from superposition of uniaxial loadings along X and Y with numerical models. To evaluate if the accuracy of the superposition approach increases with bolt spacing, the comparison between tool and FE model was performed for three different joint geometries but equal bolt diameters.

The tool considers individual strips to evaluate bolt reactions as shown in Fig.20. In the joint geometry of Fig.53, the strips have a width of 40 mm for loads in the X direction and 32 mm for loads along Y. This corresponds to a normalized strip width of 5D and 4D respectively. These values are close to the minimum spacings considered in joint design at DLR as presented in Section 7.2.1. The two additional joint geometries considered in this section are based on a scaling of the first joint geometry. A linear scaling factor SF is defined such that for SF=1 the joint geometry corresponds to the joint of Fig.53. All the dimensions were scaled in the same way, so that, for example, the plate width of 80 mm with SF=1 becomes 160 mm with SF=2 and 240 mm for SF=3. A summary of the strip width for the three geometries is provided in Table 47. Scaling the entire geometry avoids the risk of edge effects influencing the analysis as was observed in Section 7.2.1.

Table 47: Summary of strip width for the considered joint geometries

	Normalized strip width	
	Load along X	Load along Y
SF=1	5D	4D
SF=2	10D	8D
SF=3	15D	12D

For all cases, the imposed displacements resulted in forces of about P_X=23 kN and P_Y=18 kN, so that P_Y=0.78P_X. The global elastic properties of the laminate were

derived with CLT and are summarized in Table 60. Table 48 shows the results for the three geometries with the two models.

The geometries were defined solely with the goal of validating the assumption that the superposition approach is more accurate for large bolt spacing. Therefore, the fact that a strip width of 12D or 15D might be too large for the design of a real joint was deemed as unimportant.

Table 48: Load distribution comparison for three joint geometries subject to biaxial loading

		f_1 [%]	f_2 [%]	f_3 [%]	f_4 [%]
SF=1	**Tool**	25.2	27.8	25.0	22.0
	FEM	27.6	25.4	27.1	19.9
SF=2	**Tool**	25.3	27.8	24.9	22.0
	FEM	27.1	25.2	26.7	21.0
SF=3	**Tool**	25.3	27.8	24.9	22.0
	FEM	26.9	25.2	26.5	21.3

Looking at the comparison of the two models in Table 48, a few remarks can be made.

Both models predict the smallest reaction to take place at bolt 4. The difference in load fraction at this bolt ranges from 2.1% at SF=1 to 0.7% at SF=3. The tool leads to a prediction of the smallest reaction at bolt 4 since it is the least loaded bolt when considering both uniaxial loading along X and along Y.

The tool also leads to similar reactions at bolts 1 and 3, which is due to the similar bolt spacing in the two directions. In fact, bolt 1, together with 2, has the largest reaction for loading along X but the smallest for loads along Y. For bolt 3 the opposite is true. If the bolt spacing in the X and Y directions were the same, instead of 32 mm and 40 mm for SF=1, the reactions f_1 and f_3 would be the same in biaxial loading. For all geometries, the FE model confirms the reaction at bolt 1 to be similar to but larger than the reaction at bolt 3. The discrepancy with the tool is always larger at bolt 1, with a tool underprediction going from 2.4% with SF=1 to 1.6 with SF=3.

The most evident difference between the two models involves the reaction at 2. In fact, the results from the tool, unlike the prediction from the FE model, always show this load fraction to be the largest, as bolt 2 is the most loaded both in the uniaxial loading along X and along Y. As a consequence, the largest reaction predicted by the tool, while always being larger than the largest reaction from the numerical models, is not observed at the same location.

Generally, the results show a tendency of the accuracy of the superposition approach to increase for larger strip width. In fact, the average absolute difference[ix] between the predictions at the four bolts with the two models decreases from 2.26% with SF=1, to 1.81% with SF=2 and finally 1.66% with SF=3.

The results of this section showed the level of accuracy of the superposition approach for a joint loaded with P_X=23 kN and P_Y=18 kN. Before drawing any conclusion on the validity of the superposition approach for biaxial loading, an analysis on the role of the applied load was necessary and is presented in Section 7.3.3.

7.3.3 Load influence on the accuracy of biaxial superposition

In the evaluation study of the superposition approach, applied loads were considered such that P_Y=0.78P_X. Considering how the tool was designed to predict reactions with biaxial loading, the magnitude of the tensile load along one direction is only relevant when compared to the applied load in the other direction. In fact, due to the linearity of the geometry and materials, increasing P_X would lead to a larger displacement along X but equal load distribution. The same would take place for the reactions with a load increase along Y. Therefore, if P_X and P_Y were increased, or reduced, by the same factor, the load fractions along X and along Y would be equally affected. Being the total load fractions f_1 to f_4 a composition of the fractions along X and Y, they would also remain the same.

To confirm this behavior of the tool, the load distribution obtained from two FE models with different applied loads is analyzed here. The two models consider the same joint geometry, already modelled in Section 7.3.2 for SF=1. While the magnitude of the applied loads in the two models is different, their ratio is the same and equal to P_Y=0.93P_X, as shown in Table 49.

Table 49: Effects of applied load on load distribution with biaxial loading

P_Y/P_X [-]	P_X [kN]	P_Y [kN]	f_1 [%]	f_2 [%]	f_3 [%]	f_4 [%]
0.93	18.9	17.6	27.1	25.4	27.7	19.7
0.93	9.53	8.88	27.3	25.5	27.7	19.5

A comparison of the load fractions at the four bolts confirms the validity of the behavior of the tool, as no variation larger than 0.2% is observed. Despite the differences already discussed in Section 7.3.2, both the tool and the numerical models are indifferent to changes in applied load as long as the same proportionality is kept. Once again, the problem is linear both in terms of geometry and of materials, because of the strictly elastic behavior of the deformed parts. Having this assumption

---

[ix]Calculated as $\frac{1}{4}\sum_{k=1}^{4}(|f_k^{Tool} - f_k^{FEM}|)$

106

of linearity been confirmed for the considered case, it is believed that repeating a similar study for applied load ratios other than $P_Y=0.93P_X$ would lead to the same conclusions. As a consequence, for fixed joint geometry, the only parameter influencing the accuracy of the superposition approach is the ratio of the applied loads P_X and P_Y, while their absolute magnitude has no role.

Therefore, load distribution for different values of the P_Y/P_X ratio was calculated with both the tool and FE models. The considered ratios were 0.09, 0.14, 0.44, 0.78 and 0.93. The results are presented in the graph of Fig.55.

For small values of P_Y/P_X, the loading scenario is close to a case of uniaxial loading over X. Load distributions similar to those observed in Section 7.2.1 for a strictly uniaxial case are expected to be observed here. As the ratio increases towards one, the reactions in the Y direction become increasingly more relevant. The analysis was limited to the domain of P_Y/P_X between 0 and 1, since considering a case where P_Y is 2 times larger than P_X, for example, would show the same trends observed at $P_Y/P_X=0.5$ when P_X is 2 times larger than P_Y.
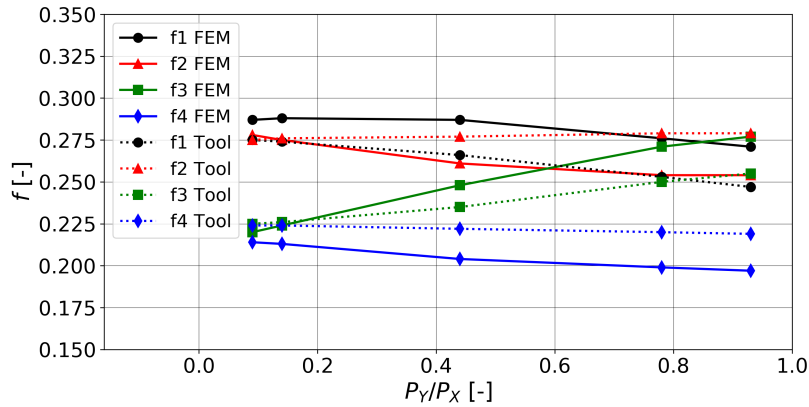
Figure 55: Comparison of load fraction predictions with superposition approach and FE model

The results of Fig.55 confirm the anticipated behavior for small P_Y/P_X values, with a load fraction f_1 similar to f_2 and f_3 similar to f_4. As the load ratio increases, the reactions at the four bolts change. The tool and the FE models show the same trends for bolts 1, 3 and 4, with the first and the last decreasing and the second increasing, but do not predict the same magnitude of change. Bolt 3 shows the clearest example in this regard: the load fraction at $P_Y/P_X=0.09$ is very similar, with a 0.5% difference, and both curves increase with P_Y/P_X. However, the curve from the tool is steeper, so that at $P_Y/P_X=0.93$ the difference is 2.2%. The load fraction for bolt 2 has a trend with the numerical results that is not fully captured by the superposition approach. In fact, the analytical model predicts an almost constant load fraction f_2, while the results from the FE model show a decrease

107

until $P_Y/P_X=0.78$, when the curve stops decreasing at 25.4%. The reduction of f_2, together with f_1 and f_4, in the numerical curves, is balanced by the already mentioned steep increase of f_3.

Generally, the predictions of the two models are reasonably close, with an average absolute difference going from 0.7% at small load ratios increasing to 1.72%, 2.26% and 2.34% at P_Y/P_X equal to 0.44, 0.78 and 0.93 respectively. However, the inaccuracy of the tool is sufficient to lead to an erroneous prediction of the largest reaction location. In fact, the tool always predicts the largest reaction to take place at bolt 2. This is due to the fact that, considering the loadings both along X and along Y, it is in the most loaded row. When combining the loads in the two directions to calculate the total reaction with Eq.25, F_2 is always the largest reaction. A possible explanation for this can be found in the modelling of the deformation direction. For uniaxial loading, the plates are known to deform in the direction of loading. Global laminate stiffness properties can be calculated and implemented in the tool knowing the exact deformation direction. In case of biaxial loading, the plate deformation is neither oriented along X nor Y. Fig.54 showed the bolt displacement in a case with $P_Y/P_X=0.78$ to take place in a direction somewhere in between the X and Y axes. As a consequence, the material properties on which the computation of the tool is based becomes more and more inaccurate. A proof of this could be found in the difference between $f_j^{FEM} - f_j^{Tool}$ which, for any value of j, is strictly increasing with the ratio P_Y/P_X. In other terms, the more biaxial effects become relevant, the larger the discrepancies.

Considering the maximum reaction predicted by the two models, the tool is conservative at P_Y/P_X equal to 0.78 and 0.93 with relative differences of 1.05% and 0.75%. For smaller load ratios, the relative difference is larger, with a value of 4.46% at $P_Y/P_X=0.14$.

The results presented here refer to a joint geometry with a scaling factor SF=1, so that the bolt spacings over X and Y of 5D and 4D are roughly equivalent to the minimum values considered for joint design at DLR. Based on the results of Section 7.3.2, the same trends can be expected to be observed for larger bolt spacings but with a larger accuracy of the tool. As already mentioned, the average absolute difference of load fractions drops from 2.26% to 1.66% for $P_Y/P_X=0.78$ going from SF=1 to SF=3.

7.3.4 Conclusions on biaxial loading modelling

Overall, for the considered conditions, the superposition approach for biaxial loading led to fairly accurate predictions. The accuracy was observed to be only dependant on the applied load ratio P_Y/P_X. The average absolute difference between the predictions from the tool and the numerical models is about 0.7% for quasi-uniaxial loading and increases as P_Y/P_X gets closer to 1, with a value of 2.34% at $P_Y/P_X=0.93$.

It was also concluded that increasing the distances between fasteners leads to more accurate tool predictions. For bolt spacings comparable to the minimum values considered in joint design, the average absolute difference of load fractions is equal to 2.26%.

The distance between the fasteners and the plate edges where boundary conditions are applied was also observed to influence load distribution. The considerations presented in this chapter apply to joints in which the plate edges are sufficiently distant from the fasteners not to greatly influence load distribution. A parametric study to estimate the impact of edge distance is presented in the Appendix (Section 11.11).

The predictions of the largest reaction in a joint was observed to be non-conservative in some cases. In addition to this, the fact that the tool incorrectly predicts the location of the largest bolt reaction raises concerns regarding the ability of the tool to fully capture the physical behavior of the joint with biaxial loading. Further investigations with different bolt patterns and plate materials are necessary to reach a definitive conclusion. In further studies, the impact of clearance should also be taken into account to evaluate the magnitude of the uncertainty it introduces.

8 Parametric studies

With the goal of providing a better understanding of the influence of key parameters on load distribution in bolted joints, parametric studies were carried out and are presented in this section. The trends observed in the results provide useful information in the context of joint design. The results of these studies are purely analytical and not derived from numerical models.

8.1 Parametric study on the uniaxial loading model

In this section are presented the results and the analysis of the studies on the geometric parameters affecting load distribution for uniaxial loading. As the tool is designed to analyze each joint column individually, the parametric studies are limited to a single-row joint. Extending the analysis to multi-column joints would not provide a better insight on the joint behavior.

A double-lap joint with three bolts is considered in the parametric studies. On the basis of model similarity, it is assumed that the same trends observed for a double-lap joint would be witnessed in the case of a single-lap configuration. The analyses were carried out for two different layups: M-DL-D-C and M-DL-Q-C. Only finger-tight torque conditions were considered since the analytical model considers preload as a source of delay in load take-up, which would have no influence on load distribution.

For all cases, a single parameter was modified at once. The non-modified parameters were kept as defined in the baseline geometry, presented in Table 50. The load distribution for an applied tensile load P=29.5 kN is the only monitored quantity in the parametric studies.

Table 50: Baseline geometry for parametric studies of Section 8.1

N [-]	D [mm]	w [mm]	p_1 [mm]	p_2 [mm]	l_{end} [mm]	t_A [mm]	t_B [mm]
3	8	48	36	36	36	2.08	4.16

As previously mentioned, when modelling a joint with the plates A having a combined stiffness equal to the stiffness of plate B, and with $p_1 = p_2$, the reactions predicted by the model at bolt 1 and 3 are exactly the same.

8.1.1 Effects of joint geometry on load distribution

As the effects of bolt-hole clearance on load distribution are analyzed in Section 8.1.2, the clearance conditions for the present parametric studies is $\boldsymbol{\lambda} = \{0, 0, 0\}$.

The results of the parametric studies are presented in Fig.56, where the load fraction curves are differentiated on the basis of the layup with letters "Q" and"D" for M-DL-Q-C and M-DL-D-C respectively.

The first modified parameter is the bolt pitch. Fig.56(a) shows the distribution evolution, where p=p_1=p_2. At baseline conditions the ratio p/D is equal to 4.5. An increase of bolt pitch leads to increasingly loaded external bolts, while the central bolt load fraction drops from 30% to about 24% with both layups. The change in load distribution due to bolt pitch variation appears to be linear.

Fig.56(b) shows the influence of variations of the w/D ratio on load distribution. Unlike in the previous analysis, an increase of plate width tends to even the load distribution, with the highest bolt load fraction dropping of about 3%. Interestingly, for large plate width to bolt diameter ratios, the load distribution becomes less and less sensitive to width increments. Increasing the width of a joint to even the load distribution would not be a fruitful approach for already large plate width to bolt diameter ratios, as the trend appears to reach saturation.
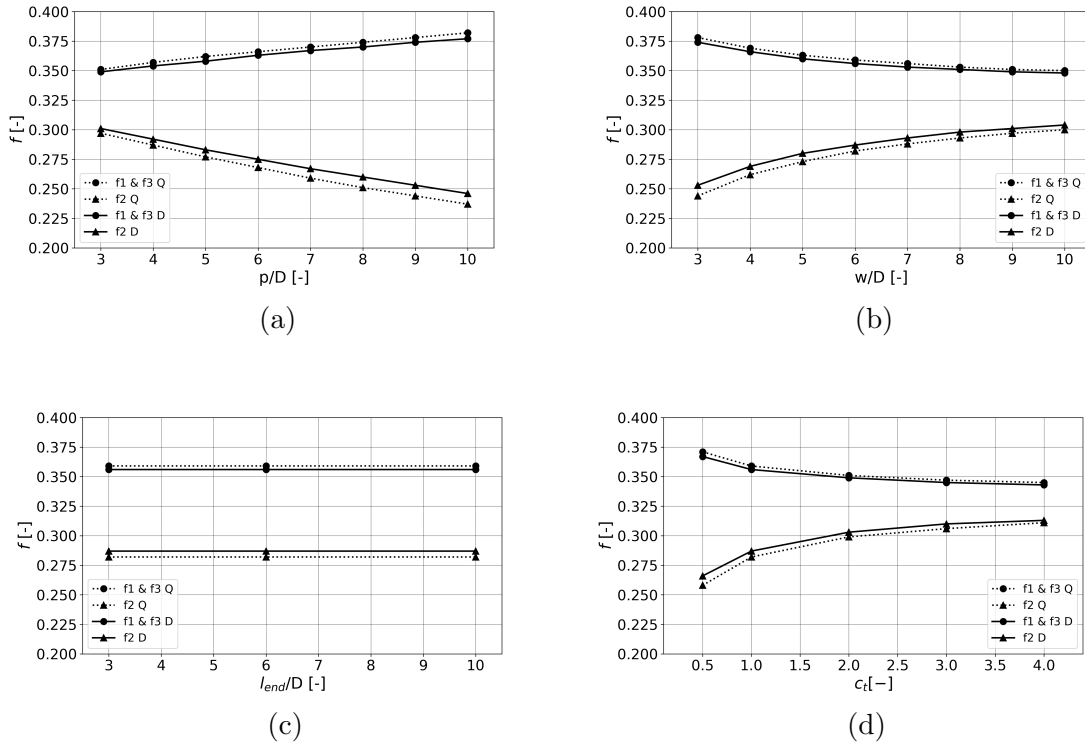
Figure 56: Influence of geometric parameters on load distribution with LC1

The distance of the first and last fastener from the plate edge l_{end} is the third parameter that was investigated. Fig.56(c) clearly shows how this quantity has no influence on the load distribution. The model for uniaxial loading could be easily

redefined not to take into account the end length, which anyway has very little impact on the model's prediction.

For the last parametric analysis of this section, the joint thickness was modified. The thickness change is expressed through the thickness factor c_t, defined as the ratio between the plate thickness at baseline conditions and the modified plate thickness. The same thickness factor is applied to plates A and plate B at the same time. The results of this study are presented in Fig.56(d). It should be noted that the joint thickness at baseline conditions is 8.32 mm, roughly equivalent to the bolt diameter. The thickness factor c_t can therefore be interpreted with little error as the ratio between the joint thickness and the bolt diameter. It is important to note from these results that changing the thickness of a thick laminate has almost no influence on the load distribution. The curves are almost flat for c_t larger than 2, with changes in load distribution at bolts 1 and 3 smaller than 1% when doubling the thickness factor from 2 to 4. With thin joints, changing the joint thickness has a more significant impact on load distribution, with a tendency of the load to increase at the external bolts for thinner joints. For a change in thickness from c_t=0.5 to c_t=1, the load fractions f_1 and f_3 decrease from 36.7% to 35.6%.

Having analyzed the results from the four studies on geometric parameters, it is possible to conclude that layup orientation has no apparent role on how much these parameters influence load distribution. For the two considered layups, the load distribution was observed to be affected equally, both in terms of trend and magnitude of the impact. In all the four studies and all parameter values, the exterior bolts were more loaded with M-DL-Q-C than with M-DL-Q-C. This is a direct consequence of the smaller global laminate stiffness in the loading direction with the former layup.

8.1.2 Effects of clearance on load distribution

The results of a study on the influence of bolt-hole clearance on load distribution are presented and discussed. A double-lap joint of geometry as described in Table 50 was considered for two different laminate layups: M-DL-D-C and M-DL-Q-C. Finger-tight torque conditions were modelled for the bolt preload, with an applied tensile load P=29.5 kN.

Different combinations of clearance conditions were considered, as summarized in Tables 51 and 52. All the values were chosen within the limits guaranteed by the f7/H10 fitting for 8 mm diameter bolts, as presented in Section 2.2. Even without investigating larger clearances, possibly resulting from manufacturing errors, significant variations were observed. As previously mentioned, for the conditions of the modelled geometry and materials, the reaction at bolt 1 is always equal to the reaction at bolt 3. For this reason, the study of both cases such as $\boldsymbol{\lambda} = \{100, 20, 20\}$ and $\boldsymbol{\lambda} = \{20, 20, 100\}$ would be redundant and was avoided, the reactions at bolt 1 and bolt 3 being simply inverted.

Table 51: Influence of clearance conditions on load distribution with uniaxial tensile loading with M-DL-D-C

λ_1 [μm]	λ_2 [μm]	λ_3 [μm]	f_1 [%]	f_2 [%]	f_3 [%]
20	20	20	35.6	28.7	35.6
100	20	20	28.1	33.2	38.7
20	100	20	40.1	19.7	40.1
20	100	100	43.2	24.2	32.6
100	20	100	31.1	37.7	31.1
70	30	70	33.4	33.2	33.4
100	100	100	35.6	28.7	35.6

Table 52: Influence of clearance conditions on load distribution with uniaxial tensile loading with M-DL-Q-C

λ_1 [μm]	λ_2 [μm]	λ_3 [μm]	f_1 [%]	f_2 [%]	f_3 [%]
20	20	20	35.9	28.2	35.9
100	20	20	31.3	31.0	37.7
20	100	20	38.7	22.6	38.7
20	100	100	40.5	25.4	34.1
100	20	100	33.1	33.8	33.1
70	30	70	34.5	31.0	34.5
100	100	100	35.9	28.2	35.9

For $\lambda = \{20, 20, 20\}$ and $\lambda = \{100, 100, 100\}$, identical load distributions are observed for both layups. This derives from the assumption of the analytical model that clearance simply introduces a delay in load take-up by the bolt. The only difference between the two cases, being applied force and load distribution equal, is the joint displacement, becoming larger for larger clearance. This load distribution is the same that would be obtained from a spring-based model for uniaxial loading that does not take into account clearance, which would assume implicitly $\lambda = \{0, 0, 0\}$

It should be noted that, for these cases of equal clearance at all bolt locations, the bolts start reacting the applied load at the same time and therefore the load distribution does not vary with the applied load. When different clearances are present in the joint, as in $\lambda = \{100, 20, 20\}$, the load distribution depends on the applied load. Fig.57 shows this evolution of the load distribution as a function of joint displacement for M-DL-Q-C. The largest displacement corresponds to the case P=29.5 kN reported in Table 52.

The conditions $\lambda = \{100, 20, 100\}$ are of great interest since, while the clearance values are within the limits prescribed by the tolerances, the load distribution con-
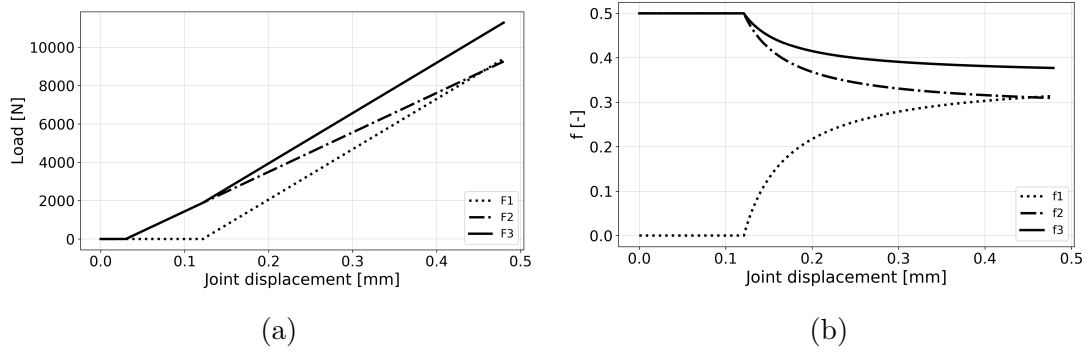
Figure 57: Bolt reactions and load fractions as a function of joint displacement with $\boldsymbol{\lambda} = \{100, 20, 20\}$ clearance conditions

tradicts a common belief about bolted joints. As M.A. McCarthy [2] and Esp [4] mention, the external fasteners, in this case 1 and 3, are often assumed to carry the largest fraction of the load. However, both with M-DL-D-C and M-DL-Q-C, the central bolt is the most loaded, by more than 6% in the case of the former layup. These results highlight the risks of neglecting the effects of bolt-hole clearance during joint analysis.

Further confirmation of the importance of clearance modelling comes from the analysis of $\boldsymbol{\lambda} = \{20, 100, 100\}$. For both layups, the largest reaction of all the parametric study appears at bolt 1 with 43.2% and 40.5% of the applied load for M-DL-D-C and M-DL-Q-C respectively. It has already been mentioned that the load distributions at cases such as $\boldsymbol{\lambda} = \{20, 100, 100\}$ correspond to the prediction of a model not accounting for clearance. For M-DL-Q-C this model would therefore estimate a maximum 35.9% load fraction while a value of 40.5% would still be possible with the f7/H10 fitting. Similarly, not modelling clearance with M-DL-D-C could lead to an underprediction up to 7.6%. The use of a higher quality hole tolerance, such as H8 or H9, would of course reduce the uncertainty.

8.2 Parametric study on the modified ICoR method

A parametric study was also carried out with the modified ICoR method. The baseline geometry in this case is equivalent to the joint presented in Fig.45. For the analyses, a coordinate system centered on the bolt group centroid was adopted. Table 53 presents the key quantities for the parametric study referred to the baseline geometry. During the parametric studies, all the quantities that were not being modified were kept equal to the values in the table. Here e_X indicates the distance of the load application point from the bolt group centroid CG. The properties of the fasteners were kept as described in previous analyses with the modified ICoR method.

Table 53: Baseline geometry for parametric studies of Section 8.2

N [-]	D [mm]	p_X [mm]	p_Y [mm]	e_X [mm]
4	8	32	40	72

Three cases were considered by modifying the values of the pitch distances p_X, p_Y and of the applied load P. The impact of these parametric variations on the position of the instantaneous center IC and Δ_{high} was monitored. Since IC is known to always be located on the line passing through CG and perpendicular to P, only the X component x_{IC} is reported.
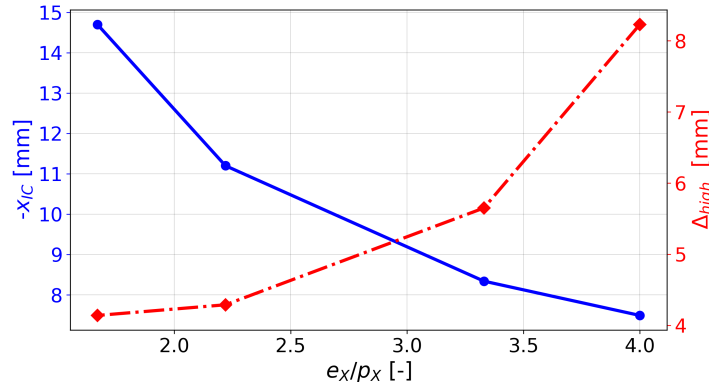
Figure 58: X direction bolt spacing influence on x_{IC} and Δ_{high}

The first parameter to be modified was p_X and the variations were monitored through the dimensionless quantity e_X/p_X. The trend for the x_{IC} curve can be interpreted by recalling the definition of the ICoR method. In fact, it is assumed that an eccentric load generates both a translation and a rotation around CG, which is equivalent to a rotation around IC. The translation can be seen as a rotation around a point set at infinity, in this case in the negative X direction. When e_X/p_X is close to zero, the load P is almost applied at CG. As a consequence the generated translation along Y is much more relevant than the rotation around CG. The joint appears to be rotating around a point at infinity and $-x_{\text{IC}}$ tends therefore to large values. In the opposite case of a very large e_X/p_X ratio, P is applied far away from the bolt group, generating a significant rotation around CG and less relevant Y translation. As the joint almost only rotates around CG, $-x_{\text{IC}}$ tends to zero. This behavior is confirmed by the blue curve in Fig.58, which is strictly decreasing for an increase in e_X/p_X. Despite this trend, a rotation purely around CG cannot be reached, and $-x_{\text{IC}}$ cannot reach zero, as bolt failure is triggered around $e_X/p_X=4$, as shown by the red curve.
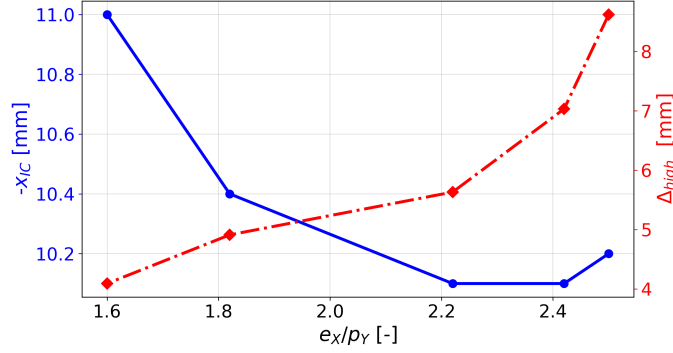
Figure 59: Y direction bolt spacing influence on x_{IC} and Δ_{high}

A similar interpretation can be given for the parametric study of Fig.59. For equal loading conditions, an infinitely tall bolt group, with large p_Y and small e_X/p_Y, would resist to rotation better than bolt group with small spacing in the Y direction. In the former case, translation is more relevant than rotation and $-x_{IC}$ tends to infinity. On the other hand, a bolt group with small e_X/p_Y would rotate more easily, so that $-x_{IC}$ tends to small values. This tendency can be observed as the blue curve is decreasing for an increase in e_X/p_Y.

The increase of the blue curve with the final increase of e_X/p_Y is probably not due to a physical phenomenon but to the imprecisions of the analytical model. In fact, x_{IC} and Δ_{high} are calculated through an iterative process in which initial guesses are updated and verified after each iteration. If the guesses led to a solution satisfying equilibrium within the defined tolerance, they are accepted as correct. This means that different solutions within these boundaries could be found, with small variations of x_{IC} and Δ_{high}. For the last point on the blue curve, $-x_{IC}=10.2$, even if imprecise, was accepted since within the tolerance. An ideal curve for an almost zero tolerance of the ICoR method would be strictly decreasing. Obviously, reducing the tolerance would lead to a more complex and lengthy calculation.
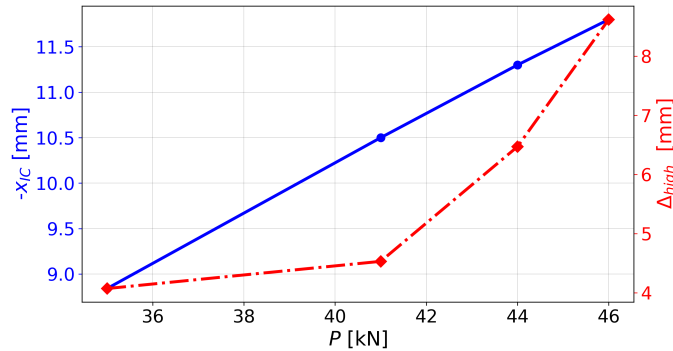
Figure 60: Applied load influence on x_{IC} and Δ_{high}

116

No study was directly carried out by modifying e_X for a constant bolt group geometry. However, it is believed that indications regarding this case can be drawn from the investigations for different spacings p_X and p_Y and constant e_X because of the similarity of the joint geometry.

Lastly, the applied load P was varied as shown in Fig.60. The red curve shows the obvious behavior of increasing with P. Without changing the load application point, a larger load leads to larger reactions in the bolts. For a sufficiently large P, around 46 kN, the shear capacity of the fastener furthest from the IC is reached and bolt failure is triggered.

The trend of the blue curve can also be easily justified. In fact, for the same bolt group geometry and load application point, a larger load P generates a larger translation along Y, thus pushing $-x_{IC}$ towards infinity. Interestingly, the curve appears to be linear.

9 Design guidelines

This chapter provides a series of guidelines for joint design based on the findings of the investigations carried out as part of the thesis study. A distinction is made for the load cases defined in Section 3.1. For each load case, the applicability of the models implemented in the tool is discussed. Considerations regarding the limits of the models, their accuracy and conservatism are also presented.

9.1 LC1 modelling with single-column joints

When considering single-column joints subject to tensile loading, the tool calculates load distribution through the uniaxial loading model for single-column joints presented in Section 4.1.2 combined with the bolt preload model for uniaxial loading from Section 4.2.1. The two methods were investigated through a comparison with numerical models, taking into account the effects of bolt-hole clearance and bolt preload. The conclusions presented here are considered to equally apply to single-lap and double lap joints, unless otherwise specified.

All the investigations confirmed that it is possible to interpret both bolt preload and clearance as sources of delay in load take-up by the fastener. In case of equal clearance at all bolts, the delay equally affects all bolts. The observations for a single case of equal clearance, such as in Fig. 34, can therefore be generalized to any case of equal clearance at all bolts or no clearance at any bolt. In such cases, the tool has shown to predict reactions rather accurately and with a level of accuracy comparable for all fasteners. The predictions at all bolts are slightly non-conservative because of the limits of the considered flexibility formulation, but only in double-lap joints, and of the implemented preload model.

In fact, all the retained fastener flexibility formulations for double-lap joints were observed to predict excessively even load distributions. As a consequence, the tool has a tendency to overpredict the reactions at the central fasteners in a column and to underpredict the reactions at the exterior bolts. Being the latter the most loaded in the joint, at least with equal clearance or no clearance at every bolt, this leads to a slightly non-conservative prediction of the largest reaction. This tendency was confirmed by a comparison of the results from the tool to experimental data from instrumented bolts. This tendency towards excessively even distributions is, however, not present with single-lap joints for which an analogous experimental comparison showed a conservative tendency to overpredict the reactions of the external bolts.

The second source of non-conservatism is the inaccuracy of the bolt preload model which was always observed to overpredict the maximum force the joint can transfer by friction. If a joint were designed to transfer loads, at least partially, through shearing of the bolts, the overestimation of the slip resistance would lead to non-conservative bolt reaction predictions. The reason for this is the fact that the delay

of bolt load take-up would be overestimated by the tool. This delay is reflected in a constant and non-conservative difference between the actual bolt reaction and the prediction of the tool.

This limit of the model for bolt preload is intrinsic to the considered friction law and equally affects all joints, independently of the geometry or the presence of clearance. A solution proposed in this study is to employ a reduced coefficient of friction. Considering a friction coefficient in the tool equal to 77% of the value implemented in the FE models led to conservative predictions of the largest reaction for all considered cases. While without further studies it is difficult to generalize if such a scaling factor would be sufficient, the approach of reducing the friction coefficient has obvious potential to ensure conservative results. Taking this idea to the extreme would be to neglect friction altogether to ensure conservative results, as done by Esp [4]. However, such a choice would lead to conservative but highly inaccurate predictions, which would then lead to overdesign of the joint. Finding a middle ground could guarantee a compromise between the needs for accuracy and conservatism.

It was previously mentioned that, in a case of equal clearance at all bolts or no clearance at any bolt, the shortcomings of the preload method and of the flexibility formulations were a source of inaccuracy. Despite this, the predictions at all bolts were observed to be slightly non-conservative but with a comparable level of accuracy. In a case of different clearance, this was observed not to be the case. When studying cases with a significantly larger clearance at one bolt, as in Figures 35 and 36, the behavior in the transition region of the bolt with larger clearance was observed to be more complex than what the tool predicted. This was shown to be due to the fact that the tool cannot take into account the friction between plates and washers which becomes relevant in presence of larger clearance at one bolt. This limit of the model prevents the tool from providing an accurate and conservative prediction of the reaction at the bolt with the largest clearance, at least for a certain range of applied loads. It was however observed that the reactions in the most loaded bolts were not affected by this phenomenon.

The fact that the reaction at the most loaded bolt could always be accurately predicted is extremely relevant for joint design. In fact, if compensation of the inaccuracy of the preload model is ensured, the tool can be used to conservatively predict the largest reaction in a joint independently of clearance or of the amount of preload. The fact that this conclusion is independent of clearance is important because the actual values of clearance at a bolt are unknown due to the uncertainty introduced by tolerances. With these conclusions in mind, joint design can then be performed conservatively for the largest reaction predicted by the tool.

All the considerations above are believed to apply to double-lap and single-lap joints, with the exception of the case of single-lap joints with high bolt preload. A definitive conclusion on the accuracy of the tool in this case could not be reached because of the shortcomings of the approach to extract forces from the FE model and the lack

of experimental data for validation.

Finally, it should be noted that the model implemented in the tool considers equal axial forces due to bolt preload at every fastener. This was assumed in the original study on which the implemented bolt preload model was based [3]. The assumption was justified by the use of instrumented bolts to measure the axial force due to preload, thus ensuring high precision in the axial force estimation. If preload control in the joint to be designed were performed with a less accurate method, an uninvestigated uncertainty in preload could be present in the joint, which the tool would not be able to keep into account. As a reference, instrumented bolts and bolt elongation measurements introduce a preload uncertainty in the order of ±5%, preload indicating washers of ±10%, while with torque measurements the uncertainty is larger than ±25% [48]. Preload relaxation is another source of uncertainty of the axial force in a bolt. While these uncertainties cannot be directly accounted for by the tool, it is possible to adopt a conservative approach when defining the coefficient of friction.

9.2   LC1 modelling with multi-column joints

Being the approach for multi-column joints based on the model for single-column joints, the considerations previously discussed also apply here.

In this case, despite the one-dimensional nature of loading, asymmetries in the joint with respect to the line along which the load is applied can result in rotational effects on the joint. In this regard, it was observed that the rotation induced by large clearance is negligible.

Before employing the tool for load distribution calculation, it is necessary to evaluate if the considered bolt pattern respects the assumptions made in the tool definition. A bolt pattern such that a division in columns is possible should always be implemented for calculation. Different column widths were considered and the assumptions underlying the multi-column approach were observed to hold also for small spacings. The minimum distances considered in joint design need however to be respected, as discussed in Section 7.2.

Additionally, the considered bolt patterns were such that all bolts were sufficiently far from the plate edges not to be affected by their presence. For some joint geometries the emergence of these edge effects was observed but not quantified and care needs to be taken when evaluating load distribution for such cases.

9.3   LC2 modelling

The study of uniaxial compression loading of single or multi-column joints is possible with the tool. The modelling approach is to consider compression and tension equiv-

alently but considering the appropriate stiffness properties for each case. Therefore, the conclusions regarding tensile loading of single and multi-column joints also apply in this case. This approach was justified by the analyses of Section 6.2.3.

It should however be noted that compression loading has some peculiarities that cannot be ignored in some cases. Specifically, compression loading can lead to structural instability, while that is not the case with tensile loading. For thin joints, the critical force triggering buckling could be smaller than the load leading to static joint failure, be that bearing failure or other forms. The tool would not be able to predict this kind of failure, nor to account for potential influences on load distribution at the onset of instability.

9.4   LC3 modelling

Two analytical models were considered and investigated in the study for joints subject to shear loading: the elastic method and the modified ICoR method.

Conservatism of the original ICoR method and of the elastic method is ensured by the use of proper factors of safety. It should be noted that neither of them consider the effects of clearance, so that the use of factors of safety is essential. Both methods, as well as the modified ICoR method defined in this thesis study, conservatively neglect bolt preload, thus assuming that no friction between the connected parts can alleviate bolt loads.

The comparison of the elastic method and of the modified ICoR method with numerical models was carried out for cases of zero bolt-hole clearance and without factors of safety. For such conditions, the modified ICoR method was observed to be more accurate than the elastic method for all considered cases. The difference in accuracy, both in terms of load distribution and largest reaction prediction, was observed to be maximum at large bolt deformation but significant also for intermediate bolt deformation. The difference is due to the possibility to take into account load re-distribution due to bolt plasticity with the modified ICoR method.

While less accurate, the elastic method was observed to always overpredict the largest reaction in a joint subject to shear loading. However, it should be noted that the reactions at the least loaded bolts were constantly underpredicted. Conservative joint design with this model is possible only if made for the largest reaction in the bolt group.

The modified ICoR method was observed to lead to conservative predictions for all bolts in most cases. The only observed underprediction, of about 1% of the force reaction, was observed for bolt failure conditions. As bolt deformation becomes smaller, the prediction of the method for the largest reaction in the joint becomes more and more conservative.

The applicability of the modified ICoR method to composite joints was demonstrated. The available empirical data allow the use of the method for different plate materials and for steel bolts with properties equivalent to grade 8.8. The use of the method for fasteners of different materials would require the derivation of more empirical relations. Nonetheless, it was demonstrated that a single empirical relation is necessary for a fastener material and is applicable to joints with different plate materials or laminate layups.

An extensive study on the effects of clearance on the prediction of the modified ICoR method would define what factors of safety should be considered for joint design. These future studies on models not accounted for clearance are also briefly discussed in Section 10.2.

Due to the limits of the current mathematical implementation of the modified ICoR method, the elastic method was implemented in the tool to calculate load distribution in case of shear loading. The modified ICoR method was programmed in a separate Python script.

9.5   LC4 modelling

In evaluating the superposition approach for biaxial loading, the results showed fairly good accuracy for the considered joint geometry with no clearance. The fasteners were assumed sufficiently far from the plate edges not to be influenced by the applied boundary conditions. The validity of such assumption should be evaluated, also through the results of the conducted parametric studies, if predictions based on superposition were to be employed for joint design.

The investigations on biaxial loading, however, also raised concerns regarding the possibility of completely and correctly modelling through superposition the phenomena taking place. A definitive conclusion on the applicability of such approach was not drawn. Further studies on different geometries and bolt patterns would allow a more complete understanding to then express a conclusive judgment. If these studies indicated that superposition can predict load distribution with reasonable accuracy when clearance is not present, it would then be possible to evaluate what factors of safety should be considered for safe joint design despite the uncertainty due to tolerances.

9.6   LC5 modelling

The investigations on the considered model demonstrated its inadequacy to accurately and conservatively predict reactions due to thermal loading.

Accounting for bolt-hole clearance and accurately estimating the expansion properties of the plates were shown to be the two necessary aspects to conservatively

predict bolt reactions. In case of isotropic plate materials, only the first aspect hinders accurate and conservative predictions. Bolt preload was also observed to have a significant impact on the behavior of the joint with thermal loading. While neglecting its effects leads to inaccurate estimations of bolt reactions, the inaccuracy was observed to be conservative.

Concerning composite laminates, if a more accurate estimation of the thermal expansion properties of the plates could be ensured, either through numerical studies or experimental measurements, clearance would be the only source of non-conservative predictions. In this case, it may be possible to employ the analytical model, neglecting clearance, with proper factors of safety. As was the case for the analytical models for LC3 and LC4, an estimation of these factors would necessitate extensive numerical studies for several joint geometries and clearance conditions.

Without such information, numerical models should be employed to evaluate load distribution in case of thermal loading. The high level of detail of 3D FE models allows to account for all the fundamental parameters driving load distribution with such loading. It would thus be possible to model the dependence of the material properties on temperature, the influence of bolt expansion or contraction and of the difference between curing and assembly conditions. This approach may not be fully suitable for early stages of preliminary design but, as the results of the investigations show, any model ignoring the fundamental aspects of load distribution with thermal loading is of no use for reaction prediction.

Finally, laminate hybridization can sometimes significantly reduce bolt loads in case of thermal loading. In some of the considered cases, bolt reactions were almost nullified by simply replacing some of the composite plies with metal sheets.

10 Conclusion

10.1 Summary

Following a review of the literature on load distribution in multi-fastener joints subject to in-plane loading, relevant studies on analytical approaches were retained. Alongside these studies, numerical studies were retained to serve as reference for the numerical models employed in this thesis work for comparison of the analytical results.

An analytical model for the calculation of load distribution in single-column joints subject to uniaxial loading was retained from the literature. It was implemented in the tool in combination with a model accounting for bolt preload. Employing the two models to predict load distribution was observed to lead to results applicable for joint design. The modification of the preload model to comply with the requirements for the tool was observed not to hinder the applicability of the approach to single-column joints with uniaxial loading. The significant impact of clearance on load distribution was highlighted.

On the basis of the results for single-column joints, an approach for multi-column joints subject to uniaxial loading was proposed. The findings of numerical investigations indicated the possibility of considering each column as independent even in presence of clearance leading to joint asymmetry and rotational effects.

The predictions of a model for thermal loading were evaluated through a series of separate studies on the parameters considered to mainly influence load distribution for such loading. In order to guarantee conservative predictions, the necessity of accounting for clearance, together with the need for a precise estimation of the thermal expansion properties of the materials, was underlined. In its current formulation, the analytical model was considered not capable of conservatively predicting loads induced by thermal loading.

The model retained from the literature for shear loading could conservatively predict the largest bolt loads in a joint. A higher level of accuracy was obtained with a modified method for shear loading based on empirical data on bolt deformation. None of the two models takes clearance into account and both are to be used with proper factors of safety.

An approach for modelling multi-fastener joints subject to biaxial loading was proposed. Fairly good accuracy was observed for the considered joint geometry. For a fixed geometry, the accuracy of the predictions was shown to solely depend on the ratio of the loads applied in the two directions. The results raised nonetheless concerns regarding the validity of such an approach which should be addressed through further investigations.

124

10.2   Outlook

In analytical studies with non-negligible preload, small variations of preload between the bolts were assumed thanks to the use of precise control measurements. If an assembly procedure with larger uncertainty were to be employed, an evaluation of the impact of differences in preload would be necessary. In fact, such uncertainty might have dangerous effects, not allowing a smooth evolution from quasi-linear region to transition region, potentially invalidating the assumptions at the basis of the analytical models.

Regarding shear loading, the modified ICoR method was observed to have a clear potential to improve the prediction of the elastic method implemented in the tool. Its applicability is currently limited by the definition of the minimization problem on which the method is based. Improvements in this regard could be easily achieved.

Single-lap joints were considered in this study and numerical models were created for comparison with studies in the literature. A comparison with the analytical models was also carried out. However, due to time constraints, it was not possible to employ them for studies on the peculiarities of single-lap configurations. In particular, the influence on load distribution of secondary bending effects due to the eccentricity of the load lines should be investigated. As previously mentioned, numerical studies on single-lap joints may need the adoption of a different approach for force extraction.

Also, despite the possibility to define stepped joints in the models for uniaxial loading, no investigation specifically on their particularities was carried out. A study on this kind of with variable thickness would increase the confidence in the analytical results for these geometries.

In the thesis study, linear deformation of the plates was considered without investigating plate failure. In the vicinity of bearing failure conditions, material non-linearity could affect load distribution without the analytical models being capable of capturing these effects. Studies on the topic could provide significant insights to correctly model load transfer in such conditions with the tool.

Finally, the great influence of even small clearance on load distribution was highlighted throughout the thesis study for different joint geometries and loadings. Higher level of accuracy was observed for the models capable of accounting for a known value of clearance. However, due to the uncertain nature of tolerances, it is not possible to exactly estimate what clearance conditions to consider as input for these models. Taking advantage of the very short computational time of the analytical models, it would be possible to define an algorithm that, for fixed geometry and loading, would repeat the load distribution calculation for many combinations of clearance conditions within the considered tolerances. The output of such a calculation would be a list of reactions in the joint for the corresponding clearance conditions. Joint design could then be made for the largest reaction possible or for the average reaction considering all clearance conditions. Such a study would also

be perfectly feasible with 3D FE models but it would require much longer computations. In this sense, the advantage of an analytical model compared to detailed numerical approaches is clear.

The described numerical approach would however be necessary for those models which cannot take into account clearance. Through a series of studies with different clearance conditions, repeated for several joint geometries, the maximum discrepancy possible between numerically computed results and analytical predictions not accounting for clearance could be estimated. From the findings of such studies, it would then be possible to define factors of safety to be employed in connection with the analytical models not accounting for clearance.

References

[1] F Liu, J Zhang, L Zhao, A Xin, and L Zhou. An analytical joint stiffness model for load transfer analysis in highly torqued multi-bolt composite joints with clearances. *Composite Structures*, 131:625–636, 2015.

[2] M A McCarthy, C T McCarthy, and G S Padhi. A simple method for determining the effects of bolt–hole clearance on load distribution in single-column multi-bolt composite joints. *Composite Structures*, 73(1):78–87, 2006.

[3] C T McCarthy and P J Gray. An analytical model for the prediction of load distribution in highly torqued multi-bolt composite joints. *Composite Structures*, 93(2):287–298, 2011.

[4] B Esp. *Practical analysis of aircraft composites, 1st edition*. Grand Oak Publishing, 2017.

[5] ISO 286. Geometrical product specifications (GPS) - ISO code system for tolerances on linear sizes. *International Organization for Standardization*, 2010.

[6] ASTM D5961 / D5961M 05. Standard test method for bearing response of polymer matrix composite laminates. *American Society for Testing and Materials International*, 2005.

[7] A Olmedo, C Santiuste, and E Barbero. An analytical model for the secondary bending prediction in single-lap composite bolted-joints. *Composite structures*, 111:354–361, 2014.

[8] C T McCarthy, M A McCarthy, W F Stanley, and V P Lawlor. Experiences with modeling friction in composite bolted joints. *Journal of composite materials*, 39(21):1881–1908, 2005.

[9] ASTM F568M-07. Standard specification for carbon and alloy steel externally threaded metric fasteners. *American Society for Testing and Materials International*, 1998.

[10] ISO 898-1. Mechanical properties of fasteners made of carbon steel and alloy steel. *International Organization for Standardization*, 2009.

[11] Y Nawab, F Jacquemin, P Casari, N Boyard, Y Borjon-Piron, and V Sobotka. Study of variation of thermal expansion coefficients in carbon/epoxy laminated composite plates. *Composites Part B: Engineering*, 50:144–149, 2013.

[12] M B Tate and S J Rosenfeld. Preliminary investigation of the loads carried by individual bolts in bolted joints. Technical report, NACA TN 1051, 1946.

[13] B L Bunin, W D Nelson, and L J Hart-Smith. Critical joints in large composite aircraft structure. NASA CR 3710, 1983.

[14] H O B Huth. *Zum Einfluss der Nietnachgiebigkeit mehrreihiger Nietverbindungen auf die Lastübertragungs-und Lebensdauervorhersage.* LBF Report No. FB-172, Dissertation, Technische Universität München, 1984.

[15] T Swift. Development of the fail-safe design features of the DC-10. *ASTM STP 486*, 1971.

[16] J M Zhang. Design and analysis of mechanically fastened composite joints and repairs. *Engineering analysis with boundary elements*, 25(6):431–441, 2001.

[17] E Madenci, S Shkarayev, B Sergeev, D W Oplinger, and P Shyprykevich. Analysis of composite laminates with multiple fasteners. *International journal of solids and structures*, 35(15):1793–1811, 1998.

[18] B Sergeev, E Madenci, and D R Ambur. Influence of bolt spacing and degree of anisotropy in single-lap joints. *Computers & Structures*, 76(1-3):89–103, 2000.

[19] American Institute of Steel Construction. *Steel Construction Manual 13th Edition.* 2005.

[20] C Reilly. Studies of iron girder bridges, recently executed, illustrating some applications of the modern theory of the elastic resistance of materials. *Minutes of the Proceedings*, 29(1870):403–500, 1870.

[21] S F Crawford and G L Kulak. Eccentrically loaded bolted connections. *Journal of the Structural Division*, 97(3):765–783, 1971.

[22] T Ireman, T Nyman, and K Hellbom. On design methods for bolted joints in composite aircraft structures. *Composite Structures*, 25(1-4):567–578, 1993.

[23] Z Kapidžić, H Ansell, Jo Schön, and K Simonsson. Quasi-static bearing failure of CFRP composite in biaxially loaded bolted joints. *Composite Structures*, 125:60–71, 2015.

[24] IASB. Load distribution in bolted/riveted, metallic joints (linear theory). *Handbuch Strukturberechnung*, HSB 21031-01 Issue C, 1991.

[25] C Santiuste, E Barbero, and M Henar Miguélez. Computational analysis of temperature effect in composite bolted joints for aeronautical applications. *Journal of Reinforced Plastics and Composites*, 30(1):3–11, 2011.

[26] T Ireman. Three-dimensional stress analysis of bolted single-lap composite joints. *Composite structures*, 43(3):195–216, 1998.

[27] W H Chen and S S Lee. Numerical and experimental failure analysis of composite laminates with bolted joints under bending loads. *Journal of composite materials*, 29(1):15–36, 1995.

[28] W H Chen, S S Lee, and J T Yeh. Three-dimensional contact stress analysis of a composite laminate with bolted joint. *Composite structures*, 30(3):287–297, 1995.

[29] B Egan, M A. McCarthy, and C T. McCarthy. Design, testing and analysis of bolted joints and connections. In *Reference Module in Materials Science and Materials Engineering*. 2015.

[30] B D Snyder, J G Burns, and V B Venkayya. Composite bolted joints analysis programs. *Journal of Composites, Technology and Research*, 12(1):41–51, 1990.

[31] M K Smith, L J Hart-Smith, and C G Dietz. Interactive composite joint design. Douglas Aircraft Company, USAF Technical Report, AFFDL-TR-78-38, 3, 1978.

[32] LJ Hart-Smith. Design methodology for bonded-bolted composite joints. Technical Report, McDonnell Aircraft Co, 1983.

[33] R L Ramkumar, E S Saether, N J Kudva, E Madenci, and R J Nuismer. Strength analysis of composite and metallic plates bolted together by a single fastener. NOR 85-278, Northrop Corporation Aircraft Division, 1985.

[34] R L Ramkumar, E S Saether, and D Cheng. Design guide for bolted joints in composite structures. NOR 86-211, Northrop Corporation Aircraft Division, 1986.

[35] M Mahler and H T Hahn. Repair methods for composite structures. *Proceedings of the 8th Japan–US conference of composite materials, Baltimore*, pages 53–62, 1998.

[36] C Poon and Y Xiong. Bolted joint technology in composite structures–analytical tools development. *Bolted/Bonded Joints in Polymeric Composites*, National Research Council of Canada, 1997.

[37] S Postupka A Kiihweg and F J Arendts. Determination of the bolt flexibility of CFRP joints. In *ECCM-8: European Conference on Composite Materials; Science, Technologies and Applications; 3-6 June, 1998, Naples-Italy*, volume 1, pages 61–68, 1998.

[38] J E Shigley. *Mechanical engineering design, 9th edition*. McGraw-Hill, 1972.

[39] W T Segui. *Steel design, 5th edition*. Cengage Learning, 2012.

[40] J H Bickford. *Introduction to the design and behavior of bolted joints: non-gasketed joints, 4th edition*. CRC press, 2007.

[41] C T McCarthy, M A McCarthy, and V P Lawlor. Progressive damage analysis of multi-bolt composite joints with variable bolt–hole clearances. *Composites Part B: Engineering*, 36(4):290–305, 2005.

[42] ABAQUS. Analysis user's manual. Version 6.14. *Dassault Systèmes SIMULIA Corp*, 2007.

[43] V P Lawlor, M A Mccarthy, and W F Stanley. An experimental study of bolt–hole clearance effects in double-lap, multi-bolt composite joints. *Composite structures*, 71(2):176–190, 2005.

[44] SAE International and National Institute for Aviation Research. Polymer matrix composites: Materials usage, design, and analysis. *Composite Materials Handbook - CMH-17-3G*, Volume 3(Chapter 8), 2012.

[45] A Fink. *Lokale Metall-Hybridisierung zur Effizienzsteigerung Hochlastfugestellen in Faserverbundstrukturen.* Dissertation, Technische Universität Braunschweig, 2010.

[46] R S Raghava. Prediction of thermal and mechanical properties of glass-epoxy composite laminates. *Polymer composites*, 5(3):173–178, 1984.

[47] American Institute of Steel Construction. *Specification for Structural Steel Buildings*, volume AISC 360-16, page 16.1-iii and page 16.1-129. 2016.

[48] NASA. Criteria for preloaded bolts,. Technical report. NSTS 08307 - Revision A, 1989.

11 Appendix

11.1 Joint displacement and bolt-hole clearance
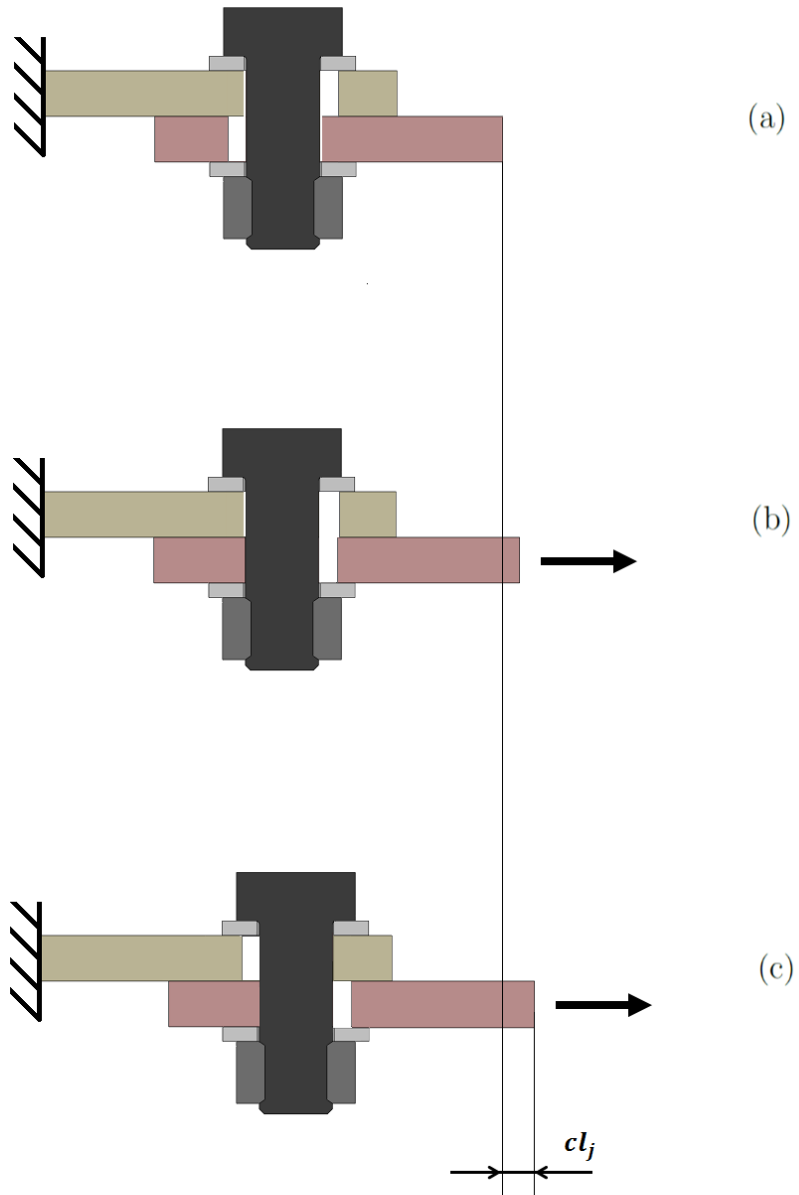
Figure 61: Bottom joint displacement due to uniaxial load: No load (a), single bolt-hole contact (b), double bolt-hole contact (c)

11.2 Generalized problem formulation for Section 4.1.2

11.2.1 $\underline{\underline{K}}$ matrix

The generalized definition of the stiffness matrix for a joint with N fasteners is provided below. The matrix has an n×n size, where n=2N+1. With the exception of rows 1, 2, n-2, n-1 and n defined below, the other rows are defined in pairs as written in rows k and k+1. In both cases, k is to be replaced by the odd row number. All the unspecified matrix components are equal to zero.

Row 1:

$$K_{1,1} = K_{\text{A\_end}} + K_{\text{A\_N-1}} + K_{\text{F\_N}}$$

$$K_{1,2} = -K_{\text{F\_N}}$$

$$K_{1,3} = -K_{\text{A\_N-1}}$$

Row 2:

$$K_{2,1} = -K_{\text{F\_N}}$$

$$K_{2,2} = K_{\text{F\_N}} + K_{\text{B\_N-1}}$$

$$K_{2,3} = -K_{\text{B\_N-1}}$$

Row k:

$$K_{k,k-2} = -K_{\text{A\_N-}\frac{(k-1)}{2}}$$

$$K_{k,k} = K_{\text{A\_N-}\frac{(k-1)}{2}} + K_{\text{A\_N-}\frac{(k+1)}{2}} + K_{\text{F\_N-}\frac{(k-1)}{2}}$$

$$K_{k,k+1} = -K_{\text{F\_N-}\frac{(k-1)}{2}}$$

$$K_{k,k+2} = -K_{\text{A\_N-}\frac{(k+1)}{2}}$$

Row k+1:

$$K_{k+1,k-1} = -K_{\text{B\_N-}\frac{(k+1)}{2}+1}$$

$$K_{k+1,k} = -K_{\text{F\_N-}\frac{(k+1)}{2}+1}$$

$$K_{k+1,k+1} = K_{\text{B\_N-}\frac{(k+1)}{2}} + K_{\text{B\_N-}\frac{(k+1)}{2}+1} + K_{\text{F\_N-}\frac{(k+1)}{2}+1}$$

$$\boldsymbol{K_{k+1, k+3}} = -K_{\text{B\_N-}\frac{(k+1)}{2}}$$

Row n-2:

$$\boldsymbol{K_{n-2, n-4}} = -K_{\text{A\_1}}$$
$$\boldsymbol{K_{n-2, n-2}} = K_{\text{A\_1}} + K_{\text{F\_1}}$$
$$\boldsymbol{K_{n-2, n-1}} = -K_{\text{F\_1}}$$

Row n-1:

$$\boldsymbol{K_{n-1, n-3}} = -K_{\text{B\_1}}$$
$$\boldsymbol{K_{n-1, n-2}} = -K_{\text{F\_1}}$$
$$\boldsymbol{K_{n-1, n-1}} = K_{\text{B\_1}} + K_{\text{B\_end}} + K_{\text{F\_1}}$$
$$\boldsymbol{K_{n-1, n}} = -K_{\text{B\_end}}$$

Row n:

$$\boldsymbol{K_{n, n-1}} = -K_{\text{B\_end}}$$
$$\boldsymbol{K_{n, n}} = K_{\text{B\_end}}$$

11.2.2 $\underline{\boldsymbol{L}}$ vector

Similarly to the definition of the stiffness matrix, the load vector $\underline{\boldsymbol{L}}$ is defined by pairs of components. The generic definitions for k and k+1 apply to any row with k values between 0 and n-2 included. The last vector component is equal to the applied load the corresponding node.

Row k:

$$\boldsymbol{L_k} = -K_{\text{F\_N-k+1}} \cdot cl_{\text{N-k+1}}$$
$$\boldsymbol{L_{k+1}} = K_{\text{F\_N-k+1}} \cdot cl_{\text{N-k+1}}$$

Row n:

$$\boldsymbol{L_n} = \text{P}$$

11.3 Additional calculations for thermal loading model

As mentioned in Section 4.1.3, the thermal loading model was derived with a direct stiffness formulation. This section provides a more detailed explanation concerning how the model was derived in the proposed formulation. The formulation was derived for a joint with three fasteners and was then generalized to any number of bolts. The equations of this section refer to the joint discretization of Fig.16.

Equations representing the displacement of the first and last node due to thermal expansion are written at first:

$$x_1 = \alpha \cdot l_{end} \cdot \Delta T \tag{40}$$

$$x_7 = x_6 + \beta \cdot l_{end} \cdot \Delta T \tag{41}$$

As a second step, because of the internal nature of thermal forces, the sum of the fastener reactions is set equal to zero:

$$F_1 + F_2 + F_3 = 0 \tag{42}$$

Nodal equilibrium equations are then written:

$$K_{A\_2}(x_3 - x_1) = K_{A\_2} \cdot \alpha \cdot p_2 + (F_2 + F_3) \tag{43}$$

$$K_{A\_1}(x_5 - x_3) = K_{A\_1} \cdot \alpha \cdot p_1 + F_3 \tag{44}$$

$$K_{B\_2}(x_4 - x_2) = K_{B\_2} \cdot \beta \cdot p_2 - (F_2 + F_3) \tag{45}$$

$$K_{B\_1}(x_6 - x_4) = K_{B\_1} \cdot \beta \cdot p_1 - F_3 \tag{46}$$

This constitutes a linear system of 7 equations to determine 7 unknown nodal displacements $\underline{x}$. Through a combination of the equations, it is possible to express the problem in the form $\underline{\underline{K}} \cdot \underline{x} = \underline{L}_{ther}$, where $\underline{x}$ are the nodal displacements due to the thermal loads expressed in $\underline{L}_{ther}$ and $\underline{\underline{K}}$ is the stiffness matrix of the structure. Since the algebraic steps after equation combination are very lengthy, only the end results are shown.

The sum of Eq.42 and Eq.43 yields:

$$(K_{F\_3} + K_{A\_2} + K_{A\_end})x_1 - K_{F\_3} \cdot x_2 - K_{A\_2} \cdot x_3$$

$$= K_{A\_end} \cdot \alpha \cdot l_{end}\Delta T - K_{A\_2} \cdot \alpha \cdot p_2\Delta T \quad (47)$$

Considering Eq.42 minus Eq.45:

$$-K_{F\_3} \cdot x_1 + (K_{F\_3} + K_{B\_2})x_2 - K_{B\_2} \cdot x_4 = -K_{B\_2} \cdot \beta \cdot p_2 \cdot \Delta T \quad (48)$$

Subtracting Eq.44 from Eq.43:

$$- K_{A\_2} \cdot x_1 + (K_{A\_2} + K_{A\_1} + K_{F\_2})x_3 - K_{F\_2} \cdot x_4 - K_{A\_1} \cdot x_5$$

$$= K_{A\_2} \cdot \alpha \cdot p_2 \cdot \Delta T - K_{A\_1} \cdot \alpha \cdot p_1 \cdot \Delta T \quad (49)$$

The difference between Eq.45 and Eq.46 leads to:

$$- K_{B\_2} \cdot x_2 - K_{F\_2} \cdot x_3 + (K_{B\_2} + K_{B\_1} + K_{F\_2})x_4 - K_{B\_1} \cdot x_6$$

$$= K_{B\_2} \cdot \beta \cdot p_2 \cdot \Delta T - K_{B\_1} \cdot \beta \cdot p_1 \cdot \Delta T \quad (50)$$

The equation for node 5 can be obtained directly from Eq.44:

$$-K_{A\_1} \cdot x_3 + (K_{A\_1} + K_{F\_1})x_5 - K_{F\_1} \cdot x_6 = K_{A\_1} \cdot \alpha \cdot p_1 \cdot \Delta T \quad (51)$$

Also here the equation can be directly obtained, in this case from Eq.46:

$$- K_{B\_1} \cdot x_4 - K_{F\_1} \cdot x_5 + (K_{B\_1} + K_{F\_1} + K_{B\_end})x_6 - K_{B\_end} \cdot x_7$$

$$= K_{B\_1} \cdot \beta \cdot p_1 \cdot \Delta T - K_{B\_end} \cdot \beta \cdot l_{end} \cdot \Delta T \quad (52)$$

Finally, the last equation is obtained by simply multiplying Eq.41 by K_{B_end}:

$$-K_{B\_end} \cdot x_6 + K_{B\_end} \cdot x_7 = K_{B\_end} \cdot \beta \cdot l_{end} \cdot \Delta T \quad (53)$$

Equations 47 to 53 are written in such a form that the components of the thermal loading vector $\underline{L}_{ther}$ can be easily identified on the right-hand side of the equations.

The left-hand side is related to the structure of the joint and is not dependent on the considered load. It is equivalent to the product $\underline{\underline{K}} \cdot \underline{x}$, which was already found for the uniaxial loading model and defined in Section 4.1.2.

In case of a joint with a generic number of fastenrs N, the proposed model can be easily adapted. The equations corresponding to the nodes 1, 2, n-2, n-1 and n are derived from equations 47, 48, 51, 52 and 53 respectively by adapting the subscripts for N fasteners. All the other equations take either the form of Eq.49, for plate A nodes, or Eq.50, for plate B nodes. With these modifications, the generalized thermal loading vector can be expressed as:

$$\underline{L}_{ther} = \begin{bmatrix} (K_{A\_end} \cdot l_{end} - K_{A\_N-1} \cdot p_{N-1})\alpha \\ -K_{B\_N-1} \cdot \beta \cdot p_{N-1} \\ (K_{A\_N-1} \cdot p_{N-1} - K_{A\_N-2} \cdot p_2)\alpha \\ (K_{B\_N-1} \cdot p_{N-1} - K_{B\_N-2} \cdot p_2)\beta \\ . \\ . \\ . \\ . \\ (K_{A\_2} \cdot p_2 - K_{A\_1} \cdot p_1)\alpha \\ (K_{B\_2} \cdot p_2 - K_{B\_1} \cdot p_1)\beta \\ K_{A\_1} \cdot \alpha \cdot p_1 \\ (K_{B\_1} \cdot p_1 - K_{B\_end} \cdot l_{end})\beta \\ K_{B\_end} \cdot \beta \cdot l_{end} \end{bmatrix} \Delta T$$

11.4   Calculation of the global CTE for a laminate

The coefficient of thermal expansion of a laminate is calculated from the CTEs of the ply material as given in Section 2.4.2.

This is done by considering the effects of hygrothermal loads which induce a "free strain" when no mechanical loads are applied. The first step is to calculate the hygrothermal loads for an isolated ply in the material system 123. In case of zero moisture gradient and non-zero temperature gradient ΔT, the free strains due to hygrothermal loads are:

$$
\begin{aligned}
\varepsilon_1^{HT} &= CTE_1 \cdot \Delta T \\
\varepsilon_2^{HT} &= CTE_2 \cdot \Delta T \\
\gamma_{12} &= 0
\end{aligned}
\tag{54}
$$

From the previously calculated strains, the strains in a rotated system are:

$$
\begin{aligned}
\varepsilon_X^{HT} &= \varepsilon_1^{HT} \cdot v^2 + \varepsilon_Y^{HT} \cdot w^2 \\
\varepsilon_2^{HT} &= \varepsilon_1^{HT} \cdot w^2 + \varepsilon_Y^{HT} \cdot v^2 \\
\gamma_{XY} &= 2\left(\varepsilon_1^{HT} - \varepsilon_2^{HT}\right)vw
\end{aligned}
\tag{55}
$$

With $v = cos\theta$ and $w = sin\theta$. Since thermal stresses are internal stresses, hygrothermal loads $\underline{\mathbf{N^{HT}}}$ are self-equilibrated and can then simply be determined from the laminate's rotated stiffness matrix $\overline{Q}$ and the free strains:

$$
\begin{bmatrix}
N_X^{HT} \\
N_Y^{HT} \\
N_{XY}^{HT}
\end{bmatrix}
= \sum_{k=1}^{q} [\overline{Q}]_k
\begin{bmatrix}
\varepsilon_X^{HT} \\
\varepsilon_Y^{HT} \\
\gamma_{XY}^{HT}
\end{bmatrix}
\cdot t_k
\tag{56}
$$

With q being the total number of plies of thickness t_k each. Knowing the effective hygrothermal loads, the laminate's coefficients of thermal expansion can be calculated as:

$$
\begin{aligned}
CTE_X &= \frac{1}{\Delta T}\left[a_{11} \cdot N_X^{HT} + a_{12} \cdot N_Y^{HT}\right] \\
CTE_Y &= \frac{1}{\Delta T}\left[a_{12} \cdot N_X^{HT} + a_{22} \cdot N_Y^{HT}\right]
\end{aligned}
\tag{57}
$$

Where a_{11}, a_{12} and a_{22} are components of the laminate's $\underline{a}$ matrix, obtained from $\underline{abd}=\underline{\underline{ABD}}^{-1}$. The temperature gradient, already applied in Eq. 54, is arbitrary.

11.5   Bolt shear capacity calculation

ASTM A325 bolts were employed in the study on bolt shear deformation on which the instantaneous center of rotation method is based. The same approach to derive bolt shear capacity used in the reference study was employed in the thesis study for consistency.

A distinction is made in [47] based on the bolt threads, which could either be included or excluded from the shear planes. In this study, it was conservatively assumed that threads are never excluded from the shear plane, thus calculating a smaller bolt shear capacity. For this case, the bolt capacity is calculated as:

$$R_N = 0.45 \cdot n_l \cdot A_F \cdot \sigma_{uts} \tag{58}$$

Where n_l represents the number of shear planes in the bolt, equal to 1 in single-lap and 2 in double-lap joints and A_F is the cross section area of the bolt. The value σ_{uts} for the considered bolts was presented in Table 7.

11.6   Mesh sensitivity study for a single-lap joint

Table 54: Monitored variables for *Plate* mesh refinements in single-lap

Mesh	P [kN]	F_{sum} [kN]	f_1 [-]	f_2 [-]	f_3 [-]	Simulation time [min]
P1-W2-BN2	19.3	16.7	22.7	37.1	40.2	24.1
P2-W2-BN2	19.2	16.6	22.8	37.0	40.2	23.8
P3-W2-BN2	19.2	16.5	22.8	37.0	40.2	35.7
P4-W2-BN2	19.2	16.5	22.7	37.0	40.2	43.4

Table 55: Monitored variables for *Washer* mesh refinements in single-lap

Mesh	P [kN]	F_{sum} [kN]	f_1 [-]	f_2 [-]	f_3 [-]	Simulation time [min]
P2-W1-BN2	19.2	16.5	22.6	37.1	40.3	22.0
P2-W2-BN2	19.2	16.6	22.8	37.0	40.2	23.8
P2-W3-BN2	19.2	16.6	22.8	37.0	40.2	34.9

Table 56: Monitored variables for *Bolt and nut* mesh refinements in single-lap

Mesh	P [kN]	F_{sum} [kN]	f_1 [-]	f_2 [-]	f_3 [-]	Simulation time [min]
P2-W2-BN1	19.2	16.5	22.8	37.0	40.2	25.6
P2-W2-BN2	19.2	16.6	22.8	37.0	40.2	23.8
P2-W2-BN3	19.3	16.6	22.7	37.1	40.2	34.6

11.7 Additional information for Section 6.2
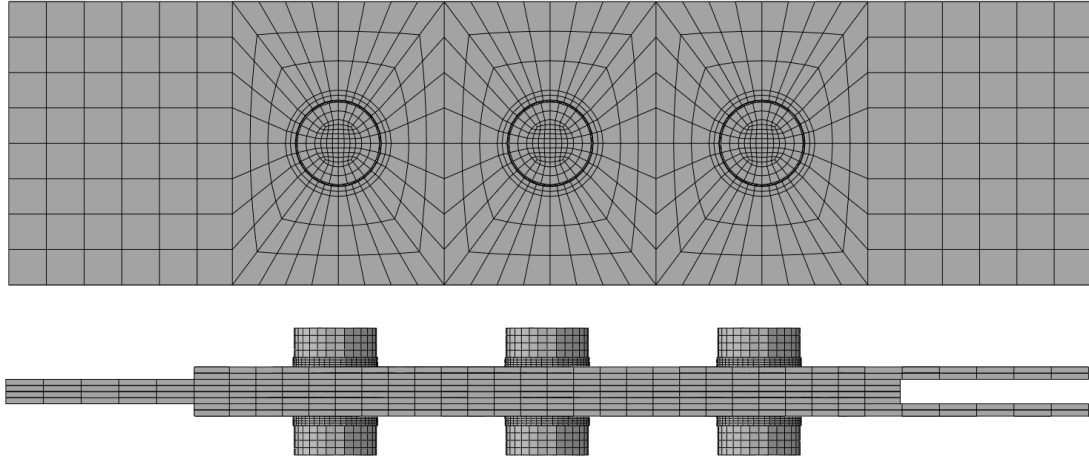

Figure 62: Mesh for the FE model of the joint considered in Section 6.2
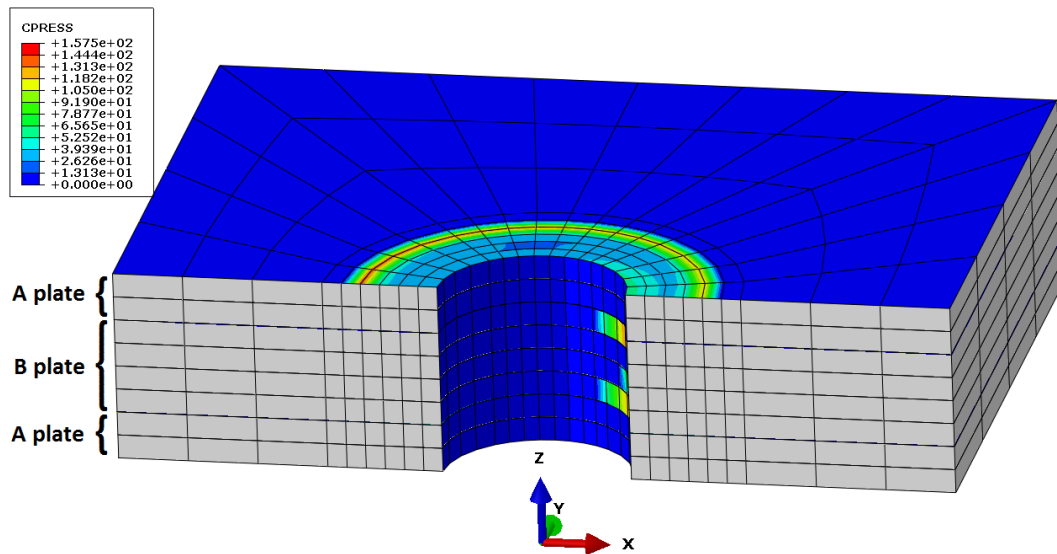

Figure 63: Bolt 2 - hole contact status at 27 kN of applied load for $\boldsymbol{\lambda} = \{40, 100, 40\}$
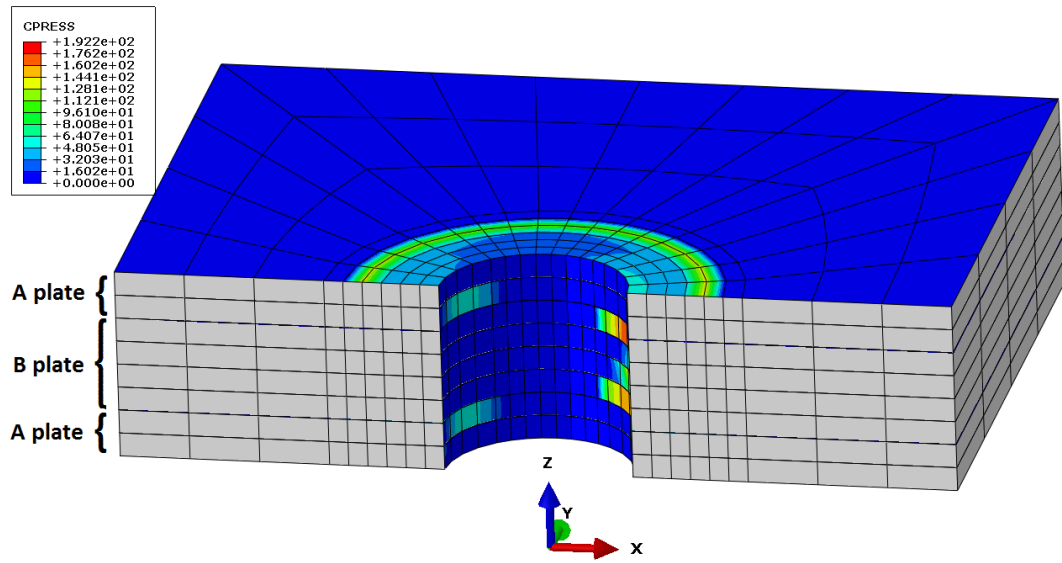
Figure 64: Bolt 2 - hole contact status at 42 kN of applied load for $\boldsymbol{\lambda} = \{40, 100, 40\}$

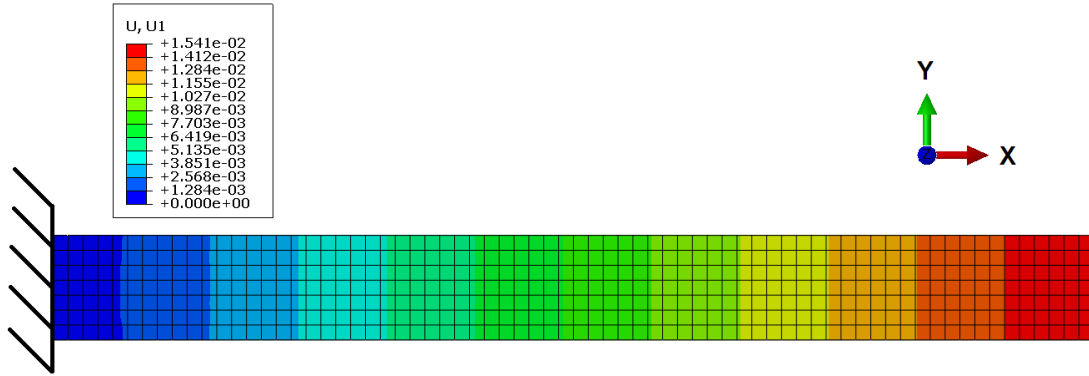## 11.8 Additional information for Section 6.3

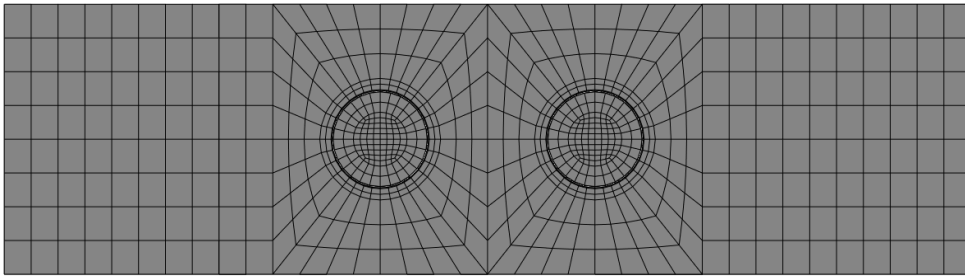Figure 65: Top view of the rectangular plate from Section 6.3.1

Figure 66: P2-W2-BN2 mesh for sensitivity study with thermal loading
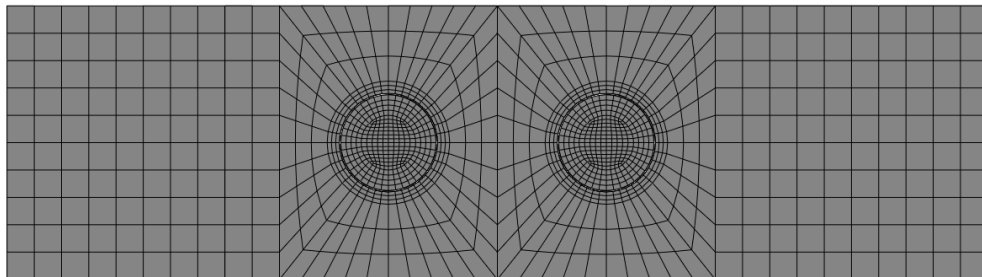

Figure 67: P3-W2-BN3 mesh for sensitivity study with thermal loading

11.9 Additional information for Section 7.1
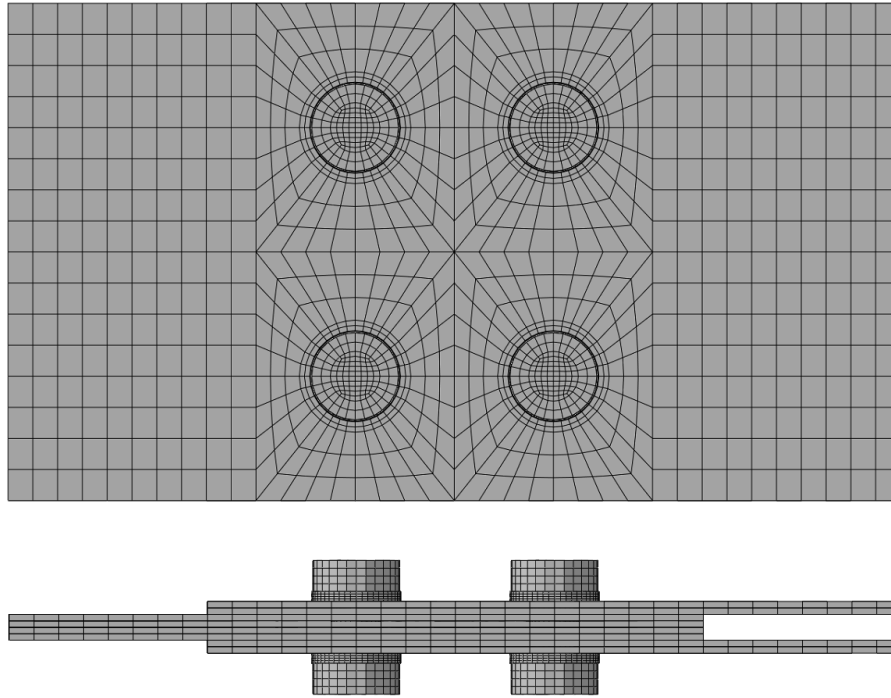
Figure 68: Mesh for the FE model of the joint considered in Section 7.1

Table 57: Bolt loads comparison for Δ_{high}=0.01 mm (P=2 kN)

	FEM		Modified ICoR		Elastic	
	F_S [kN]	f_S [%]	F_S [kN]	f_S [%]	F_S [kN]	f_S [%]
Bolt 1	1.40	24.0	1.54	22.3	1.31	20.3
Bolt 2	1.34	23.1	1.54	22.3	1.31	20.3
Bolt 3	1.53	26.4	1.92	27.7	1.91	29.7
Bolt 4	1.54	26.5	1.92	27.7	1.91	29.7

Table 58: Bolt loads comparison for Δ_{high}=2.86 mm (P=35 kN)

	FEM		Modified ICoR		Elastic	
	F_S [kN]	f_S [%]	F_S [kN]	f_S [%]	F_S [kN]	f_S [%]
Bolt 1	25.2	23.8	25.8	23.0	22.9	20.3
Bolt 2	24.9	23.4	25.8	23.0	22.9	20.3
Bolt 3	28.1	26.5	30.3	27.0	33.5	29.7
Bolt 4	28.0	26.3	30.3	27.0	33.5	29.7

Table 59: Bolt loads comparison for Δ_{high}=8.636 mm (P=47.7 kN)

	FEM		Modified ICoR		Elastic	
	$\mathbf{F_S}$ [kN]	$\mathbf{f_S}$ [%]	$\mathbf{F_S}$ [kN]	$\mathbf{f_S}$ [%]	$\mathbf{F_S}$ [kN]	$\mathbf{f_S}$ [%]
Bolt 1	35.0	24.2	34.7	24.2	31.2	20.3
Bolt 2	35.1	24.3	34.7	24.2	31.2	20.3
Bolt 3	37.2	25.8	36.9	25.8	45.7	29.7
Bolt 4	37.0	25.7	36.9	25.8	45.7	29.7

Table 60: Global plate stiffness for considered layups from CLT

	$\mathbf{E_x}$ [GPa]	$\mathbf{E_y}$ [GPa]
M-DL-D-C	86.7	29.8
M-DL-Q-C	48.0	48.0

Table 61: Elastic model loads prediction with CFRP plates for Δ_{high}=0.409 mm (P=15 kN)

	Elastic	
	$\mathbf{F_S}$ [kN]	$\mathbf{f_S}$ [%]
Bolt 1	9.82	20.3
Bolt 2	9.82	20.3
Bolt 3	14.4	29.7
Bolt 4	14.4	29.7

11.10 Additional load-distribution calculation for Section 7.2.2

To obtain reactions F_1 and F_4 on one hand and F_2 and F_3 on the other, two separate FE models with single-column approach were employed. In both cases, a displacement u_x=0.3 mm was imposed to the free end of the joint. This displacement value corresponds to different applied loads for the two columns, for example 27.4 kN and 21.3 kN in Table 62. This discrepancy is a consequence of the presence of bolt-hole clearance only in one of the two single-column models.

The results for the case *1-col (Bolts 1-4)* were scaled, maintaining the same proportionality, to consider the same F_{sum} value as in *1-col (Bolts 2-3)*, thus yielding the line *1-col (Bolts 1-4)**. This is equivalent to consider that the load distribution for the single-column joint with bolts 1 and 4 remains the same for different applied loads. This approach is justified by considering the elastic nature of material deformation, the absence of clearance in bolts 1 and 4 and the fact that the slip-critical friction force has been overcome.

Table 62: Bolt reactions scaling for *1-col* with M-DL-D-C and $\boldsymbol{\lambda} = \{0, 100, 0, 0\}$

Joint	P [kN]	F_{sum} [kN]	F_1 [-]	F_2 [-]	F_3 [-]	F_4 [-]
1-col (Bolts 1-4)	27.4	27.0	15.2			11.8
1-col (Bolts 2-3)	21.3	20.8		4.7	16.1	
1-col (Bolts 1-4)*		20.8	11.7			9.13

Based on these scalings, the results could be compared to obtain the load distribution at the four fasteners for the single-column approach, as shown in Tables 63 and 65 and reported in Section 7.2.2.

Table 63: Load distribution for *1-col* with M-DL-D-C and $\boldsymbol{\lambda} = \{0, 100, 0, 0\}$

Joint	P [kN]	F_{sum} [kN]	f_1 [-]	f_2 [-]	f_3 [-]	f_4 [-]
1-col	21.3	(20.8)	28.1	11.3	38.7	21.9

The scaling procedure for comparison of the results described above was equally applied to the quasi-isotropic laminate case. The results are presented in Tables 64 and 65.

Table 64: Bolt reactions scaling for *1-col* with M-DL-Q-C and $\boldsymbol{\lambda} = \{0, 100, 0, 0\}$

Joint	P [kN]	F_{sum} [kN]	F_1 [-]	F_2 [-]	F_3 [-]	F_4 [-]
1-col (Bolts 1-4)	20.9	20.5	12.3			8.16
1-col (Bolts 2-3)	15.9	15.5		2.85	12.6	
1-col (Bolts 1-4)*		15.5	9.30			6.17

Table 65: Load distribution for *1-col* with M-DL-Q-C and $\boldsymbol{\lambda} = \{0, 100, 0, 0\}$

Joint	P [kN]	F_{sum} [kN]	f_1 [-]	f_2 [-]	f_3 [-]	f_4 [-]
1-col	15.9	(15.5)	30.1	8.9	39.6	19.9

11.11 Parametric study on the effect of boundary condition distance

A parametric study was carried out to validate the hypothesis that the two modelling approaches *1D BCs* and *2D BCs* tend to give equal results when the fasteners are far from the plate edges. The study was carried out for the joint geometry presented in Fig.53 by considering five different values for the length s. It was not necessary to modify the joint geometry also in the other direction since only a load along the X direction is considered. This makes it easy to monitor the impact of edge distance since, for *1D BCs* conditions, an equal distribution at 1-2 and 3-4 is known to be observed. The results are summarized in Table 66.

Table 66: Influence of boundary conditions distance for uniaxial tensile loading

	s	f_1	f_2	f_3	f_4	X_{re}	
	[mm]	[%]	[%]	[%]	[%]	BC_X [%]	BC_Y [%]
1D BCs	40	28.3	28.3	21.7	21.7	100	0
2D BCs	10	30.1	23.8	18.6	27.5	66.0	34.0
2D BCs	40	29.4	26.1	19.9	24.6	84.6	15.4
2D BCs	160	28.5	27.9	22.3	21.3	98.7	1.34
2D BCs	240	28.4	28.1	21.5	22.0	99.6	0.37
2D BCs	320	28.3	28.1	21.6	21.9	99.9	0.10

For large s values, the load distribution prediction with the *2D BCs* approach tends to the prediction obtained with *1D BCs*, as had been anticipated. Modifying s with the latter approach is not expected to modify the load distribution and only the case with s=40 mm was considered. For the case s=160 mm, roughly four times the bolt pitch, the difference between the two approaches at the two most loaded bolts is of 0.2%.

Based on these results, it is believed that repeating the study by considering loads in two directions would lead to the same trends. However, it is possible that the variations of load fraction between *1D BCs* and *2D BCs* would be larger with biaxial loading than with uniaxial loading for the same edge distance. This fact should, of course, be kept in mind when interpreting these findings for loading in two directions.